Impact of Dicer on the Embryonic Stem Cell Epigenome and Androgen Mediated AMPK-PGC-1α Signaling in Prostate Cancer

A

Dissertation

Presented to

The Faculty of the Department of Biology and Biochemistry

University of Houston

In Partial Fulfillment

of the Requirements for the Degree

Doctor of Philosophy

in Cell and Molecular Biology

by

Jayantha H.B.Tennakoon

August 2013

Impact of Dicer on the Embryonic Stem Cell Epigenome and Androgen Mediated AMPK-PGC-1α Signaling in Prostate Cancer

_____
Jayantha H.B. Tennakoon

Approved:

_____
Dr. Preethi H. Gunaratne, Co-Chairman

_____
Dr. Daniel E. Frigo, Co-Chairman

_____
Dr. Dan E. Wells

_____
Dr. Xiaolian Gao

_____
Dr. Thomas P. Zwaka,
Baylor College of Medicine 77030

_____
Dean, College of Natural Sciences and Mathematics

ACKNOWLEDGEMENTS

In bringing this dissertation to existence I was richly blessed to receive the support of numerous individuals who were of remarkable substance. In fact all of them deserve to be personally acknowledged, hence I make an earnest effort to show my gratitude in an all-encompassing manner. To begin with, sincere thanks are offered to my two principle mentors Dr. Preethi Gunaratne and Dr. Daniel Frigo who exercised enormous effort in guiding me through the complex problems I attempted to address during the work presented in this dissertation. Some of them were very trying times where I was tested to the limits. When I ponder with hindsight, I now realize if it weren't for the challenges that the three of us as a team had to overcome I would not have been as refined as I am today to confidently face an arduous scientific career which lies ahead. I am grateful to my committee members Dr. Dan Wells, Dr. Thomas Zwaka and Dr. Xiaolian Gao who constantly offered insightful advice. A special word of thanks is offered to Dr. Austin J. Cooney and the members of his laboratory who were generous in providing material support. Dr. Cristian Coarfa is thankfully acknowledged for generating the genetic maps, which provided the basis to formulate the initial hypothesis, tested in the first chapter of this work. Dr. Yan Shi did an excellent job in producing mitochondrial photographs presented in chapter two. Jenny Han who always provided sound technical support and Efrosini Tsouko who generated the clinical data graphs from the Oncomine database presented in the second chapter are wholeheartedly acknowledged for their contributions. It was indeed a pleasure working with the numerous co-authors with whom I had the opportunity to publish several manuscripts while in Houston and they are thanked indeed. All present and past laboratory members of Dr. Preethi Gunaratne and Dr. Daniel Frigo who provided support in numerous ways are also remembered. Finally, I would like to mention that I am truly indebted to my family and friends who were near and dear to me at all times providing moral support.

Impact of Dicer on the Embryonic Stem Cell Epigenome and Androgen Mediated AMPK-PGC-1α Signaling in Prostate Cancer

An

Abstract of a Dissertation

Presented to

The Faculty of the Department of Biology and Biochemistry

University of Houston

In Partial Fulfillment

of the Requirements for the Degree

Doctor of Philosophy

in Cell and Molecular Biology

by

Jayantha H.B.Tennakoon

August 2013

ABSTRACT

What mechanisms govern a cellular phenotype is a fascinating question for which answers are yet being sought. The work presented in this dissertation is an effort to address two fundamental questions, which relate to cellular transition of pluripotent stem cells to a differentiated state and the ability of prostate cancer to have increased proliferative potential. Dicer is an evolutionary conserved RNAse III type endoribonuclease enzyme, which plays a pivotal role in the biogenesis of microRNAs and silencing RNAs (siRNAs). Within the first chapter herein using *in vitro* cultures of embryonic stem cells, I show that loss of Dicer leads to changes in the ES cell epigenome resulting in a shift in transcriptionally favorable versus transcriptionally unfavorable histone modifications and thereby affect gene expression critical for precise cellular differentiation. In the second chapter, employing a combination of molecular biological and modern metabolomics approaches I show that androgen signaling deregulated in almost all forms of metastatic prostate cancers can lead to increased mitochondrial biogenesis and ATP production affording a distinct proliferative advantage. The underlying mechanism is linked to androgen mediated AMPK- PGC-1α signaling which results increased oxidative capacity in addition to elevated glycolytic capacity quite well established in numerous types of cancers. The pathway uncovered provides an interesting option for targeted therapeutics of prostatic cancers that are particularly resistant to androgen ablation therapies. Finally in the third chapter I show the significance of Dicer in maintaining expression levels of developmentally critical mammalian imprinted genes. The combined results of this thesis provide mechanistic insights into developmentally critical cellular pathways in embryonic stem cells and cancer having high potential to be manipulated in stem cell and molecular intervention based therapeutics.

TABLE OF CONTENTS

LIST OF FIGURES

LIST OF TABLES

SCOPE OF RESEARCH

A cell represents the fundamental unit of life (1, 2). Since the first discoveries of cells were made by Robert Hooke (3) science has developed to an extent where the organelle composition of cells is well defined. Numerous discoveries made in the past have shed much light on fundamental phenomena that define a cells ability to develop, replicate, migrate, evolve to carry out specialized functions, and eventually undergo cell death. For example, Matthias Schleiden and Theodor Schwann's observations provided a foundation for the well-established modern cell theories (1, 2). Studies by Gregor Mendel in 1866 led to the idea of the genetic basis of heritable traits (4). More recently, with the advent of new technologies, subcellular structures were identified and it was shown that these structures have specialized functions. Today we know transfer of heritable traits is facilitated by genetic elements coded by different combinations of base pairs in DNA packaged into chromosomes with histone proteins and linkers (5-7). When transcribed DNA produces pieces of RNA molecules (8), which are eventually translated to protein molecules (9, 10). Messenger RNA molecules are translated into proteins, which can undergo post-translational modifications (11). More recent studies have shown that several non-messenger RNA molecules have different functions other than protein coding (12) out of which miRNAs have been actively researched due to their ability to regulate messenger RNA through 3'UTR elements (13-17). The different varieties of molecules formed within a cell and their interactions can have different attributes from a cellular perspective, which can range in a variety of structural and functional events (18-21). During the latter part the twentieth century massive technological advancement in the tools utilized for cellular investigation have provided opportunities to more closely observe the coordinated activities within and in-between cells that are largely facilitated by biochemical mechanisms at

the molecular level. As evidenced today, high-throughput methods combined with powerful computing tools have completely revolutionized the scope of molecular life sciences (22).

Interestingly, in spite of advancements in the technological spheres, the biochemical and molecular mechanisms that determine the fate of a cell within a given context still are largely not well understood. This of course is of utmost importance because as much as healthy cells form life, cells which depart from the mechanistic principles designed by nature to sustain living organisms in a healthy state can lead to undesirable consequences which span a gamut of illnesses. The main effort of this dissertation has been studying the underlying molecular events that define two important aspects of cellular dynamics: 1) the regulatory events that determine fate of embryonic stem cells and 2) the unlimited survival and proliferative potential of prostatic cancer cells. The former is of immense significance as it is still a burgeoning field where discoveries are being made and the knowledge generated through studies are applied to developing cell-based therapies. The latter is a problem, which has been relatively well studied compared to stem cell biology. Nonetheless prostate cancer remains a very elusive disease for which effective therapies are still being sought.

To address the first issue of probing the regulatory mechanisms that govern the cellular transition from a pluripotent stem cell state to the differentiated state I initially employed a discovery based genomic approach using a state of the art next generation sequencing platform (Illumina GA-II) to examine the impact of Dicer-on the embryonic stem cell epigenome and examined global changes in H3K9me2 modifications typically associated with long term silencing of chromatin regions during the transition of pluripotent embryonic stem from the state of self-renewal to a differentiated state. I validated the information generated through ChIP-seq in the discovery with respect to a number of genes established to be involved in the

maintenance of the two states of self-renewal and differentiation. Subsequently, I examined the impact of Dicer loss on histone modifications at a number of imprinted loci in the mouse genome. In order to get a handle on mechanistic principles, which facilitate stem cellular transition from a pluripotent state to a differentiated state I also utilized siRNAs and microRNAs to identify Ezh2 up-regulation due to decreased let-7 in Dicer null ES cells to be in part responsible for some of the epigenetic changes in genes regulating ES cell self-renewal and differentiation. The model system I have used for studies relevant to the first and third chapters is based on a Dicer deficient mouse embryonic stem cell line (23), which I compare to a wild type mouse embryonic stem cell line.

Dicer is an evolutionarily conserved RNAse, which is necessary for microRNA biogenesis. It is an essential component for the generation of a majority of miRNAs in mammals (12, 14). Previous studies have shown that Dicer deficient embryonic stem cells are incapable of differentiation and do not survive beyond day 6.5 of embryonic development (23-25). While the role of Dicer in the post-transcriptional regulation of genes is well established its' contribution to the mammalian epigenome is less clear. Here I report findings on the impact of Dicer on genome-wide H3K9me2 in mouse embryonic stem cells (ES) and the local impact of Dicer on H3K9me2, H3K4me3, H3K27me3 and H3K36me3 on promoters of key regulators of ES cell self-renewal, differentiation and the transition from one state to another using a retinoic acid-induced differentiation model of ES cells. Comparing, the epigenetic profiles which favor H3K4me3 modifications versus H3K9me2 and H3K27me3 modifications in wild type and Dicer deficient ES cells I found that one of the key impacts of loss of Dicer is the loss of critical balance between the transcriptionally favorable H3K4me3 and transcriptionally unfavorable H3K27me3 modifications at the promoters of differentiation genes Hoxa1 and Cdx2. Failure to down-regulate these genes at the same rate as wild type ES cells is likely in

large part to be instrumental in the differentiation block of Dicer KO ES cells that ultimately lead to the untimely death of Dicer KO embryos at Day 6.5. Through further studies I have also established that the increase in H3K27me3 is in part due to an increase in the levels of the polycomb repressor gene Ezh2, which facilitates H3K27me3. Ectopic expression of let7g miRNA or siRNAs targeting Ezh2 in Dicer null ES cells was able to reverse these conditions leading to reduced H3K27me3 enrichment at Hoxa1 and Cdx2 while elevating mRNA expression of these genes to comparable levels in wild type stem cells. This is an observation, which proves in principal the potential of using let7g, or interfering RNA molecules in directed reprogramming of stem cells for therapeutic purposes.

In the second chapter I mainly utilize two established cellular models of human prostate cancer to evaluate proliferative capacity due to Androgen-mediated AMPK-PGC-1α signaling. The two models which were used are LNCaP cells, which are a lymph node, metastasized prostate cell line and VCaP cells which are a bone metastasized prostate cancer cell line (26, 27). Androgen signaling is known to be deregulated in almost all prostate cancers (28-32). Through a series of experiments I was able to ascertain that androgen signaling can affect AMPK-PGC-1α mediated cellular ATP production. The consequences of Androgen signaling through the AMPK-PGC-1α axis are, increased mitochondrial volume, oxidative capacity and cellular proliferative potential of the two cell lines. These observations provide the opportunity to develop targeted therapeutics directed at the uncovered pathway for further investigation.

Finally in the third chapter, using mouse embryonic stem cells, I show that microRNAs in conjunction with Dicer play a role in regulating genetic imprinting in mammals. While attempting this study I carried out a comparative messenger RNA expression analysis of three cell types, which are wild type embryonic stem cells, trophoblastic stem cells (33), and Dicer

null mouse embryonic stem cells. Close investigation of the developmentally critical PWCR1, ATP10a, and the imprinted polycomb group repressor Sfmbt2 cluster mRNA levels indicate that the expression of these genes is enriched in trophoblastic stem cells, elevated in the Dicer null cell lines and minimal in wild type ES cells. This implies a potential role for Dicer in conjunction with miRNAs in regulating the trophoblastic lineage decision and expression of genes in the developmentally critical imprinted regions of mammals.

Taken together the three chapters covered in this dissertation provide molecular mechanistic insights to different levels of regulation, which affect cellular state, proliferative capacity and imprinting in different model systems. All of which have potential to be further investigated for therapeutic purposes in future.

CHAPTER 1:

Loss of Dicer results in a shift in transcriptionally favorable and unfavorable histone marks to influence genes in embryonic stem cells.

ABSTRACT

Loss of Dicer, an enzyme critical for microRNA biogenesis, results in lethality due to a block in embryonic stem cell (ES) differentiation. We found that the ES (Dicer$^{-/-}$) mutant epigenome was characterized by a shift in the overall balance between transcriptionally favorable

(H3K4me3) and unfavorable (H3K9me2 and H3K27me3) marks at key genes regulating ES cell differentiation. Using ChIP-seq we found increased H3K9me2 at over 900 CpG islands in the Dicer$^{-/-}$ES epigenome to specifically impact chromatin regulators. We therefore, extended the study to include H3K4me3 and H3K27me3 marks for selected genes. An increase in H3K9me2/H3K27me3 in the promoters of differentiation genes Hoxa1 and Cdx2 in Dicer$^{-/-}$ES cells was coincident with an inability to up-regulate these genes at the same rate as ES upon Retinoic acid (RA)-induced differentiation. siRNAs and microRNA let-7g rescued this effect by down-regulating Ezh2 suggesting that Ezh2 up-regulation is in part responsible for increased H3K27me3 and decreased rates of up-regulation of differentiation genes in Dicer$^{-/-}$ES. Pluripotency genes Oct4, Sox2 and Nanog showed no changes in H3K9me2/H3K4/me3/H3K27me3 coincident with no changes in rates of RA-induced down-regulation between Dicer$^{-/-}$ES and ES. Promoters of genes regulating the transition from self-renewal to differentiation (Lin28b and Gcnf) were associated with increased H3K4me3 coincident with down-regulation of Lin28b at a lower rate and up-regulation of Gcnf at a higher rate upon RA-induction in Dicer$^{-/-}$ES.

MATERIALS AND METHODS

Cell Culture:

mES cells were cultured on gelatin coated plates using DMEM (Gibco, Invitrogen, Carlsbad California catalog number-31053) containing 15% FBS (Invitrogen, Carlsbad California catalog number-10439-024), 1X Penstrep (Gibco, Grand Island New York catalog number-15140-122), 1X Glutamine (Gibco, Grand Island New York catalog number-25030-024), 1X

non-essential amino acids (Gibco, Grand Island New York catalog number-11140-035), 1X Pyruvate Solution (Gibco, Grand Island New York catalog number- cat#11360), 0.1mM 2-mercaptoethanol (Sigma, St. Louis Missouri catalog number-M7522) and 1000U/ml LIF (LIF 2010, Millipore, Billerica, Massachusetts) during day 0 by seeding at a density of 250,000 cells per well. LIF containing media was replaced with RA containing media to induce differentiation after day 0. Thereafter the cells were maintained in RA containing medium by feeding on a daily basis. Mouse ES and ES (Dicer-/-) cells were provided by Gregory Hannon, Cold Spring Harbor Laboratories(34).

miRNA and siRNA transfections*:*

Mature let-7g miRNAs and *Ezh2* siRNAs were purchased from Invitrogen Inc Carlsbad USA. Cells were transfected with let-7g and si*Ezh2* RNAs on day 0 on six well format plates using standard protocols for Lipofectamine 2000 transfection reagent (Catalog number11668-019, Invitrogen, Carlsbad, California). Each well was transfected with 5 ul of Lipofectamine 2000 reagent and let-7g miRNA at a final concentration of 10 nM and a final concentration of 50 nM si*Ezh2*. In order to sustain overexpression, the cells were re-transfected using the same protocols at day 3 after RA induction.

RNA Extraction:

RNA was extracted from the cell lines using a Qiagen miRNAeasy mini extraction kit (Catalog number 217004), Qiagen, Maryland, USA according to manufacture's instructions. In order to make sure that the RNA samples were free of DNA contamination an on column DNAse

treatment was carried out according to manufactures' protocols using a Qiagen DNAse reagent kit.

Quantitative real time PCR:

Quantitative real-time reactions were performed on Chromatin immunoprecipitated DNA and reverse transcribed RNA samples on a 96 well format Applied Biosystems 7500 real time PCR machine using SYBR green dye according to manufacturer's protocols (catalog number 4385112, Applied Biosystems, New Jersey, USA). A mouse 18S ribosomal subunit mRNA was used as an endogenous control. mRNA fold changes of candidate genes were calculated by normalizing against the ES day zero samples in respective experiments of a given panel. Total mRNA was extracted from cell samples using a Qiagen RNA easy kit (catalog number 74104, Qiagen, California, USA). In order to ensure the RNA samples were free of genomic contamination an on column DNAse digestion treatment was carried out using a Qiagen RNase free DNase kit (catalog number 79254, Qiagen, California, USA). CDNA synthesis of isolated RNA was carried out using a Taqman Reverse transcription kit according to manufacturer's protocol (catalog number N8080234, Applied Biosystems, New Jersey, USA).

Chromatin Immunoprecipitation:

Chromatin immunoprecipitation was performed on genomic DNA samples from cell lines using antibodies specific to H3K4me3, HK9me2 and H3K27me3 as previously described (35). $5x10^6$ cells were used for each ChIP assay. The cells were Formaldehyde (1%) cross-linked for 10 minutes. The cell lysates were sonicated to shear DNA to lengths between 200 and 1000 bp.

The following antibodies were used for the chromatin immunoprecipitation assays: Rabbit anti- Dimethyl-H3K9 (Cat# 39765, Active Motif 914 Palomar Oaks Way # 150, Carlsbad, CA) 92008-6509Rabbit anti-Trimethyl-H3K4 (Cat# 07-473, Upstate Biotechnology, Lake Placid, NY), Rabbit anti- Trimethyl-H3K27 (Cat# 07-449, Upstate Biotechnology, Lake Placid, NY). The DNA/antibody complexes were pulled down by the protein A/G plus-agarose (cat# sc- 2003, Santa Cruz Biotechnology, Inc., Santa Cruz, CA) Enrichment of a given histone modification in the promoter regions of respective genes were calculated as a percentage of the input samples used for each experiment.

Solexa Library preparation:

Libraries for ChIP-Seq analysis were prepared using standard protocols of the Solexa Illumina paltform provided by the manufacturers and outlined in our previous descriptions (35). Sheared DNA fragments of Chromatin immunoprecipitated samples were end repaired to fill 5'overhangs employing a T4 DNA polymerase reaction. 3'overhangs were removed employing Klenow polymerase. 5' hydroxyl groups were phosphorylated using T4PNK. Adapter ligation was then carried out using Illumina's patented oligo mix according to recommended protocols. The adapter ligated constructs were PCR amplified (using matching primers) within the linear range for 18 cycles to ensure non-saturation. Quality verified DNA was then run on on TBE gels and gel purified at desired lengths. Finally 10nM of the purified samples were run on an Illumina GA-2 genome analyzer and data collected for downstream mapping purposes.

Genomic Mapping:

Genomic mapping of chromatin immunoprecipitated sequence libraries for ES and *Dicer*$^{-/-}$ were performed using the Pash algorithm as previously described (36). Uniquely mapping reads were selected, then read coverage was computed over 100bp windows tiling across the entire genome. The read density maps were normalized employing a quantile normalization step. For each genomic window the difference between ES and *Dicer*$^{-/-}$ and the associated p-value was computed; windows with a false discovery rate (FDR) below 0.001 were selected, and then a segmentation algorithm was applied. Finally, genomic feature sets such as gene promoters, gene exons, microRNAs, piRNA clusters, CpG islands and others were annotated for individual elements with enriched bindings in either ES or *Dicer*$^{-/-}$. Virtual genome maps in Figure 1.1A and 1.1B were generated using the VGP feature of the Genboree tool.
(http://www.genboree.org/java-bin/login.jsp).

Primers:

All primers for real time quantitative PCR and ChIP-qPCRwere designed using the publicly available primer 3 tool (http://frodo.wi.mit.edu/primer3/). Primers for qRT-PCRs as listed in Table 1.1 were designed to span intronic regions whenever possible to avoid background resulting from genomic contamination of RNA samples. Primers for ChIP-qPCR were designed to span promoter regions of the assayed genes derived from the Cold Spring Harbor

mammalian promoter database (http://rulai.cshl.edu/CSHLmpd2/). The complete lists of primers used for ChIP-qPCR assays are listed in Table 1.2

Statistical analysis:

Statistical analyses were carried out using Graph pad Prism and Excel software. Students' t-tests were carried out to assess significance in differences in quantitative real time PCR results while false differential ratios were calculated to assure quality of chromatin immunoprecipitated sequence mapping. Unless otherwise stated all statistical analyses were carried out and tested at confidence levels of 0.05 or less.

Table 1.1 List of Primers used for qPCR assays

Gene	Forward primer	Reverse primer
Oct4	AGAGGGAACCTCCTCTGAGC	CCAAGGTGATCCTCTTCTGC
Sox2	CACAACTCGGAGATCAGCAA	CGGGGCCGGTATTTATAATC
Nanog	ATGCCTGCAGTTTTTCATCC	GAGCTTTTGTTTGGGACTGG
Ronin	AAGAGGGCTTCCCTGACACT	CGGATGCTACCCTTCATCTC
Lin28b	GAGAGGGAAATCCCTTGGATA	TGTTACCCGTATTGACTCAAGG
Gcnf	TTGCAACAAACGGGTGTATC	GGCATGCCATCTTCTCTGAT
Hoxa1	GCAGACCTTTGACTGGATGA	AGCTCTGTGAGCTGCTTGGT
Cdx2	ACCTGTGCGAGTGGATGC	TGAAACTCCTTCTCCAGCTC
Ezh2	GCGGAAGCGTGTAAAATCAG	GCTGCTTCCACTCTTGGTTT
Setd2	CCGAAGATGGGGGATTTCTA	TTTTGTCTTCGTGCCTTTGG
G9a	CCTGAGCTTCGGAACAAAGA	ATTGACACAGGGGATGGGTA
Ash1l	CCAGTTGCCGGAAGAAATTA	TGATCGCTGGGAAGGTTTAT
Dnmt3a	GAGAGGAACAGGAGGAGAACC	TGAGACTTGGTGGTCACTGC
Dnmt3b	TGGGAATGGCTCTGATATTCT	ATTCTGGGGGAGGCTCTTT
18S	AGTTCCAGCACATTTTGCGAG	TCATCCTCCGTGAGTTCTCCA

Table 1.2 List of Primers used for ChIP-qPCR assays

Gene	Forward primer	Reverse primer
Oct4	TAGGTGAGCCGTCTTTCCAC	CCCTGCTGACCCATCACC
Sox2	GCGGCCCCTGCATCC	TTCAGCTCCGTCTCCATCAT
Nanog	TTTGGTTGTTGCCTAAAACCTT	CTGCAGGCATTGATGAGG
Ronin	CGTCGAAGAGCTCGAGAGG	CGTCCTTGGGAAACGTGTAG
Lin28b	ATCAAGATGTTAGACTGATGCTGAA	GAGAAAAGAAGAGAGGAATCACAG
Gcnf	CCCGTGGAAGACCAGGAC	GCTAGGTGGCCGTTCGTC
Hoxa1	CATATCATTTTTCTTCTCTGGTCCT	ACTGCCAAGGATGGGGTATT
Cdx2	CCTCTGGCAGCCTTCAAC	CGCACGGAGCTAGGATACAT

INTRODUCTION

Dicer is an RNAse III type endoribonuclease with specific enzymatic activity of cleaving double stranded RNA molecules (37). It is evolutionary conserved among worms, flies, plants, fungi and mammals (37). Dicer-dependent microRNAs are initiated through RNA polymerase II activity to generate a primary miRNA that forms a stem and loop structure which is cleaved by the combined activities of two enzymes Drosha and Pasha (14). The resultant stem loop precursors are then transported to the cytoplasm through Exportin-5 action where Dicer catalyzes the second cleavage event to produce 18 to 25 nucleotide mature miRNA duplex structures (14). Mature miRNAs are known to regulate gene expression by either cleaving mRNA molecules by binding to respective 3'UTR elements or by translational repression (14, 38, 39). Sequence analysis using Dicer deficient mES cells show that a large majority of miRNAs native to the wild type (WT) cells is absent in the $Dicer^{-/-}$ES cells (40, 41). The conventional role of miRNAs in post-transcriptional gene silencing is well established, however the full extent of the role of Dicer-dependent pathways beyond their established role in regulatory mechanisms such as epigenetic silencing critical for biological processes is yet to be determined. In spite of several studies having shown small RNA molecules regulating epigenetic modifications in plants, flies and fission yeast (42-44) it remains unclear whether similar regulation occurs in higher order mammals in particular through direct effects of Dicer-dependent pathways or through Dicer-dependent miRNA mediated post-transcriptional regulation. In addition to roles in which Dicer has been implied thus far in regulatory mechanisms, it has also been implied in events as diverse as genome surveillance in C. elegans, nuclear exclusion in tetrahymena and differentiation control in ES cells (45-47).

Studies have shown that Dicer deficient mouse embryos show morphological abnormalities at day 6.5 of embryonic development (23, 24, 34). Critical events that Dicer-dependent miRNAs play in maintaining mammalian stem cell pluripotency and cellular transition by functioning as repressors of transcription factors, chromatin modifiers and cell signaling molecules have been elaborately reviewed by (48). Moreover it is known that miRNAs are needed for proper maintenance of DNA methylation in mES cells (49). The currently proposed mechanistic principle is that proper DNA methylation is invoked in ES cells by down regulation of repressors of DNA methyltransferases 3A and 3B (Dnmt3) such as Rbl by miRNAs in the miR-290-295 cluster ensuring availability of DNA methyltransferases for de novo DNA methylation (49). The critical roles which histone modifications play in determining cellular transition and stem cell plasticity is all the more emphasized through observations made by (50) that polycomb group proteins repress key developmental regulators in mES cells through repressive histone H3K27me3 modifications during the pluripotent state. Mechanistic details complementing these observations and the subtle role that different histone modifications play have been made clear through striking observations by (51) demonstrating the occupation of key developmental regulators by transcriptionally unfavorable H3K27me3 as well as transcriptionally favorable H3K4me3 modifications which render these subsets of genes to be repressed during the pluripotent state poised for activation upon differentiation (51). These combined observations strongly argue for a case where reversible histone modifications regulate gene expression by decorating the genomic landscape of pluripotency factors with marks favoring transcription H3K4me3 while keeping the other transcription factors in downstream genetic cascades involving genes associated with differentiation in a poised state for activation through bivalent domains comprising H3K4me3 as well as H3K27me3 modifications. Given the connotations of miRNAs in defining stem cell pluripotency and the roles that small RNAs play in epigenetic regulation in species other than higher order mammals we hypothesized that Dicer-dependent pathways, either

directly or indirectly through miRNA mediated regulation, guide epigenetic changes in mES cells and affect transcriptional expression that potentially define cellular fate.

To address our hypothesis we chose to carry out a genome-wide ChIP-seq analysis of mES cells and Dicer$^{-/-}$ES cells for H3K9me2 modifications. We then extended this work to include ChIP-qPCR assays for H3K9me2, H3K27me3 and H3K4me3 marks in the promoter regions of key developmental genes. This was motivated by the uncovering of chromatin regulators as the top Gene Ontology group to be impacted by the loss of Dicer in the H3K9me2 study. H3K9me2, H3K27me3 are considered context dependent repressive marks and H3K4me3, which is favorably associated with polymerase recruitment, is typically associated with transcriptional activation. Focusing on key genes involved in mES self-renewal and pluripotency (Oct4, Nanog, Sox2 and Ronin), differentiation (Cdx2 and Hoxa1) and genes regulating the transition between these states (Lin28b and Gcnf) we carried out qRT-PCR assays. (52-54). As reversible histone silencing modifications could potentially function as tracers, mapping genetic regions for subsequent DNA methylation, and thus more profoundly repressing gene expression, we probed the expression levels of a host of histone methyl transferases responsible for the modifications H3K9me2 (G9a) H3K4me3, (Setd2), H3K36me3 (Ash1l) and H3K27me3 (Ezh2). Taken together our data show that Dicer directly or indirectly regulates gene expression in mES cells at the epigenetic as well as post-transcriptional levels and point to a critical role Dicer plays in mammalian embryogenesis.

RESULTS

Loss of Dicer has a strong impact on H3K9me2 in the epigenomic landscape in mES cells.

It has been shown that small RNAs regulate epigenetic changes in plants, flies and fission yeast (42-44). However a potential role for Dicer-dependent pathways and miRNAs in mammals in particular remain hitherto unexplored. It has also been shown that miRNAs regulate DNA methylation via the miR-290-295 candidates functioning as repressors of Rbl2, which in turn is a repressor of Dnmt3 (49). H3K9me2 modifications are widely considered precursors or tracers demarcating genetic regions bound to undergo DNA methylation (55, 56). In order to assess Dicer's effect on potential upstream events regulated via H3K9me2 modifications, which could have significant implications on gene expression programs in mammalian cells, we carried out genome-wide H3K9me2 ChIP-seq analysis using the Illumina platform. We then generated genome-wide H3K9me2 maps on the mES cell genome using the PASH algorithm (36). Of the regions showing differential H3K9me2 modification we found increased H3K9me2 in Dicer$^{-/-}$ ES cells in 71% of promoter regions and 98% of CpG islands, (Fig 1.1A). Comparison of ratios of H3K9me2 occupation by the number of tags mapping to different genomic features revealed that on a global scale Dicer$^{-/-}$ ES cells showed fold changes of 60 at CpG islands, 5 at exons and 2 at promoters and <1 in whole genes, introns, 3'UTR whole gene, 3'UTR piRNA and miRNA clusters respectively (Fig 1.1B). These observations strongly suggested a potential role for either a direct or indirect role for Dicer-dependent pathways in regulating the mES cell epigenome via H3K9me2 modifications. In order to see if the biological processes that are impacted by the large number of genes associated with increased CpG island H3K9me2 and the small number of genes associated with decreased CpG island H3K9me2 in Dicer$^{-/-}$ ES are distinct we carried out GO

analyses on the gene sets. From data shown in Table 1.3 we see that genes with equivalent levels of CpG island H3K9me2 in WT and Dicer$^{-/-}$ ES and genes exhibiting higher levels of CpG island H3K9me2 in WT were associated with housekeeping functions such as nucleosome and cellular component assembly, amino acid biosynthesis, protein acetylation and cation transport. In sharp contrast genes associated with higher levels of CpG island H3K9me2 in Dicer$^{-/-}$ ES cells included chromatin regulators, genes regulating DNA damage and repair and cell cycle. The same was true when we examined key genes involved in ES cell self-renewal and differentiation. Pluripotency genes such as Oct4 and Nanog showed equivalent levels of H3K9me2 in WT and Dicer$^{-/-}$ ES (Fig 1.1C). In contrast, genes in the Sox2 cluster that are repressed during ES cell differentiation showed increased CpG island H3K9me2 in Dicer$^{-/-}$ ES (Fig 1.1D). To more closely assess the effects of loss of Dicer on promoter H3K9me2 enrichment levels of key developmental genes we carried out ChIP-qPCR assays on key developmental genes and found subtle differences in H3K9me2 levels between the two cell lines subject to RA induced differentiation Figures (1.1F to 1.1K).

Figure 1.1A to D

A

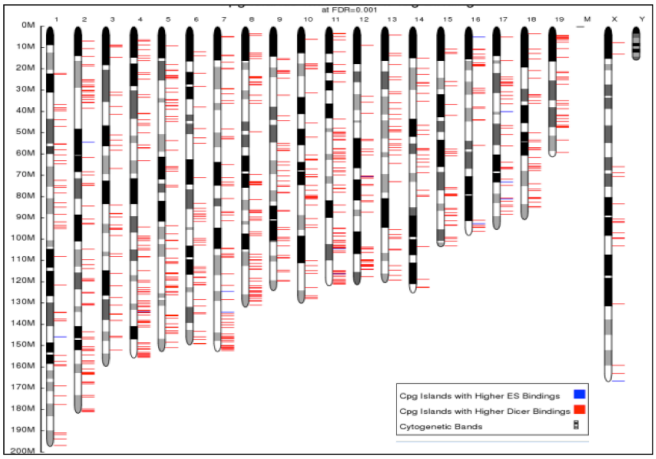

B

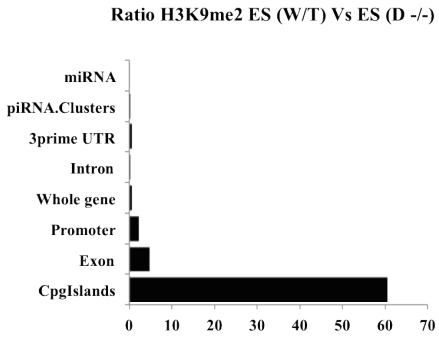

C Oct4

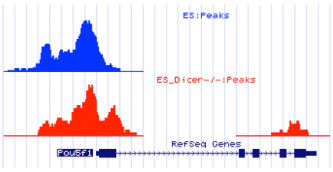

D Sox2

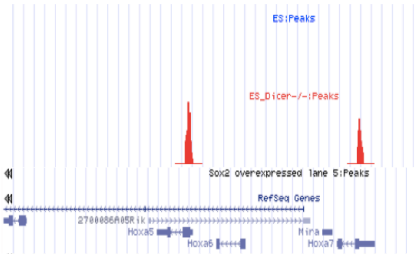

Figure 1.1E to K

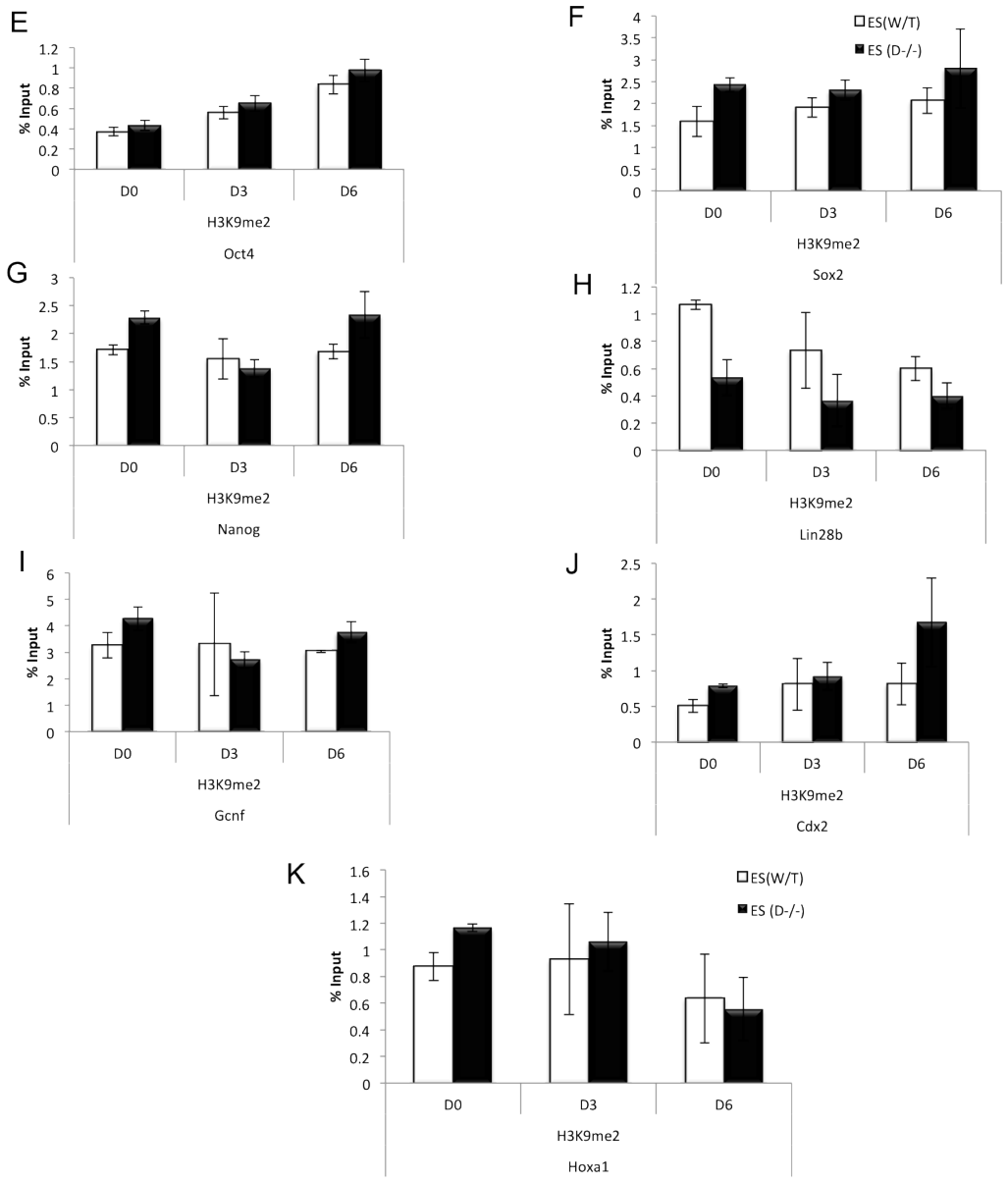

Figure 1.1 Dicer's effect on H3K9me2 distribution patterns in mES cells

A) Differential distribution of H3K9me2 in mouse chromosomes. Blue bars represent loci where higher enrichment levels were observed in mES while red bars represent loci where enrichment levels were higher in Dicer$^{-/-}$ ES cells. B) Bar graph showing ratio of H3K9me2 occupation in Dicer$^{-/-}$ ES cells compared to WT ES cells in different genomic elements. C and D) Sequence tags from H3K9me2 ChIP-seq experiment mapped to the UCSC genome browser to show enrichment at Oct4 and Sox2 gene clusters promoter regions of WT and Dicer$^{-/-}$ ES cells. Blue peaks represent WT ES cells and red peaks represent Dicer$^{-/-}$ ES cells. (E,F,G,H,I,J and K) ChIP-qPCR results showing H3K9me2 enrichment in Oct4, Sox2, Nanog, Lin28b, Gcnf, Cdx2 and Hoxa1 promoters respectively.

Table 1.3 Gene ontology terms of differentially methylated CpG island H3K9me2 sites.

Dicer Specific	ES Specific	Common ES-Dicer
Chromatin regulator DNA damage DNA repair GO:0000166~nucleotide binding GO:0000785~chromatin GO:0003676~nucleicacid binding GO:0003677~DNA binding GO:0004672~protein kinase activity GO:0004674~protein serine/threonine kinase activity GO:0005488~binding GO:0005515~protein binding GO:0005524~ATP binding GO:0005622~intracellular GO:0005634~nucleus GO:0005694~chromosome GO:0005737~cytoplasm GO:0005921~gap junction GO:0006139~nucleobase, nucleoside, nucleotide and nucleic acid metabolic process GO:0006259~DNA metabolic process GO:0006323~DNA packaging GO:0006325~establishment and/or maintenance of chromatin architecture GO:0006333~chromatin assembly or disassembly GO:0006464~protein modification process GO:0006468~protein amino acid phosphorylation GO:0006793~phosphorus metabolic process GO:0006796~phosphate metabolic process GO:0007049~cell cycle GO:0007242~intracellular signaling cascade GO:0008152~metabolic process GO:0008270~zinc ion binding GO:0009987~cellular process GO:0016310~phosphorylation GO:0016773~phosphotransferase activity, alcohol group as acceptor GO:0017076~purine nucleotide binding GO:0022403~cell cycle phase	BP00014:Amino acid biosynthesis BP00066:Protein acetylation BP00143:Cation transport BP00201:Skeletal development BP00204:Cytokinesis BP00289:Other metabolism	GO:0000786~nucleosome GO:0006334~nucleosome assembly GO:0022607~cellular component assembly GO:0022829~wide pore channel activity GO:0065003~macromolecular complex assembly MF00101:Guanyl-nucleotide exchange factor phosphoprotein GO:0048471~perinuclear region of cytoplasm MF00060:Damaged DNA-binding protein MF00178:Extracellular matrix Nucleosome core

Transcripts of H3K27me3 modifying enzyme Ezh2 are overexpressed in Dicer$^{-/-}$ ES cells whereas H3K4me3/H3K36me3/H3K9me2 modifying enzyme transcript levels are comparable in both cell lines.

To ascertain how loss of Dicer affects the transcript levels of histone modifying and DNA modifying enzymes, which contribute downstream to elevated levels of corresponding epigenetic modifications, we carried out qRT-PCR analysis on a panel of epigenetic modifier genes in WT and Dicer$^{-/-}$ ES cells. While we found no significant differences in H3K4me3, and H3K36me3 modifying Setd2 and Ash1l gene transcript levels (Figure 1.2A and 1.2C) we found slightly elevated levels of H3K9me2 modifying enzyme G9a transcripts in Dicer$^{-/-}$ ES cells (Figure 1.2B). Most notably the transcript levels of H3K27me3 modifying enzyme Ezh2 (57) was consistently overexpressed in Dicer$^{-/-}$ ES cells compared to WT cells from D0 through D6 of RA induction (Figure 1.2D).

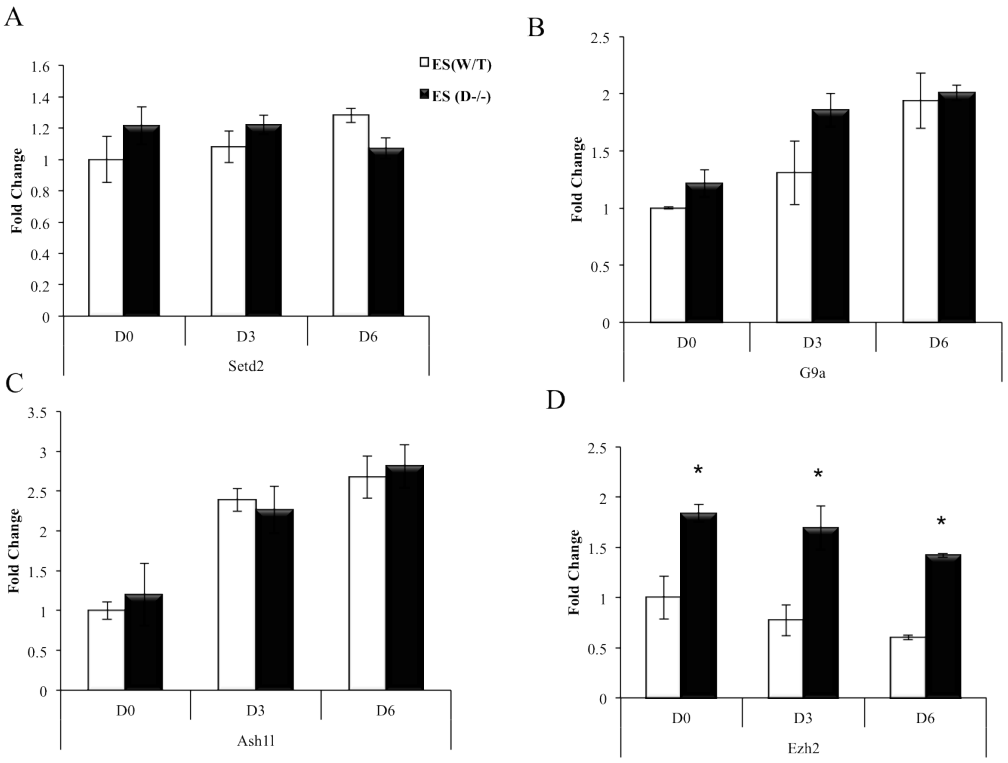

Figure 1.2 Ezh2 transcripts in Dicer$^{-/-}$ ES cells are overexpressed compared to WT ES cells, while Setd2, G9a and Ash1l levels remain relatively similar in both cell lines.

A, B C and D bar graphs showing expression levels of the histone methyl transferases Setd2, G9a, Ash1l and Ezh2 in WT and Dicer$^{-/-}$ ES cells upon RA treatment through days 0 (D0) to day 6 (D6). Note that the transcripts of enzymes Setd2 and Ash1l, which promote H3K36me3 and H3K4me3 modifications respectively show comparable results while H3K9me2 promoting G9a is slightly elevated in Dicer$^{-/-}$ ES cells and Ezh2 is significantly high in Dicer$^{-/-}$ ES cells. The symbol* indicates that the results of a given time point were significantly different between the two cell lines at a confidence level of 0.05 when a students t-test was performed.

Pluripotency genes Oct4, Sox2 and Nanog are not impacted by loss of Dicer but Ronin levels are significantly lower in Dicer$^{-/-}$ ES cells.

Dicer-deficient embryos tend to show morphological abnormalities as early as day 6.5 of development (23, 24). It has also been shown that Dicer-deficient ES cells are defective in their ability to properly differentiate (24). In order to assess the degree to which Dicer-deficient ES cells differentiate and to uncover mechanisms through which Dicer potentially regulates cellular transition we carried out ChIP-qPCR assays in the promoter regions of key genes regulating self-renewal and differentiation for transcriptionally favorable H3K4me3 versus transcriptionally unfavorable H3K27me3 marks side by side with qRT-PCR assays to determine gene expression. We particularly chose the H3K27me3 mark because Ezh2 mRNA levels were high in Dicer -/- ES cells and H3K4me3 mark as it is associated with active polymerase recruitment. Upon RA induction transcripts of pluripotency factors Oct4 Sox2 and Nanog gradually went down in both WT and Dicer$^{-/-}$ ES cells at comparable rates (Figures 1.3A-C). However transcripts of Ronin (Figure 1.3D) a pluripotency factor, known to be translationally regulated, was found to be significantly lower in Dicer$^{-/-}$ ES cells. ChIP-qPCR results in the regions of promoter regions of four pluripotency genes indicated high levels of H3K4me3 marks and low levels of H3K27me3 in both WT and Dicer$^{-/-}$ ES cells.

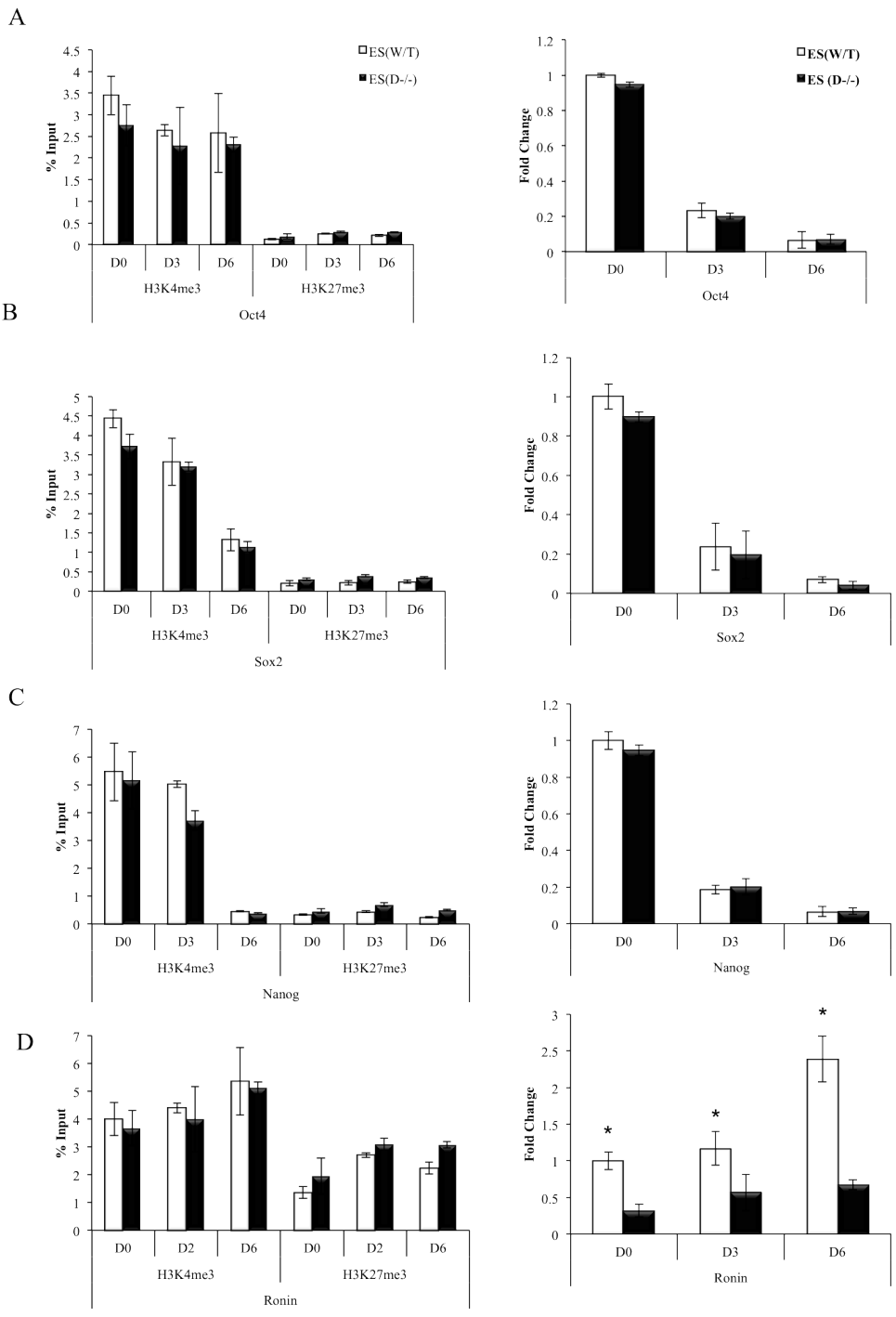
A
ES(W/T)
ES(D-/-)
% Input
D0
D3
D6
H3K4me3
H3K27me3
Oct4
ES(W/T)
ES (D-/-)
Fold Change
Oct4
B
Sox2
C
Nanog
D
D2
Ronin
*

Figure 1.3 The balance in enrichment levels between transcriptionally favorable versus transcriptionally unfavorable histone modifications affects pluripotency factor expression in mES cells.

A, B, C and D ChIP-qPCR and qRT-PCR results of relative mRNA levels in Oct4, Sox 2, Nanog and Ronin in WT and Dicer$^{-/-}$ ES cells upon RA induced differentiation through days 0 (D0) to 6 (D6). A and B transcripts of Oct4 and Sox2 go down both in mES and Dicer$^{-/-}$ ES cells upon RA treatment. Both in ES and Dicer$^{-/-}$ ES cells transcriptionally favorable H3K4me3 marks go down gradually. In both cell lines Oct4 and Sox2 H3K9me2 levels gradually go up upon RA treatment while H3K27me3 levels remain very low. C) Expression levels of Nanog go down upon RA induction while transcriptionally favorable H3K4me3 marks gradually go down. D) Transcripts of Ronin go up in WT and Dicer$^{-/-}$ ES cells, while transcriptionally favorable H3K4me3 marks go up both in WT and Dicer$^{-/-}$ ES cells. * Indicates that the difference for a given time point between the two groups were significant at 0.05 confidence levels when a students t-test was performed.

Transcriptionally favorable histone modifications in promoter regions impede the down-regulation of Lin28b and accelerate the up-regulation of Gcnf.

Lin28b and Gcnf are genes known to facilitate the transition from ES self-renewal to differentiation. Lin28b decreases and Gcnf increases upon RA-induced differentiation (47, 58, 59). We examined both changes in promoter regions and transcript levels of these genes in Dicer$^{-/-}$ ES cells treated with RA and compared this with WT. In Dicer-/- ES cells the promoter region of Lin28b exhibited high enrichment of H3K4me3 compared to ES cells while the Gcnf promoter region showed slightly elevated yet comparable levels of enrichment. At the transcript level Lin28b failed to go down at the same rate in Dicer$^{-/-}$ ES cells upon RA induction as compared to WT (Figure 1.4A). It is possible that the presence of higher levels of H3K4me3 marks at their promoter regions favoring transcription in Dicer$^{-/-}$ ES cells is in part responsible for this. Gcnf as well was observed to go up at a faster rate in Dicer$^{-/-}$ ES cells upon RA induction as compared to WT although with elevated yet comparable enrichment of transcriptionally favorable H3K4me3 at its promoter region (Figure 1.4B).

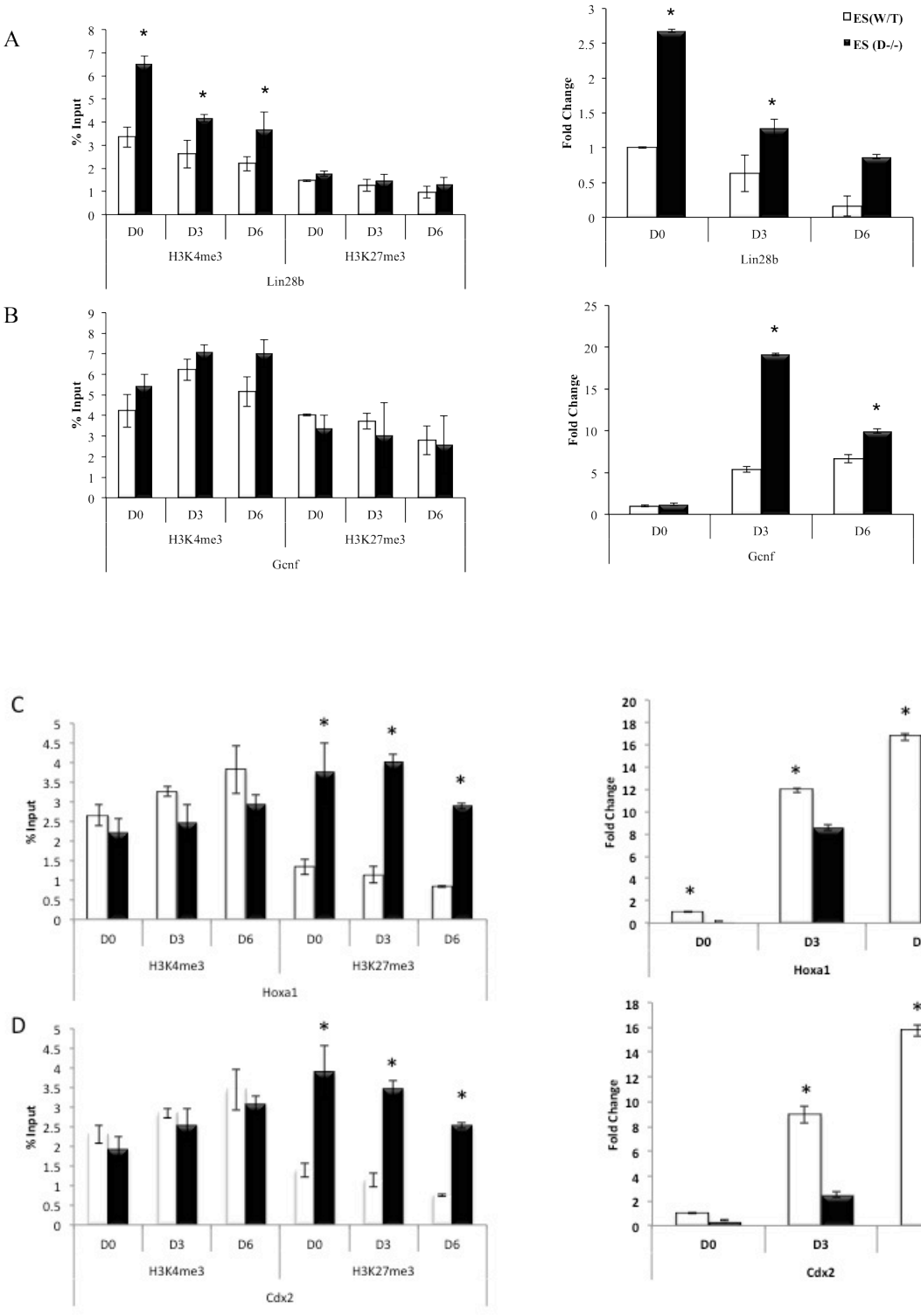
A
B
C
D
% Input
Fold Change
ES(W/T)
ES (D-/-)
D0
D3
D6
H3K4me3
H3K27me3
Lin28b
Gcnf
Hoxa1
Cdx2

Figure 1.4 Transcriptionally favorable histone modifications in promoter regions promote expression levels of Lin28b and GCNF in Dicer$^{-/-}$ES cells relative to WT ES cells, while transcriptionally unfavorable histone modifications disfavor Hoxa1 and Cdx2 expression in Dicer$^{-/-}$ES cells relative to WT.

A B C and D, ChIP- qPCR results on promoter regions and qRT-PCR results of Lin28b, Gcnf, Hoxa1 and Cdx2 respectively upon RA induction from day 0 (D0) through day 6 (D6). Note higher enrichment levels of H3K4me3 in the promoter regions of Lin28b and Gcnf, which affect increased expression levels in Dicer$^{-/-}$ ES cells in A and B. As shown in C and D higher enrichment of H3K27me3 in Hox a1 and Cdx2 down regulates the expression levels of corresponding genes in Dicer$^{-/-}$ ES cells compared to WT ES cells. The symbol * indicates that the difference for a given time point between the two groups were significant at 0.05 confidence levels when a students t-test was performed.

Transcriptionally unfavorable histone modifications impede the up-regulation of Hoxa1 and Cdx2 during RA-induced differentiation in Dicer$^{-/-}$ ES cells.

In order to examine the impact of Dicer-dependent histone modifications on genes promoting ES cell differentiation we carried out ChIP-qPCR and qRT-PCR analysis on Cdx2 and Hoxa1. Here we noted an entirely different outcome to the other genes. Dicer$^{-/-}$ ES cells retained the ability to induce transcripts upon RA-treatment but failed to do so at the same rate as WT cells (Figures 1.4C and 1.4D). In addition the promoter regions of Cdx2 and Hoxa1 had significantly higher levels of H3K27me3 levels in promoter regions in Dicer$^{-/-}$ ES cells compared to WT cells, which likely explains the attenuated up-regulation of these genes upon RA-induction of Dicer$^{-/-}$ ES cells. Comparable and high H3K4me3 marks were found in both cell lines.

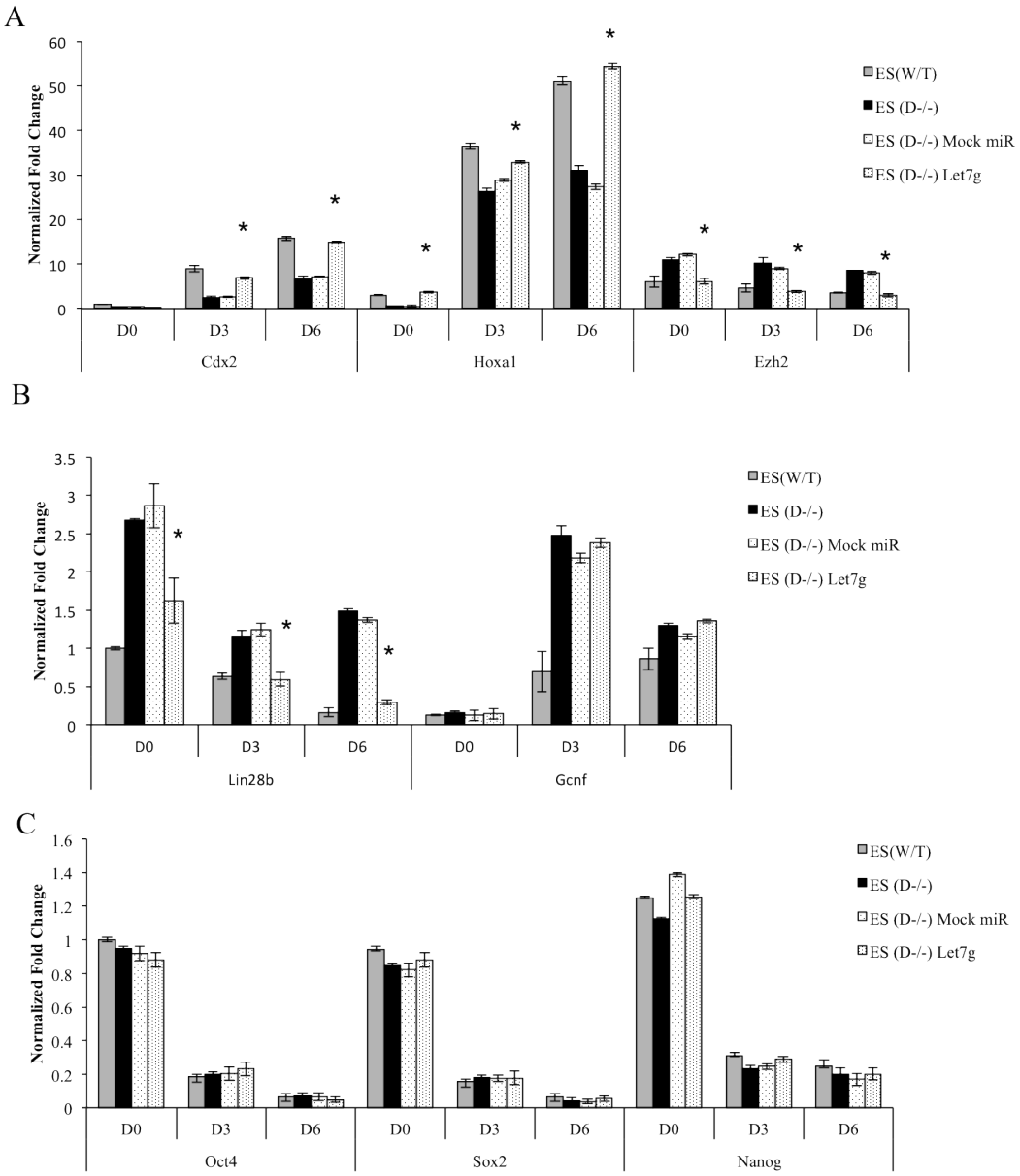
A
Normalized Fold Change
60
50
40
30
20
10
0
ES(W/T)
ES (D-/-)
ES (D-/-) Mock miR
ES (D-/-) Let7g
D0
D3
D6
Cdx2
Hoxa1
Ezh2
B
Normalized Fold Change
3.5
3
2.5
2
1.5
1
0.5
0
Lin28b
Gcnf
C
Normalized Fold Change
1.6
1.4
1.2
1
0.8
0.6
0.4
0.2
0
Oct4
Sox2
Nanog

Figure 1.5 Transfecting Dicer$^{-/-}$ES cells with let-7g miRNA rescues Hoxa1 and Cdx2 transcript levels.

A) Hoxa1 and Cdx2 transcript levels increase upon transfecting Dicer$^{-/-}$ES cells with miRNA let-7g while Ezh2 transcript levels go down. B) Lin28b transcripts are significantly reduced in Dicer$^{-/-}$ES cells cells upon transfecting with miRNA let-7g. C) Pluripotency factors Oct4, Sox2 and Nanog remain relatively unchanged upon transfecting Dicer$^{-/-}$ES cells with let-7g. * indicates that the difference for a given time point between Dicer$^{-/-}$ES cells and Dicer$^{-/-}$ES cells with let-7g were significant at 0.05 confidence levels when a students t-test was performed.

Reduced transcript levels of Hoxa1 and Cdx2 in Dicer$^{-/-}$ ES cells can be rescued by overexpressing let-7g miRNA or siRNAs targeting Ezh2.

Based on 1) the failure of Hoxa1 and Cdx2 to be fully transcriptionally induced upon RA induction in Dicer$^{-/-}$ ES cells, 2) increased enrichment of H3K27me3 in the promoter regions of Hoxa1 and Cdx2 in Dicer$^{-/-}$ ES cells, and 3) significant increase in transcript levels of Ezh2 that has been established to regulate H3K27me3 in WT cells we hypothesized that a key developmentally regulated miRNA lacking in Dicer$^{-/-}$ ES cells due to miRNA biogenesis defects may play a mechanistic role in facilitating higher levels of Ezh2 transcripts and hence higher enrichment of H3K27me3 marks in Hoxa1 and Cdx2 in promoter regions. Moreover Lin28b, which is known to play a critical role in facilitating cell fate through a double negative feed back loop between let-7g and itself (59), was found to be substantially increased in Dicer$^{-/-}$ ES cells and mmu-let-7g is predicted to target Ezh2. From these observations we hypothesized that the loss of let-7g in Dicer$^{-/-}$ ES cells led to the increase in its predicted target Ezh2, which in turn led to increased H3K27me3 at the Hoxa1 and Cdx2 promoter regions. It is possible that failure to fully induce genes that are critical for embryonic differentiation such as Hoxa1 and Cdx2 are a result of the failure to down-regulate epigenetic modifiers such as Ezh2 which potentially play an important role in the embryonic lethality of the Dicer$^{-/-}$ embryos.

To functionally validate our hypothesis we overexpressed mature let-7g in WT and Dicer$^{-/-}$ ES cells and assayed the expression levels of developmentally significant genes, those in particular, which are critical in determining cell fate. Upon over-expression of mature let-7g, both Lin28b and Ezh2 transcript levels were down-regulated in Dicer$^{-/-}$ ES cells (Figure 1.5A and 1.5B), while Cdx2 and Hoxa1 transcript levels were increased in Dicer$^{-/-}$ ES cells compared to WT cells (Figure 1.5A). In sharp contrast, overexpression of let-7g has very little effect on pluripotency genes (Figure 1.5C). In order to assess the effect of Ezh2 exclusively on the expression levels of genes in the absence of concomitant down-regulation of Lin28 with Ezh2 we carried out a rescue

experiment using siRNAs targeting Ezh2. We found that siRNAs to Ezh2 was sufficient to increase levels of Cdx2 and Hoxa1 transcripts in Dicer$^{-/-}$ ES cells (Figure 1.6A). Reciprocally, to test whether introducing miRNA let7g and siRNA specifically targeting Ezh2 reduces H3K27me3 enrichment at Hoxa1 and Cdx2 loci in Dicer$^{-/-}$ ES cells we carried out treatments with let7g and siEzh2 along with respective controls and chromatin immunoprecipitated genomic DNA from the cell lines using an H3K27me3 specific antibody. Upon assaying for enrichment of H3K27me3 at Hoxa1 and Cdx2 loci we noticed significant reductions in Dicer$^{-/-}$ ES cells treated with the mentioned interfering RNA candidates compared to mock and control treated samples (Figure 1.7).

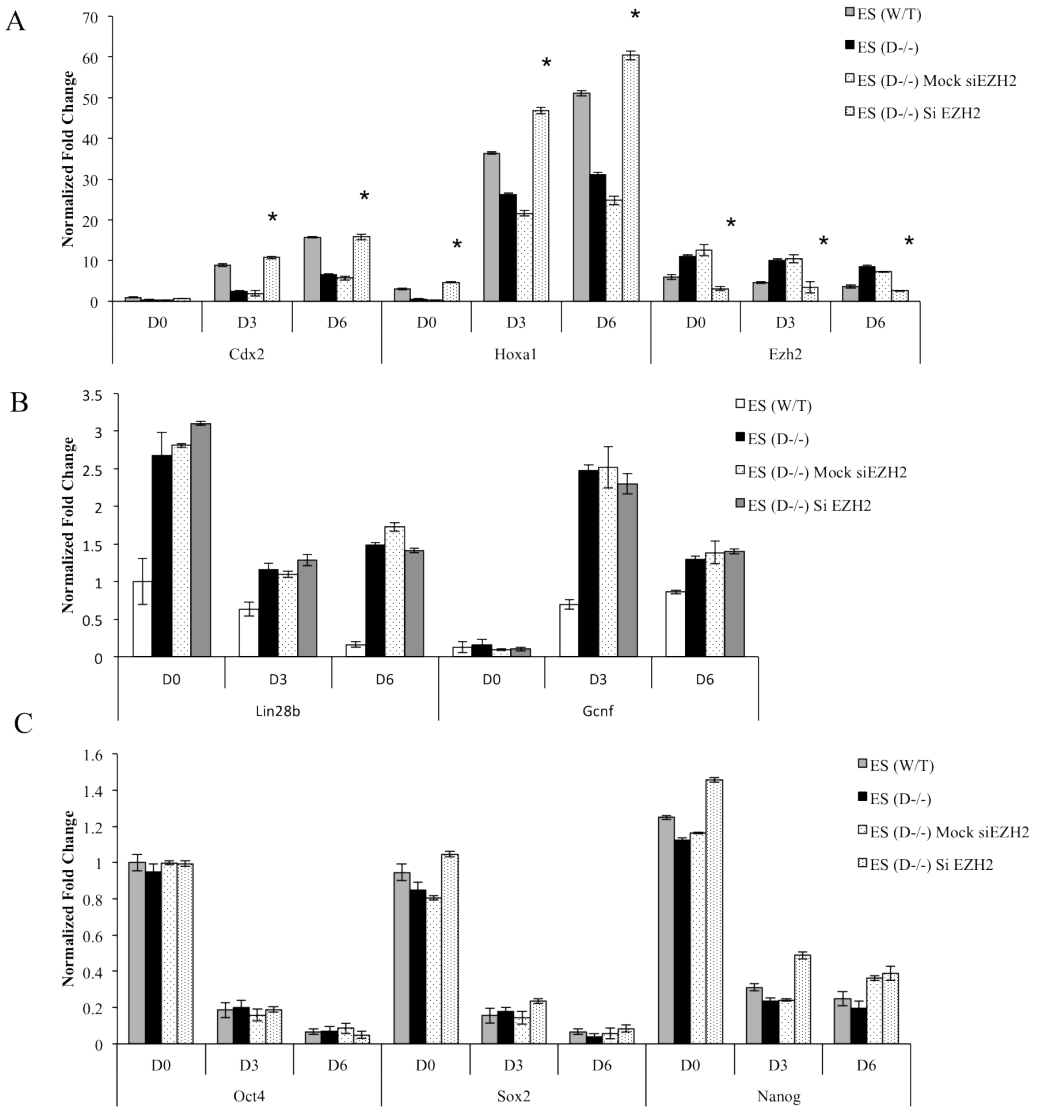
A
Normalized Fold Change
70
60
50
40
30
20
10
0
ES (W/T)
ES (D-/-)
ES (D-/-) Mock siEZH2
ES (D-/-) Si EZH2
D0
D3
D6
Cdx2
Hoxa1
Ezh2
B
Normalized Fold Change
3.5
3
2.5
2
1.5
1
0.5
0
ES (W/T)
ES (D-/-)
ES (D-/-) Mock siEZH2
ES (D-/-) Si EZH2
D0
D3
D6
Lin28b
Gcnf
C
Normalized Fold Change
1.6
1.4
1.2
1
0.8
0.6
0.4
0.2
0
ES (W/T)
ES (D-/-)
ES (D-/-) Mock siEZH2
ES (D-/-) Si EZH2
D0
D3
D6
Oct4
Sox2
Nanog

Figure 1.6 Transfecting Dicer$^{-/-}$ES cells with siRNAs specifically targeting Ezh2 rescues Hoxa1 and Cdx2 transcript levels.

A) Ezh2 transcript levels reduce while Hoxa1 and Cdx2 transcript levels increase upon transfecting Dicer$^{-/-}$ ES cells with siRNA specific to Ezh2. B) Lin28b transcripts remain significantly unchanged upon transfecting Dicer$^{-/-}$ES cells with siRNA specifically targeting Ezh2. C) Pluripotency factors Oct4, Sox2 and Nanog remain relatively unchanged upon transfecting Dicer$^{-/-}$ ES cells with siRNA targeting Ezh2. * indicates that the difference for a given time point between Dicer$^{-/-}$ES cells and Dicer$^{-/-}$ES cells with siEzh2 were significant at 0.05 confidence levels when a students t-test was performed.

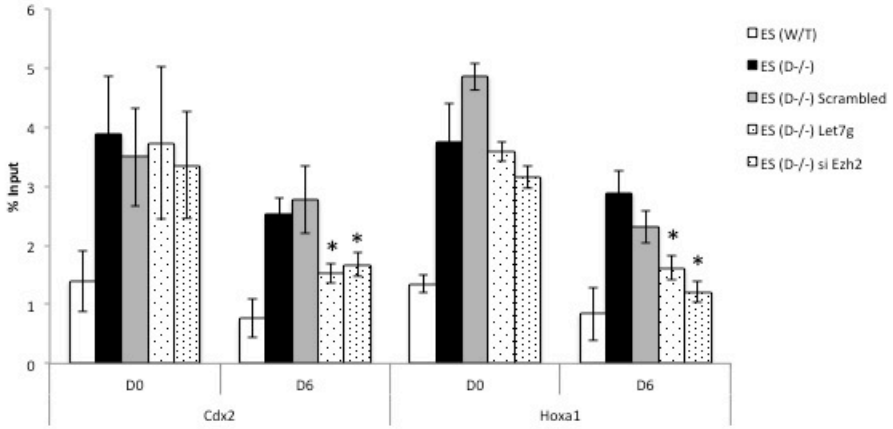

Figure 1.7 Transfecting Dicer$^{-/-}$ ES cells with let7g miRNA and siRNA targeting Ezh2 reduces H3K27me3 at Hoxa1 and Cdx2 during retinoic acid induced differentiation.

Cells were treated with let7g miRNA and siRNA targeting Ezh2 along with a scrambled negative control as described in the methods section and chromatin immunoprecipitated using an H3K27me3 specific antibody. Thereafter enrichment of H3K27me3 at Hoxa1 and Cdx2 loci were assayed by quantitative real time PCR.

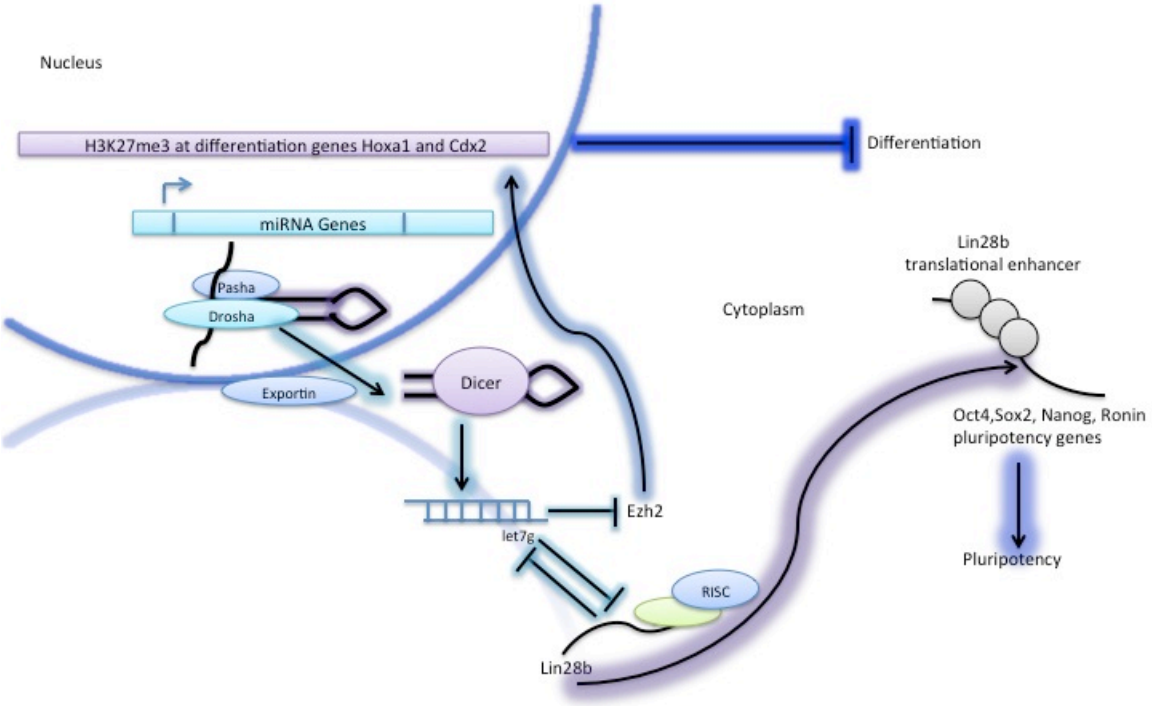
Nucleus
H3K27me3 at differentiation genes Hoxa1 and Cdx2
Differentiation
miRNA Genes
Pasha
Drosha
Exportin
Dicer
Cytoplasm
Lin28b
translational enhancer
Oct4,Sox2, Nanog, Ronin
pluripotency genes
Pluripotency
Ezh2
let7g
RISC
Lin28b

Figure 1.8 Putative model explaining Dicer mediated regulation of mouse ES cell differentiation.

When ES cells are induced to differentiate by RA treatment let7g levels increase. Hence Let7g suppresses Ezh2 resulting in reduced H3K27me3 favoring transcription of Hoxa1 and Cdx2 differentiation genes. As let7g increases during differentiation Lin28b levels are reduced as a result translational enhancement of pluripotency factors by Lin28b is reduced, this event in turn favors differentiation.

DISCUSSION

The role of Dicer, in post-transcriptional regulation of embryonic stem cell genes is well established. Sinkkonen *et al*., (49) have shown that regulating DNA methylation in ES cells require the miR-290-295 cluster. Members of this cluster ensure the availability of DNA methyltransferases 3A and 3B in ES cells by downregulating Rbl a known repressor of the enzymes. This in turn facilitates appropriate DNA methylation at developmentally critical genes(49). Here we report that Dicer-dependent differences in histone methyl modifications can affect transcription of genes by functioning as an additional layer of epigenetic regulation in conjunction with DNA methylation. To examine the role of Dicer in regulating histone modifications that are critical to self-renewal and differentiation of embryonic stem cells we examined genome-wide changes in H3K9me2 in the presence and absence of Dicer and local changes in H3K27me3 and H3K4me3 in the promoters of key regulators of self-renewal and pluripotency (Oct4, Nanog, Sox2 and Ronin), differentiation (Cdx2 and Hoxa1) and genes promoting the transition between these states (Lin28b and Gcnf). The critical role, which Dicer plays in mammalian embryogenesis, is highlighted by the fact that mouse embryos lacking Dicer do not successfully progress beyond day 6.5 in development (23, 24). Using the ability to maintain Dicer-deficient ES cells in long-term culture and RA-mediated differentiation cues to our advantage we specifically show that loss of Dicer can lead to changes in the landscape of the embryonic stem cell epigenome by impacting histone modifications in genes critical for embryonic stem cell differentiation. Loss of Dicer in particular led to a global increase in H3K9me2 modifications at over 900 CpG islands. Using a publicly available microarray data set from the GEO database we found that in spite of increased H3K9me2 at their promoter regions some of the associated genes showed relatively higher level of transcripts in Dicer$^{-/-}$ ES cells compared to WT (data not shown). We confirmed this observation by performing qRT-PCR experiments on a panel of key developmentally critical genes.

In order to examine how H3K9me2 modifications work with other histone modifications at the promoters of genes critical for stem cell function we also integrated data for H3K4me3 and H3K27me3 modifications.

Upon carefully evaluating genes regulating different aspects of ES cell functions (pluripotency, differentiation and transition points between the two states) we uncovered a higher level of complexity where the presence and comparative abundance levels of transcriptionally favorable (H3K4me3) marks versus transcriptionally unfavorable (H3K27me3) marks affect mRNA expression levels. An increase in H3K9me2/H3K27me3 in the promoters of differentiation genes Hoxa1 and Cdx2 in Dicer$^{-/-}$ES cells was coincident with an inability to up-regulate these genes at the same rate as ES upon Retinoic acid (RA)-induced differentiation. siRNAs and microRNA let-7g rescued this effect by down-regulating Ezh2 suggesting that Ezh2 up-regulation is in part responsible for increased H3K27me3 and decreased rates of up-regulation of differentiation genes in Dicer$^{-/-}$ES. Pluripotency genes Oct4, Sox2 and Nanog showed no changes in H3K9me2/H3K4/me3/H3K27me3 coincident with no changes in rates of RA-induced down-regulation between Dicer$^{-/-}$ES and ES. Gcnf, which is induced upon RA-induction, has been shown to be responsible for repression of Oct4 and Nanog (58, 60, 61) and Lin28b mediated repression of let-7, has been shown to block ES cells from differentiating (59). Promoters of genes regulating the transition from self-renewal to differentiation (Lin28b and Gcnf) were associated with increased H3K4me3 coincident with down-regulation of Lin28b at a lower rate and up-regulation of Gcnf at a higher rate upon RA-induction in Dicer$^{-/-}$ES.

It is possible that H3K27me3 patterns in the promoter regions of the aberrantly expressed differentiation genes Cdx2 and Hoxa1 genes, contribute as potential causative factors, which render Dicer$^{-/-}$ embryos incompetent to differentiate to their full potential. As it is explained in the

putative model, which we present in Figure 1.8, it is plausible that increased H3K27me3 at Hoxa1 and Cdx2 loci render Dicer deficient ES cells unable to differentiate under retinoic acid induced conditions. In contrast to Dicer$^{-/-}$ ES cells wild type ES cells show reduced H3K27me3 enrichment at these loci affording expression as Ezh2 is repressed by the presence of miRNA let7g, which increases upon RA, induced differentiation. Moreover unlike in Dicer$^{-/-}$ ES cells in wild type ES cells, increasing let7g levels upon RA induction reduce Lin28b, which is a translational enhancer of pluripotency factors, and thereby facilitate differentiation. Surprisingly, in spite of the fact that Ezh2 transcript levels were significantly increased in the Dicer$^{-/-}$ ES cells we did not see a global impact on increased H3K27me3 at all promoter regions within the gamut of the developmentally critical genes we scanned but indeed specific effects on two of the key differentiation genes Hoxa1 and Cdx2 were strikingly noticeable. It has been shown in Drosophila that accessory proteins direct enzymes to specific locations bound to be heterochromatin (62), however at this point it remains unclear as to how an elevated enzyme catalyzing a particular histone modification preferentially chooses its target loci in mammalian cells.

Understanding the interactions between transcription factors miRNAs and the epigenetic landscape is a fundamental requirement to develop strategies aimed at cellular reprogramming. From the perspective of reprogramming cells for therapeutic purposes introducing miRNAs such as let-7g, is investigated as a potential candidate to target various cancers. Our observations suggest that a single miRNA (let-7g) alone can significantly alter the phenotype of a cell by means of transcriptional, epigenetic, as well as post-transcriptional changes. Taken together our findings point to the numerous roles that Dicer mediated events play at different levels of regulation in a cellular context. Our findings emphasize the significance of Dicer in regulating stem cell phenotype via epigenetic and transcriptional regulation. But most importantly we note

that evidence emerging from this study highlights Dicer mediated pathways involving miRNAs, PcGs and epigenetic marks, which could be potentially manipulated to direct cellular fate in engineering cells for therapeutic applications in future.

CHAPTER 2:

Androgens Regulate Prostate Cancer Cell Growth via an AMPK-PGC-1α-Mediated Metabolic Switch

ABSTRACT

Prostate cancer is the most commonly diagnosed malignancy among men in industrialized countries, accounting for the second leading cause of cancer-related deaths. While we now know that the androgen receptor (AR) is important for progression to the deadly advanced stages of the disease, it is poorly understood what AR-regulated processes drive this pathology. Here, we demonstrate that AR regulates prostate cancer cell growth via the metabolic sensor 5'-AMP-activated protein kinase (AMPK), a kinase that classically regulates cellular energy homeostasis. Using a combination of radiolabeled assays and emerging metabolomic approaches, we show that prostate cancer cells respond to androgen treatment by increasing not only rates of glycolysis as is commonly seen in many cancers, but also glucose and fatty acid oxidation. Importantly, this effect was dependent on androgen-mediated AMPK activity. Our results further indicate that the AMPK-mediated metabolic changes increased intracellular ATP levels and peroxisome proliferator-activated receptor gamma coactivator 1-alpha (PGC-1α)-mediated mitochondrial biogenesis, affording distinct growth advantages to the prostate cancer cells. Correspondingly, we used outlier analysis to determine that PGC-1α is overexpressed in a subpopulation of clinical samples. Taken together, our findings converge to demonstrate that androgens co-opt the AMPK-PGC-1α signaling cascade, a known homeostatic mechanism, to increase prostate cancer cell

growth. The current study points to the potential utility of developing metabolic-targeted drug therapies directed towards the AMPK-PGC-1α signaling axis for the treatment of prostate cancer.

MATERIALS AND METHODS

Extracellular acidification rate (ECAR) and oxygen consumption rate (OCR) measurements:

ECAR, reflective of the rate of glycolysis, and OCR, reflective of the rate of OXPHOS, were measured using a Seahorse Bioscience XF24 analyzer. Cells were plated at 30,000 cells/well in Seahorse XF24 plates coated with BD Cell-Tak (BD Biosciences) and incubated for 48 hours. For R1881 dose response experiments, the cells were then treated for 72 hours. For knockdown experiments, cells were transfected with indicated siRNAs overnight prior to treatment. For ECAR and OCR measurements in the presence of inhibitors (oligomycin-1.3 mM; Carbonyl cyanide 4-(trifluoromethoxy)phenylhydrazone (FCCP)-1 mM; rotenone-1 mM; antimycin A-1 mM), the samples were treated with R1881 and then incubated for 72 hours. During the initial/basal phase of assaying no inhibitors were present. Thereafter at respective time points inhibitor-containing media were sequentially injected to the assay wells through automated instrument ports. Data were normalized to cell numbers using the DNA content assay described herein.

Metabolic profiling:

Measurements of intracellular acetylcarnitine levels, which are reflective of acetyl-CoA levels, and organic acid/TCA cycle intermediates were performed using tandem mass spectrometry (MS/MS) or gas chromatography/mass spectrometry (GC/MS) as previously described (63).

Quantitation of mitochondrial volume using fluorescence microscopy:

Cells were seeded on poly-L-lysine (0.01% in PBS, sterile-filtered)-coated coverslips, transfected with respective siRNAs as described in the methods and materials section and treated with R881 after overnight incubation. To visualize mitochondria, cells were cultured at 37°C with 200 nM MitoTracker Deep Red (Life Technologies) for 30 minutes, then washed with PBS and fixed with 4% *paraformaldehyde,* stained with 200 nM DAPI as a counter stain and mounted in ProLong Gold Antifade Reagent (Life Technologies). Cells were visualized using an Olympus FV-1000 confocal microscope under a ×60 oil immersion objective lens. To obtain a volumetric measurement, the Z-axis was acquired in 15-20 planes with 0.5 μm steps. Collected images were analyzed by 3D software Amira 5.2.1 for mitochondria volumetric measurement (Visage Imaging). Whole cytoplasmic mitochondrial volumes were calculated and normalized to the number of cells/image as determined by DAPI staining.

Statistical analysis:

Two-sample comparisons were performed using Student's *t*-tests. Multiple comparisons were performed using a one-way ANOVA and *post-hoc* Dunnett's test with GraphPad Prism, Version 4 (GraphPad Software). Significant changes were determined at the $P < 0.05$ level.

Cell culture

LNCaP and VCaP human prostate carcinoma cell lines and PWR-1E and RWPE-1 immortalized nontumorigenic cell lines were all purchased from ATCC and maintained and validated for androgen responsiveness as previously described (32). Prior to all experiments, cells were plated and incubated for 72 hours in charcoal-stripped FBS to minimize endogenous hormone signaling.

siRNA transfection of human prostate cells

Stealth siRNA (Life Technologies) transfections were carried out as previously described (32). The sequences of all siRNAs used in this study are listed in Table 2.1. 50ul of 100uM stocks of siRNA and were mixed with 950ul of Optimem medium, vortexed and allowed to incubate at room temperature for five minutes. Similarly 20ul of Dharmafect reagent was mixed with 980ul of Optimem medium, vortexed and allowed to incubate at room temperature for five minutes. The two stocks were then combined, vortexed and allowed to stand for further twenty minutes at room temperature and introduced in appropriate quantities to wells in culture plates to yield desired concentrations of specific assays.

Western blot analysis

Western blots were conducted using whole cell lysates as previously described (64). Densitometry was performed using ImageJ software (NIH) and normalized to the indicated controls. Cells were seeded at a density of 500000 cells per well on the six well formats for 72-hour incubation based assays. On the day of harvesting the media were siphoned and while keeping the plates on ice the cells treated with 200ul of Phospho RIPA buffer with 50mM NaF, 2mM Na_3VO_4 and 1X protease inhibitor. The lysates were then transferred to pre-chilled 1.5ml eppendorf tubes and rotated at 4^{o}C for 30 minutes. The lysates were then centrifuged at 14000 rpm @ 4 ^{o}C for 15 minutes and the supernatant was transferred to new pre-chilled tubes. The lysates were then stored at -80 ^{o}C or immediately utilized for blotting applications. For each well on SDS PAGE gels 20ug of total protein sample were loaded and run at 90volts up to the stacking gel and at 110 volts further at room temperature. The proteins were transferred to nitrocellulose membranes at 4 ^{o}C and 30 mA overnight in blotting chambers. The blots were then blocked in 5% milk in TBST buffer for 1 hour. The block solution was then poured off and allowed to incubate in primary antibodies diluted in blocking solution at a rate of 1:1000 and allowed to incubate for 72 hours at 4 ^{o}C. Thereafter the primary antibody was removed and the blots were washed thrice in TBST buffer for 15 minutes in each instance. The secondary antibody diluted at the rate of 1:5000 in blocking solution was then introduced to the blots and allowed to incubate at room temperature for one hour. Finally, following three more washes with TBST buffer the blots were quantified using a Perkin Elmer ECL reagent kit according to manufacturer's protocols.

Cell proliferation assay

Cell proliferation assays were carried out as previously described (65) by measuring the cellular DNA content using a FluoReporter Blue fluorometric double-stranded DNA Quantitation Kit (Life Technologies) following the manufacturer's protocol. LNCaP cells were seeded at a density of 10000 cells per well and VCaP cells were seeded at a density of 5000 cells per well in charcoal stripped 8% FBS and phenol red free RPMI and DMEM media respectively on CellBIND (Corning) plates. The media were supplemented with 1% non-essential amino acids and sodium pyruvate. On the third day following incubation at 5% CO2 and 37 ^{o}C, siRNA was introduced by removing 20 ul of media and then adding 20ul of siRNA in fresh media to yield a final concentration of 100 nM in each well. The cells were then allowed to incubate for further 24 hours. Thereafter 50 ul of existing media were removed and topped up with 50ul of R1881 in fresh media to yield a final concentration of 10nM per well, the cells were then allowed to incubate for an additional day. After that, an extended treatment of siRNA was done by removing 20ul of existing media and introducing 20ul of siRNA in fresh medium to yield a final concentration of 100nM in each well. After one more day of incubation, R1881 was introduced to maintain a final concentration of 10nM as in the previous instance. Following two more days of incubation the media were removed from the wells by inverting the plates. Subsequently the plates were stored at -80 ^{o}C for a further day. Then the cells were thawed to room temperature and 100ul of water was introduced to each well and refrozen. Finally the cells were thawed to room temperature and 100ul of FluoReporter dye diluted at a consistency of 25ul of dye in 10ml of TNE buffer were introduced to each well and assayed using a PerkinElmer-2030 Victor X4 microplate reader.

Radiolabelled CO_2 trap assays

Cells were plated in 24-well CellBIND (Corning) plates at a density of 60,000 cells per well in phenol red-free steroid-starved medium. All assays were carried out 72 hours post-treatment. For siRNA experiments, cells were transfected overnight prior to treatment. For glucose oxidation assays, cells were preincubated with 3 mM glucose for one hour. Thereafter, the cells were further incubated with 0.5 ml of 3 mM or 12 mM ^{14}C U-glucose for 2 hours. $^{14}CO_2$ was trapped using modified traps as previously described (66, 67). 100 μl of perchloric acid (PCA) was added to each well and the evolved $^{14}CO_2$ was absorbed in adjacent wells with hyamine hydroxide-soaked Whatman filter paper. Trapping devices were rotated on a shaker platform at 125 rpm for two hours. Finally, scintillation counting was done on a PerkinElmer Tri-Carb Counter. Data were normalized to cell numbers using the DNA content assay described above. For fatty acid oxidation assays, palmitate or oleate complexed with bovine serum albumin (BSA) were diluted in culture media to constitute final concentrations of 500 μM fatty acid and 0.5% BSA at 0.1 μCi/ml labeled ^{14}C. The complexed BSA-radiolabelled fatty acid was diluted in culture media to achieve the final working concentrations. Carnitine and HEPES were then incorporated into the ^{14}C-labeled fatty acid culture media mix to yield 1 mM and 12.5 mM final concentrations, respectively. 500 μl of labeled media was transferred to each assay well. CO_2 trapping devices were assembled as previously described (66, 67). Thereafter, 50 μl of PCA was added to each well and $^{14}CO_2$ was measured and normalized as described above.

ATP assay

Intracellular levels of ATP were assayed using an ATP Bioluminescence Assay Kit CLSII (Roche) according to the manufacturer's instructions and normalized to cell numbers using the

DNA content assay described above. Measurements were carried out on a PerkinElmer-2030 Victor X4 microplate reader.

RNA isolation, cDNA preparation, and quantitative reverse transcription (RT)-PCR (qPCR)

RNA isolation, cDNA preparation, and qPCR were carried out as previously described using 36B4 as a control (32). All primers used in this study are listed in Table 2.1. Cells were seeded at desired densities contingent to specific assays and lysed in buffer supplied by the manufacturer in Biorad RNA gold isolation kits. An on column DNAse treatment was carried out in each instance to ensure extracting RNA free of genomic DNA contamination. For quality assurance purposes all RNA samples were quantified using a Nanodrop instrument. Based on 230, 260 and 280 nm spectral readings it was ascertained that RNA samples were free of protein, carbohydrate and DNA contaminants. A maximum quantity of 2ug of RNA was loaded to each 20ul cDNA synthesis reaction carried out using a BioRad iScript cDNA suntheis kit. Thermocycling were carried out on a Biorad thermocycler according to manufacturer's recommendations. The resultant cDNA were diluted at a rate of 1:10 using ultrapure DNAse free water and utilized for quantitative real time PCR reactions based on standard SYBR green based methods on an Applied Biosystems Fast 96 well qPCR instrument.

Transmission electron microscopy (TEM)

For TEM, cells were plated in 6-well plates at 500,000 cells/well and treated as described above. Cells were then washed twice in serum-free media and fixed for 3-5 minutes at room temperature

with 4% glutaraldehyde in 0.1 M cacodylate buffer pH 7.0. Cells were gently scraped and centrifuged at 5,000 x g for 3 minutes in a swinging bucket rotor followed by additional fixing for 1 hour. Pellets were then embedded and sectioned at the Duke University Department of Pathology's Electron Microscopy Core (Durham, NC). Grids were viewed using a Philips/FEI CM 12 Transmission EM with AMT 2k x 2k digital camera. Mitochondria (> 30/group) were counted blindly from randomly selected sections.

Table 2.1 List of Primers and siRNA sequences

Primer/siRNA	Sequence
qPCR primers	
36B4	Forward: 5'-GGACATGTTGCTGGCCAATAA-3'
36B4	Reverse: 5'-GGGCCCGAGACCAGTGTT-3'
PGC-1α	Forward: 5-AGTACAACAATGAGCCTTCAA-3'
PGC-1α	Reverse: 5-CATCAAATGAGGGCAATC-3'
siRNA sequences	
AMPKα1 #1	5'-CCCAUCCUGAAAGAGUACCAUUCUU-3'
AMPKα1 #2	5'-CCCUCAAUAUUUAAAUCCUUCUGUG-3'
AMPKα1 #3	5'-ACCAUGAUUGAUGAUGAAGCCUUAA-3'
PGC-1α #1	5'-GGGCAGAUUUGUUCUUCCACAGAUU-3'
PGC-1α #2	5'-CCCAUUUGAGAACAAGACUAUUGAA-3'
PGC-1α #3	5 -AGUAAGAGCUUCUUAAGUAGAGACG-3'

INTRODUCTION

Since the 1920's, it has been known that cancer cells possess the unique ability to alter their metabolism and, as such, are distinguishable from benign cells (68). However, it was only in the past decade that the reprogramming of energy metabolism has been acknowledged as one of the true emerging hallmarks of cancer (69). Interestingly, while the majority of metabolic cancer research focuses on the role of glycolysis, it has recently become apparent that the tricarboxylic acid (TCA) cycle and oxidative phosphorylation (OXPHOS) also play major roles in many types of cancers including prostate cancer (70-73). Both the genetic deletion or pharmacological inhibition of key steps in the TCA cycle and/or OXPHOS can block cancer cell growth *in vitro* and disease progression *in vivo* (74-77). Further, metabolic signatures of the TCA cycle and OXPHOS correlate with cancer progression and unfavorable outcomes (76, 78-84). Also, 2-^{18}F-fluoropropionic acid and ^{11}C-acetate, new tracers being used for positron emission tomography (PET) imaging, are more sensitive detectors of prostate cancer than the glycolysis marker ^{18}F-fluorodeoxyglucose (85-88). These data indicate that prostate cancers can exhibit unique metabolic profiles. What is not understood is specifically how androgen receptor (AR)-signaling, elevated in 100% of metastatic prostate cancers (89), impacts cellular metabolism and what role this plays in disease progression.

Prostate cancers express the AR and rely on androgens for growth and survival (29). Consequently, androgen ablation therapies are the standard of care for late-stage disease. While patients with advanced prostate cancer initially respond favorably to androgen ablation therapy, most experience a relapse of the disease within 1-2 years. Following this hormone-refractory relapse, patients have limited treatment options. Although the hormone-refractory disease is unresponsive to androgen-deprivation, AR-regulated signaling pathways remain active and are

necessary for cancer progression (29). Thus, both AR itself and the processes downstream of the receptor remain viable targets for therapeutic intervention.

The master metabolic regulator AMP-activated protein kinase (AMPK) governs overall cellular homeostasis by modulating the use of sugars, fats and/or proteins as sources of cellular fuel. Recent work from our laboratory has demonstrated that androgens increase cellular migration and invasion through the direct upregulation of Ca^{2+}/calmodulin-dependent protein kinase kinase b (CaMKKβ) and subsequent phosphorylation/activation of AMPK (32). Later, two more independent groups confirmed our CaMKKβ findings *in vitro* and in multiple clinical cohorts and suggested CaMKKβ also promotes glycolytic flux (90, 91). Correspondingly, Park *et al.,* demonstrated that levels of the serine-79 phosphorylated form of acetyl-CoA carboxylase (ACC), a direct target of AMPK, are increased in clinical prostate cancer samples (92). Because of the importance of androgen signaling in prostate cancer and the increasing evidence from other laboratories as well as our own that suggests AMPK may have an oncogenic role in certain cancer contexts (32, 90-94), we wanted to determine whether AR signaling promoted prostate cancer cell growth in part through AMPK signaling. Further, given AMPK's role as a central regulator of cellular metabolism, we also wanted to determine whether AR-mediated AMPK signaling influenced prostate cancer cell biology through additional mechanisms beyond those classically attributed to cancer (i.e. glycolysis).

RESULTS

AMPK is required for androgen-mediated prostate cancer cell growth

Our previous work identified a role for CaMKKβ-AMPK signaling in AR-mediated prostate

cancer cell migration and invasion (32). Subsequent studies confirmed AR's regulation of CaMKKβ in prostate cancer and demonstrated its additional importance in regulating prostate cancer growth both *in vitro* and *in vivo* (90, 91). Additionally, Massie *et al.*, showed that CaMKKβ augmented cell growth in part through increased glucose metabolism, an effect they suggested may be mediated through AMPK (91). In that study, the role of AMPK was inferred from experiments that used pharmacological AMP mimetics that, while known activators of AMPK, cause cellular stress and therefore, may indirectly affect cell growth. We wanted to confirm a direct role for AMPK in AR-mediated prostate cancer cell growth using molecular approaches. To do so, we blocked AMPK activity using siRNAs targeting three separate regions of the predominant catalytic subunit of AMPK found in the prostate (32). In both LNCaP and VCaP human prostate cancer cells, siRNA-mediated knockdown of AMPKa1 decreased the levels of both total AMPKa and the threonine-172/activation loop phosphorylated form of AMPKa, indicating blocked AMPK activity (Figs. 2.1 A and B). Importantly, all three siRNAs targeting AMPK significantly inhibited R1881 (a synthetic androgen)-mediated prostate cancer cell growth in both cell types (Figs. 2.1 C and D).

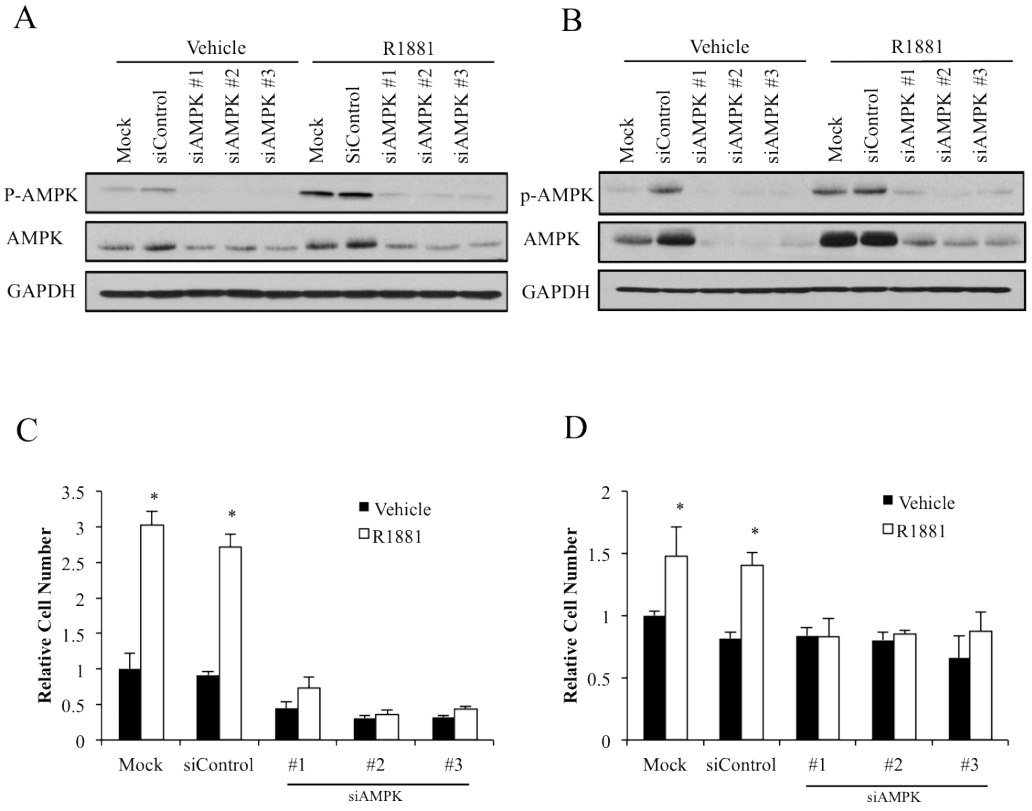

Figure 2.1 AMPK is required for androgen-mediated prostate cancer cell growth.

A and B, LNCaP (A) or VCaP (B) cells were transfected with mock or siRNAs targeting a b-lactamase negative control (siControl) or AMPKa1 (#1-3). The following day, cells were treated for 72 hours ± 10 nmol/L R1881 (synthetic androgen). Whole cell extracts were subjected to Western blot analysis using GAPDH as a loading control. C and D, LNCaP (C) and VCaP (D) cells were transfected the same as in A and B and then treated for 7 days ± R1881. Cells were then lysed and the relative number of cells was quantified using a fluorescent DNA-binding dye. Results are expressed as mean relative cell number + SE (n = 3). *, significant changes from vehicle-treated cells.

Androgens promote both glycolysis and OXPHOS

Given AMPK's role as a master regulator of metabolism and its regulation by AR in the prostate, we next asked what effects androgens had on prostate cancer cell metabolism. To quantitate glycolytic rates, we measured the extracellular acidification rate (ECAR) in prostate cancer cells following treatment with R1881. In both LNCaP and VCaP cells, R1881 increased glycolysis in a dose-dependent manner (Figs. 2.2A-C). Consistent with what has previously been shown (95), the dose response was unaffected by various modulators of mitochondrial function (Fig. 2.2C), highlighting the cytoplasmic nature of glycolysis. Interestingly, simultaneous measurement of the oxygen consumption rate (OCR) indicated that androgens also increased oxygen consumption in a dose-dependent manner (Figs. 2.2D-F). This androgen-mediated increase in OCR was dependent on mitochondrial function as combined treatment of rotenone and antimycin, inhibitors of mitochondrial respiration, collapsed the response (Fig. 2.2F). The increased oxygen consumption indicated androgens promote metabolism not only through glycolysis, but also through the TCA cycle. In support of this, we used MS/MS to show that androgens increased intracellular levels of acetyl-CoA, the entry molecule for the TCA cycle (Fig. 2.2G). Importantly, GC/MS was used to demonstrate that androgens also increased the levels of all TCA cycle intermediates tested, suggesting that acetyl-CoA is not only entering the TCA cycle, but also metabolized completely through it (Fig. 2.2H). These data are in contrast to Massie *et al.,* who found that androgen treatment increased citrate but not succinate levels nor oxygen consumption (91). To verify whether complete oxidation was occurring, we used a radiolabeled CO_2 trap assay to demonstrate that androgens increase complete glucose oxidation (Fig. 2.3 A and C). These results indicate that androgens promote the uptake and metabolism of radiolabeled glucose through at least ~1.5 turns of the TCA cycle prior to the radiolabeled 1-carbon of glucose being release in the form of CO_2.

While the majority of metabolic cancer research focuses on the role of glucose, recently several groups have demonstrated an important role for fatty acid metabolism in prostate cancer (85, 96-98). Correspondingly, in our hands, b-oxidation was required for maximal androgen-mediated prostate cancer cell growth as co-treatment with etomoxir, an inhibitor of carnitine palmitoyltransferase I—the rate-limiting step of b-oxidation, suppressed androgen-mediated LNCaP growth (Fig. 2.2 I). We therefore tested whether androgens could also promote fatty acid oxidation in prostate cancer cells by tracking the metabolism of radiolabeled fatty acids. Treatment of either LNCaP (Figs. 2.3 B and C) or VCaP (Figs. 2.3 E and F) cells with increasing concentrations of androgens promoted, in a dose-dependent manner, the complete oxidation of both the saturated fatty acid palmitate and the monounsaturated fatty acid oleate, two of the most common b-oxidation substrates. Taken together, these findings indicate that androgens increase both glycolysis and OXPHOS in prostate cancer cells.

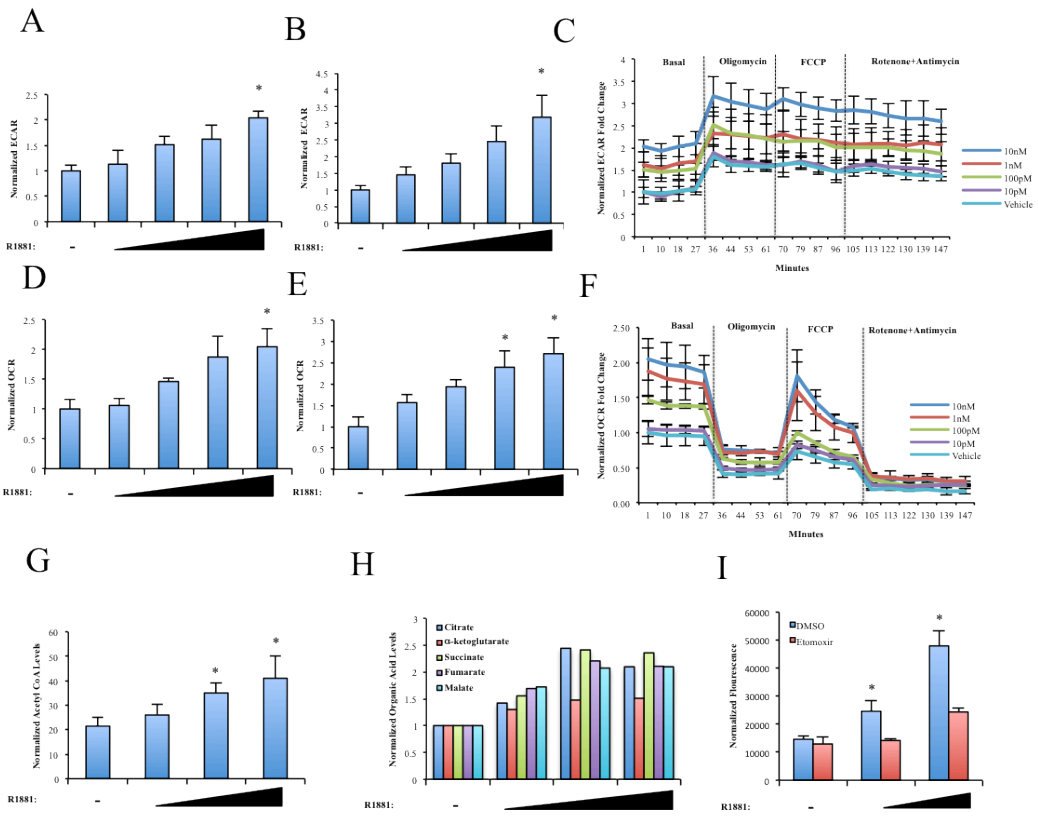
A
B
C
Normalized ECAR
R1881:
Basal
Oligomycin
FCCP
Rotenone+Antimycin
Normalized ECAR Fold Change
Minutes
10nM
1nM
100pM
10pM
Vehicle
D
E
F
Normalized OCR
Normalized OCR Fold Change
G
H
I
Normalized Acetyl CoA Levels
Normalized Organic Acid Levels
Citrate
α-ketoglutarate
Succinate
Fumarate
Malate
Normalized Fluorescence
DMSO
Etomoxir

Figure 2.2 Androgens promote glycolysis and OXPHOS in prostate cancer cells.

A and B, LNCaP (A) or VCaP (B) cells were treated for 72 hours with increasing concentrations of R1881 (0, 0.01, 0.1, 1, and 10 nmol/L). Extracellular acidification rates (ECARs) were then measured using a Seahorse XF Analyzer and values were normalized to cell numbers. Results are expressed as ECAR normalized to cell numbers + SE (n = 3). C, LNCaP cells were treated and analyzed for ECAR as in A but were also tested for effects on ECAR in the sequential presence of oligomycin, FCCP and a combination of rotenone and antimycin A. D and E, LNCaP (D) and VCaP (E) cells were treated the same as in A and B. At the same time ECAR rates were being measured, simultaneous oxygen consumption rates (OCRs) were measured and normalized the same as in A and B. F, LNCaP cells were treated and analyzed for OCR as in D but were also tested for effects on OCR in the sequential presence of oligomycin, FCCP and a combination of rotenone and antimycin A. G, LNCaP cells were treated for 72 hours with increasing doses of R1881 (0, 0.1, 1, and 10 nmol/L). Acetyl-CoA levels were then measured using MS/MS and normalized to total protein. Results are expressed as acetyl-CoA levels normalized to total protein + SE (n = 3). H, LNCaP cells were treated as in G. TCA cycle intermediate levels were then measured using GC/MS and normalized to total protein. Results are expressed as metabolite levels normalized to total protein + SE (n = 2). I, LNCaP cells were cotreated for 7 days with increasing doses of R1881 in the presence of vehicle (DMSO) or the b-oxidation inhibitor etomoxir (100 mmol/L). Relative cell numbers were then determined as described in Fig. 1.

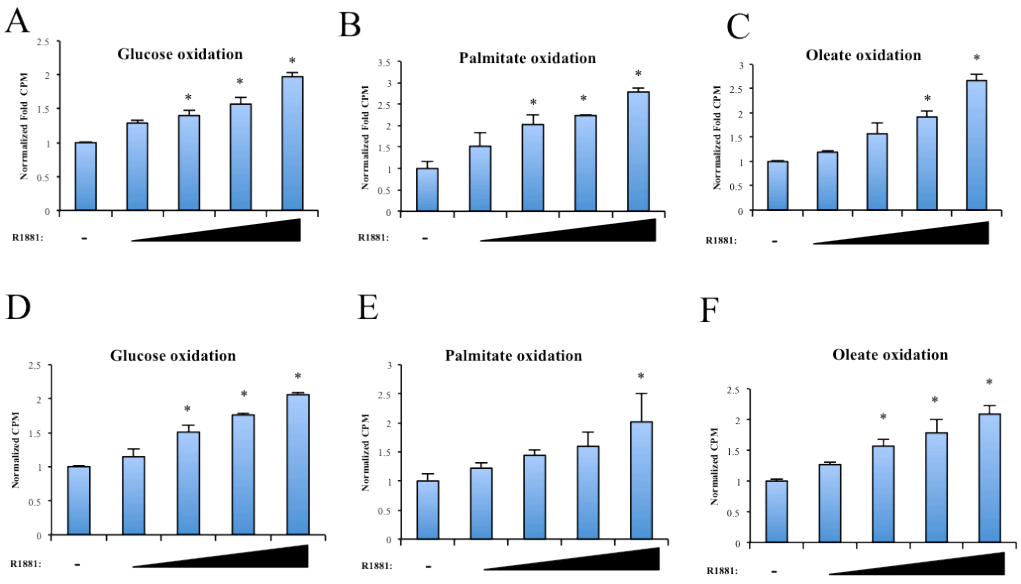

Figure 2.3 Androgens regulate glucose and fatty acid oxidation in prostate cancer cells.

(A) LNCaP cells were treated with R1811 for 72 hours, thereafter incubated with ^{14}C-labeled glucose and subjected to a CO_2 trap assay to measure complete glucose oxidation and normalized to cell numbers. Results are expressed as fold counts per minute (CPM) normalized to cell numbers + SE (n = 3). B and C, LNCaP cells were treated and subjected to a CO_2 trap assay the same as in A, but using ^{14}C-labeled palmitate (B) or oleate (C) to quantitate the levels of fatty acid oxidation. *, significant changes from vehicle-treated cells. D, E and F Same as A, B and C, respectively carried out with VCaP cells.

AMPK is required for androgen-mediated OXPHOS

AMPK is a positive regulator of OXPHOS. Given that AMPK is required for androgen-mediated prostate cancer cell growth (Fig. 2.1), we next wanted to determine whether the androgen-mediated increase in OXPHOS was mediated by AMPK. To do this, we used two different approaches. First, we demonstrated in both LNCaP and VCaP cells that molecular knockdown of AMPK decreased androgen-mediated oxygen consumption (Figs. 2.4A and 2.4B). Second, knockdown of AMPK significantly inhibited the androgen-mediated oxidation of radiolabeled glucose (Figs. 2.4C and 2.4D), palmitate (Figs. 2.4E and 2.4F) and oleate (Figs. 2.4G and 2.4H). Collectively, these data confirm that androgens increase OXPHOS through AMPK signaling.

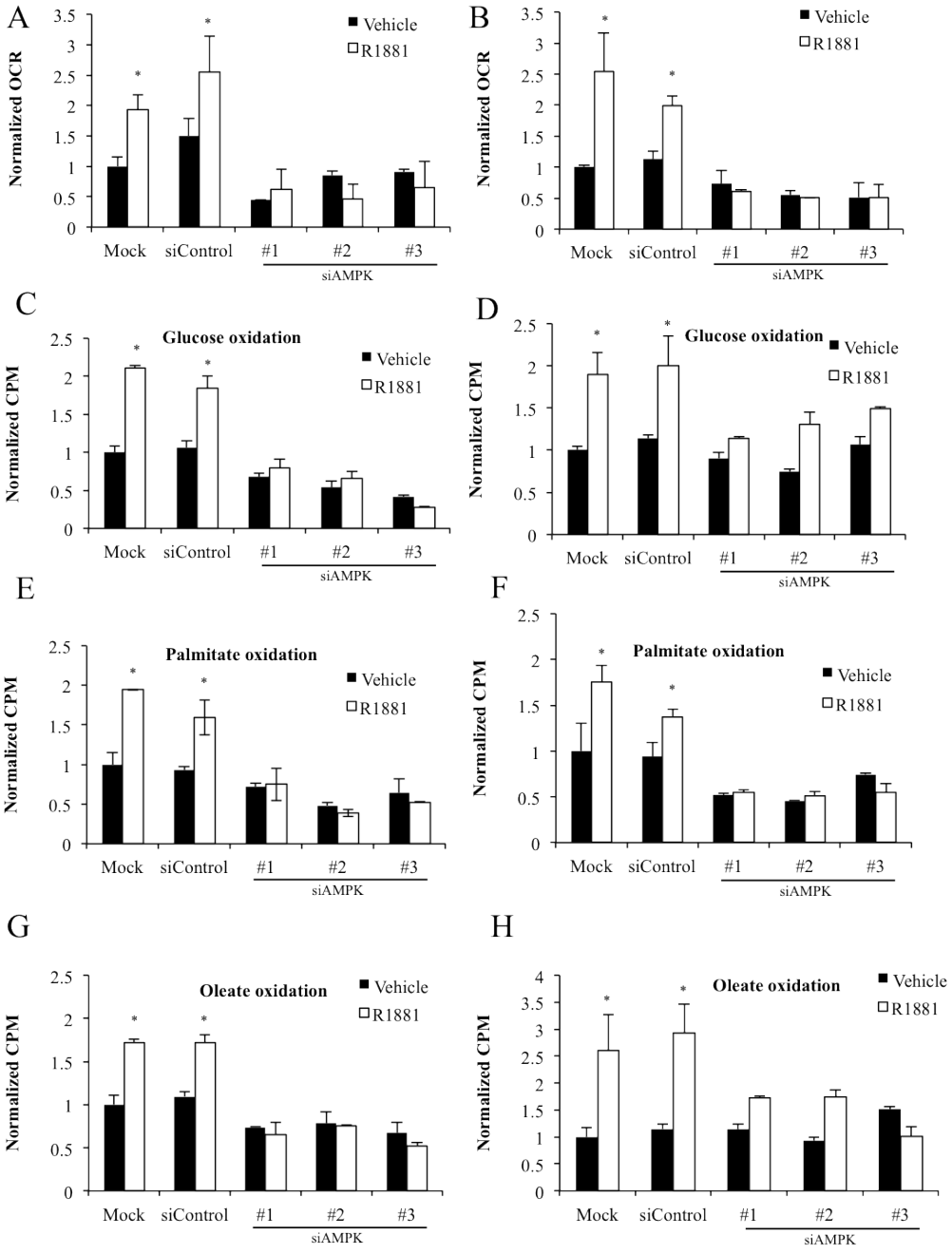
A
Normalized OCR
Vehicle
R1881
Mock
siControl
#1
#2
#3
siAMPK
B
Normalized OCR
C
Glucose oxidation
Normalized CPM
D
Glucose oxidation
E
Palmitate oxidation
F
Palmitate oxidation
G
Oleate oxidation
H
Oleate oxidation

Figure 2.4 Androgen-mediated OXPHOS requires AMPK.

A and B, LNCaP (A) or VCaP (B) cells were transfected and treated as described in Figs. 1A and B. OCRs were then measured using the Seahorse Analyzer and normalized to cell numbers as described in Fig. 2. C and D, LNCaP (C, E, G) or VCaP (D, F, H) cells were transfected and treated as described in A and B. Oxidation of radiolabeled glucose (C and D), palmitate (E and F) and oleate (G and H) were then measured using CO_2 trap assays and normalized to cell numbers as described in Fig. 2. *, significant changes from vehicle-treated cells.

AR-AMPK signaling increases intracellular ATP levels

One of the major functions of mitochondrial OXPHOS is to generate ATP. We therefore wanted to determine whether the androgen-mediated OXPHOS indeed led to an increase in intracellular ATP levels and hence, helped fulfill the cancer cell's bioenergetic demands. Using a luciferase-based ATP assay, we determined that R1881 increased intracellular ATP levels in a dose-dependent manner (Fig. 2.5A). This R1881-mediated increase in ATP levels was blocked by transfection with the siRNAs targeting AMPK (Fig. 2.5B). These results indicate that androgens increase mitochondrial function through AMPK.

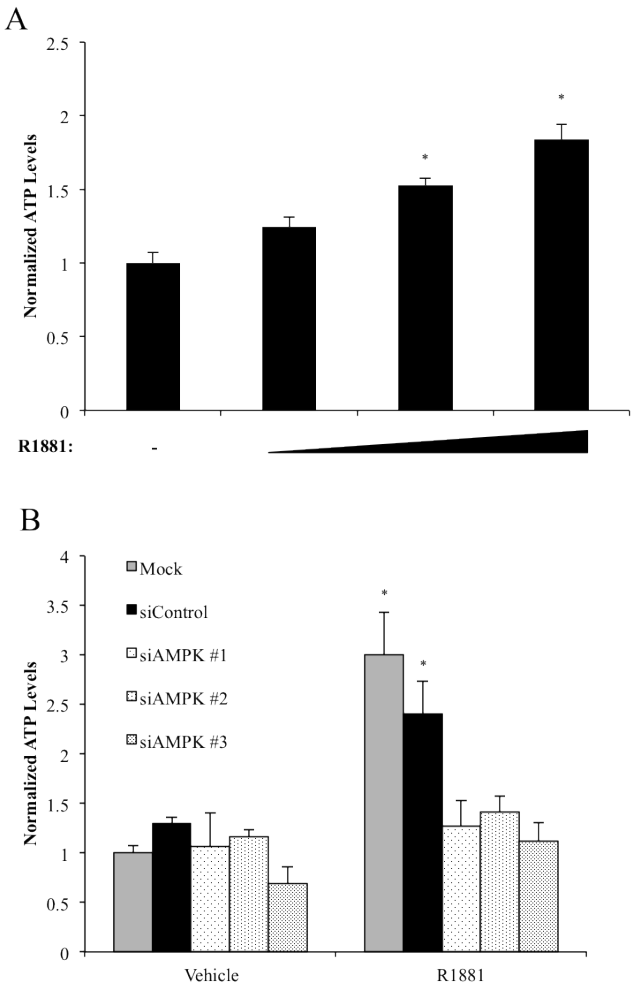

Figure 2.5 Androgens increase intracellular ATP levels through AMPK.

A, LNCaP cells were treated the same as in Fig. 2.1A. Intracellular ATP levels were then quantitated using a luciferase-based assay and data were normalized to cell numbers. Results are expressed as relative ATP levels normalized to cell numbers + SE (n = 3). B, cells were transfected and treated as described in Fig. 1A. ATP levels were then quantitated and normalized as described in A. *, significant changes from vehicle-treated cells.

Androgen-mediated AMPK signaling increases PGC-1α levels, which are elevated in a subpopulation of prostate cancers

Our data indicate that androgens increase overall mitochondrial function. However, the mechanism for this effect was still unknown. One of the known targets of AMPK is peroxisome proliferator-activated receptor gamma coactivator 1-alpha (PGC-1α), a transcriptional coactivator that is a master regulator of mitochondrial biogenesis and function (99). Therefore, we tested whether androgens could increase PGC-1α levels in prostate cancer cells. Androgens, starting at 100 pM R1881, significantly increased PGC-1α protein levels in a dose-dependent manner in both LNCaP (Fig. 2.6A) and VCaP (Fig. 2.6B) prostate cancer cells. Using qPCR, we found that increasing concentrations of R1881 could also increase PGC-1α mRNA levels in LNCaP (Fig. 2.6C) and VCaP (Fig. 2.6D) cells after a 72 hour treatment. This induction was not seen following a 24-hour treatment nor was it seen in the immortalized benign PWR-1E and RWPE-1 prostate cells, indicating an indirect regulatory mechanism that is cancer-specific (Fig. 2.7).

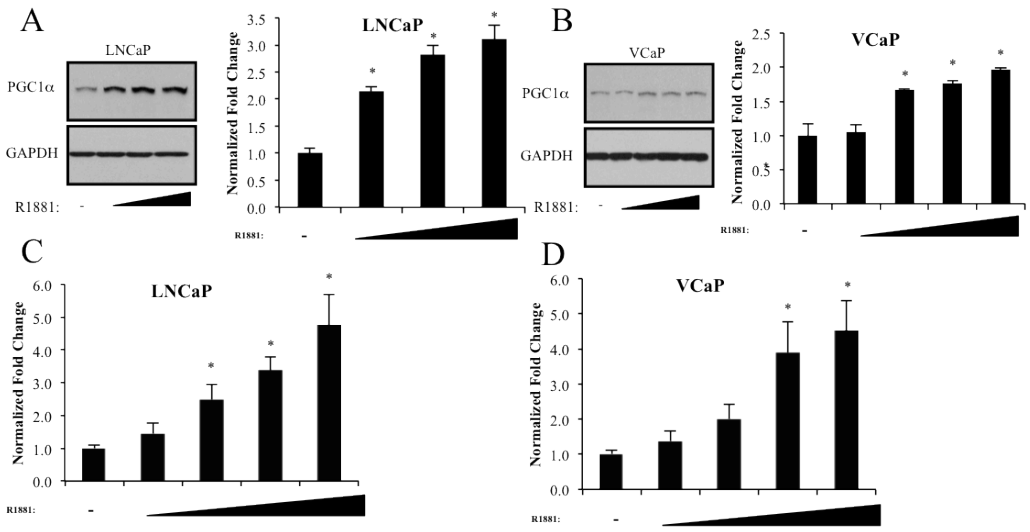

Figure 2.6 AR-AMPK signaling increases PGC-1α levels.

A-D, prostate cancer cells were treated with increasing concentrations of R1881 for 72 hours. A left, representative LNCaP Western blots following treatment (0, 0.1, 1 and 10 nmol/L R1881). A right, densitometry values for LNCaP Western blots. PGC-1α levels were normalized to GAPDH levels (n = 4). B left, representative VCaP Western blots following treatment (0, 0.01, 0.1, 1 and 10 nmol/L R1881). B right, densitometry values for VCaP Western blots. PGC-1α levels were normalized to GAPDH levels (n = 4). C and D, LNCaP (C) and VCaP (D) cells treated for 72 hours with 0, 0.01, 0.1, 1 or 10 nmol/L R1881. After treatment, cells were lysed and RNA was isolated and reverse transcribed. The expression of PGC-1α was assessed using qPCR (n = 3). *, significant changes from vehicle-treated cells.

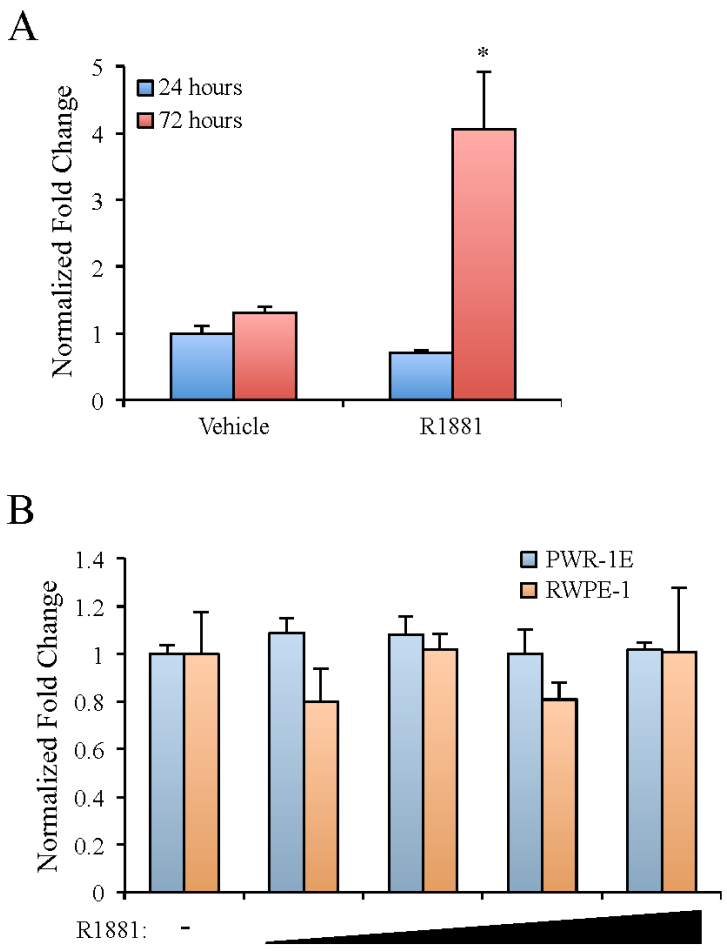

Figure 2.7 Androgens increase PGC-1α mRNA levels in an indirect and cancer cell-specific manner.

A, LNCaP cells were treated for 24 or 72 hours with vehicle or 10 nmol/L R1881. B, PWR-1E or RWPE-1 cells were treated for 72 hours with increasing concentrations of R1881 (0, 0.01, 0.1, 1, and 10 nmol/L). After treatment, cells were lysed, RNA isolated, and reverse transcribed. PGC-1α mRNA levels were assessed using qPCR and normalized to 36B4 levels. Results are expressed as fold induction over vehicle-treated cells + SE. *, significant changes from vehicle-treated cells.

To test whether AMPK was responsible for the androgen-mediated increase in PGC-1α levels, we used the same siRNAs targeting AMPK described in Figure 2.1 to determine what effects they had on both basal and androgen-mediated PGC-1α levels (Figs. 2.8 and 2.9) In LNCaP and VCaP cells, knockdown of AMPK led to a significant decrease in both PGC-1α protein (Fig. 2.8 and 2.9 A and B) and mRNA (Fig. 2.8C and 2.9C) levels, demonstrating a clear requirement for AMPK in AR-mediated induction of PGC-1α.

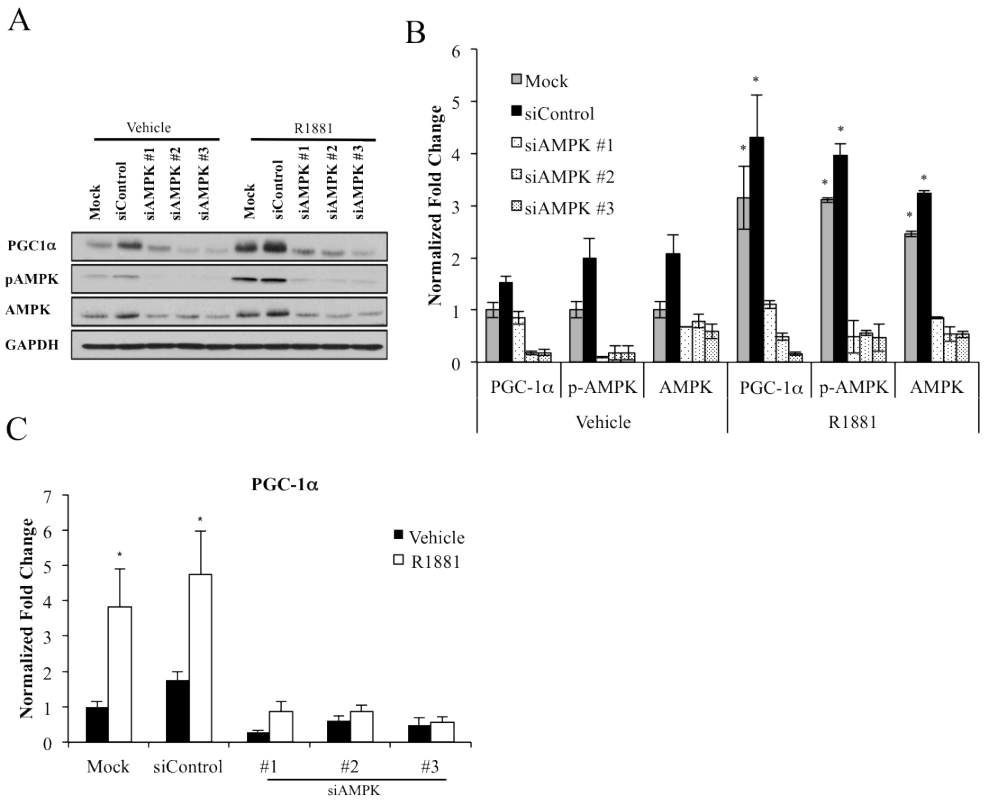

Figure 2.8 AR-AMPK signaling increases PGC-1α levels in LNCaP Cells.

LNCaP (A, B and C) prostate cancer cells were transfected with indicated siRNAs and treated ± R1881 as described in Figs. 2.1A and 2.1B. Cells were then subjected to Western blot (A and B) or qPCR (C) analysis (n = 3). A , representative LNCaP Western blots. B, densitometry values for LNCaP Western blots *, significant changes from vehicle-treated cells.

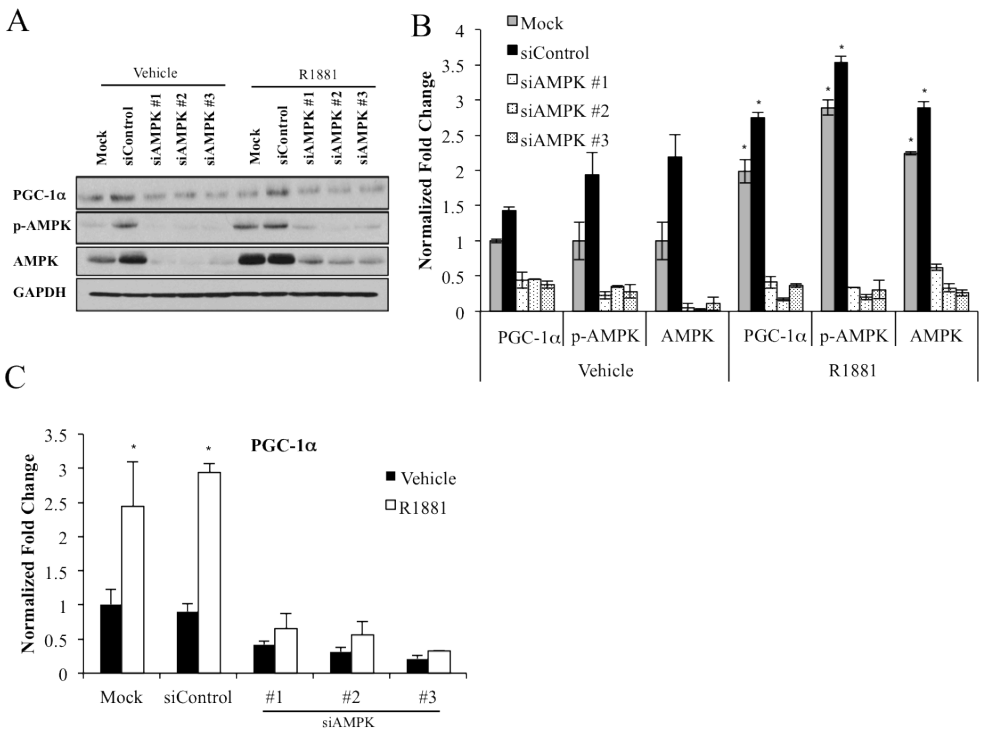

Figure 2.9 AR-AMPK signaling increases PGC-1α levels in VCaP cells.

VCaP (A, B and C) prostate cancer cells were transfected with indicated siRNAs and treated ± R1881 as described in Figs. 2.1A and 2.1B. Cells were then subjected to Western blot (A and B) or qPCR (C) analysis (n = 3). A, representative LNCaP Western blots. B, densitometry values for VCaP Western blots *, significant changes from vehicle-treated cells.

PGC-1α is overexpressed in a subpopulation of prostate cancers in multiple clinical cohorts.

Given that PGC-1α levels were increased in multiple cellular models of prostate cancer, we next determined if its expression correlated with prostate cancer in patients. Analysis of clinically annotated prostate cancer data sets accessible through Oncomine revealed that PGC-1α expression was significantly higher in cancers compared to controls (Fig 2.10A) (100). While this increase was significant, it was derived from a study with a modest cohort size (19 patients). Because of the high degree of heterogeneity in prostate cancer, we asked whether PGC-1α levels might be elevated in a subset of cancers. Using outlier analysis, we found that PGC-1α was indeed overexpressed in a subpopulation of prostate cancers in multiple clinical cohorts (Fig 2.10B) (98, 100-103).

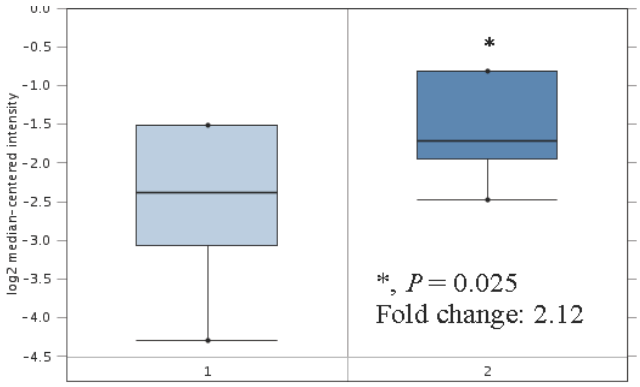

1. Prostate Gland (6)
2. Prostate Carcinoma (13)

- Varambally et. al., Cancer Cell, 2005

B

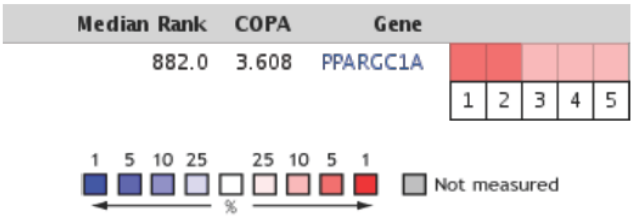

1. Arredouani et. al., Clin Cancer Res, 2009; (n = 21)
2. Chandran et. al., BMC Cancer, 2007; (n = 31)
3. Liu et. al., Cancer Res, 2006; (n = 57)
4. Tamura et. al., Cancer Res, 2007; (n = 35)
5. Varambally et. al., Cancer Cell, 2005; (n = 19)

Figure 2.10 PGC-1α levels are increased in a subpopulation of clinical prostate cancer. samples.

Independent microarrays were analyzed using the Oncomine resource. A, PGC-1α levels were elevated in prostate cancer samples (group 2) compared to normal prostate controls (group 1). B, five separate studies determined using outlier analysis that PGC-1α was significantly overexpressed in a subpopulation of prostate cancers. Cancer Outlier Profile Analysis (COPA) identifies oncogene expression profile where high gene expression is seen in a fraction of samples in the total population within a cancer type. The calculated median COPA value of 3.608 across all five clinical cohorts indicates that a subset of prostate cancers demonstrate marked PGC-1α overexpression.

AR-AMPK-PGC-1a signaling promotes mitochondrial biogenesis and cell growth

Mitochondrial function is essential for both basic cellular homeostasis as well as increased cell growth (70). Given recent studies that suggest a previously underappreciated role for mitochondrial function in cancer (70-84), we decided to test whether androgens could increase mitochondrial biogenesis in prostate cancer cells. Using TEM, we found that LNCaP cells treated for 72 hours had significantly more mitochondria (Fig. 2.11 A). To test whether the AMPK-mediated induction of PGC-1α promoted androgen-mediated mitochondrial biogenesis in a more unbiased manner, we used confocal microscopy and subsequent image analysis to quantitatively assess if AMPK and/or PGC-1α were required (Figs 2.11 C-D). Using our two most efficacious siRNAs targeting either AMPK (32) or PGC-1α. siRNA-mediated knockdown of either AMPK or PGC-1α significantly decreased mitochondrial volume in LNCaP and VCaP cells (Figs. 2.12 A and B). Importantly, similar to knockdown of AMPK (Fig. 2.1), and in concordance with what others have reported (104), molecular inhibition of PGC-1α also blocked androgen-mediated prostate cancer cell growth (Fig. 2.13), indicating a role for the AR-AMPK-PGC-1α signaling cascade in prostate cancer cell growth.

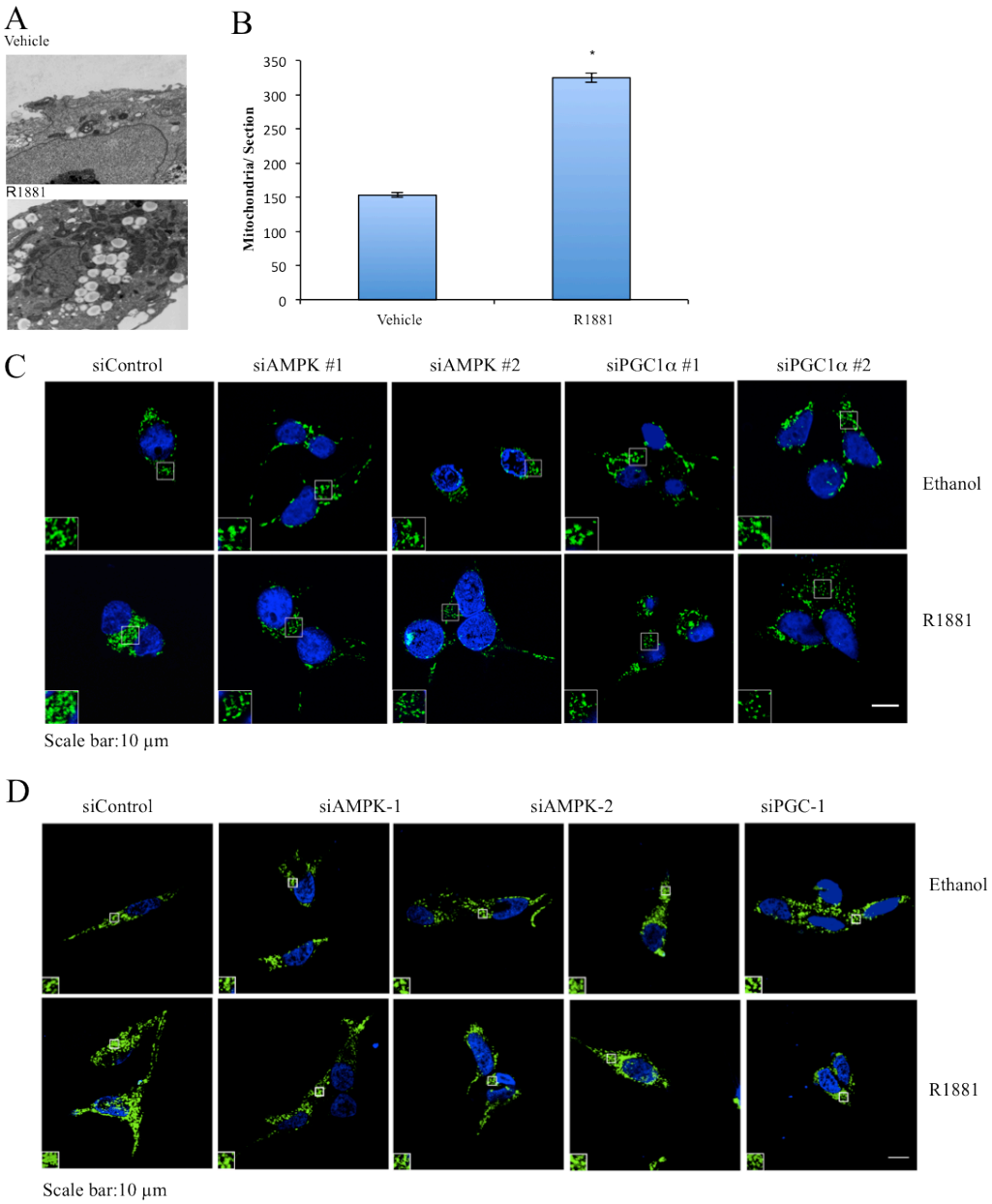
A
Vehicle
R1881
B
Mitochondria/ Section
350
300
250
200
150
100
50
0
*
Vehicle
R1881
C
siControl
siAMPK #1
siAMPK #2
siPGC1α #1
siPGC1α #2
Ethanol
R1881
Scale bar:10 μm
D
siControl
siAMPK-1
siAMPK-2
siPGC-1
Ethanol
R1881
Scale bar:10 μm

Figure 2.11 AR-AMPK signaling increases PGC-1α-mediated mitochondrial biogenesis.

A, LNCaP cells were treated ± 10 nmol/L R1881 for 72 hours and then subjected to TEM analysis. Shown are representative images A and results from blinded scoring of mitochondrial numbers/section B. C and D VCaP and LNCaP cells were respectively transfected with indicated siRNAs and treated as in Figs. 2.1A and 2.1B. Mitochondrial volume was then assessed using fluorescence confocal microscopy and subsequent image analysis. Shown are representative images.

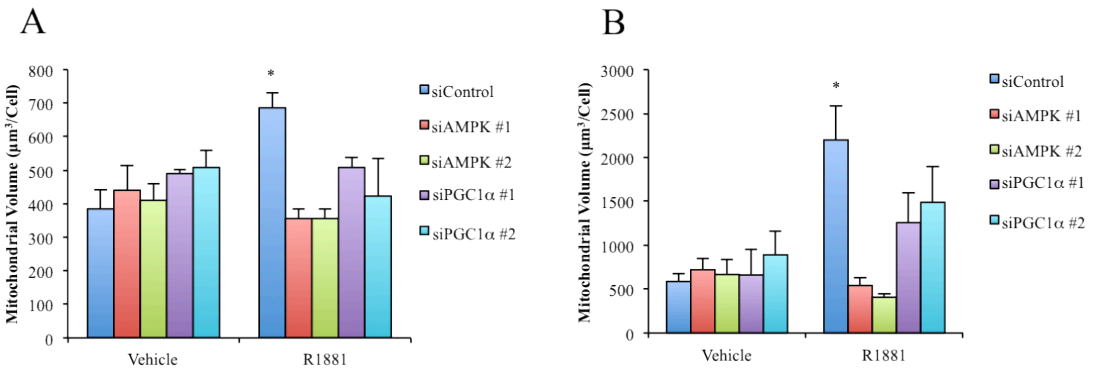

Figure 2.12 AR-AMPK signaling increases PGC-1α-mediated mitochondrial volume.

A and B Quantitated morphometric analysis results of 2.11 C and D. Scale bar, 10 mm.

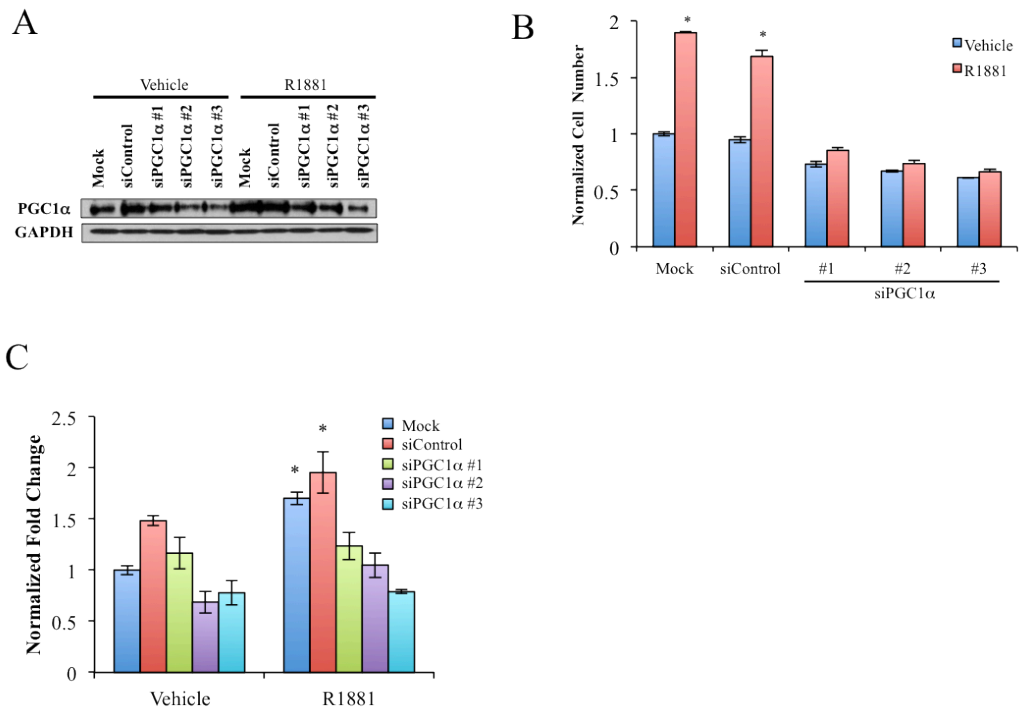

Figure 2.13 AR-AMPK signaling increases PGC-1α-mediated cell growth.

A. Representative western blot showing PGC-1α knockdown using siRNA. B, LNCaP cells were transfected as in E and then treated for 7 days ± R1881. Relative cell numbers were determined using the assay described in Fig. 2.1A. C, Normalized densitometry analysis of western blots in A. *, significant changes from vehicle-treated cells.

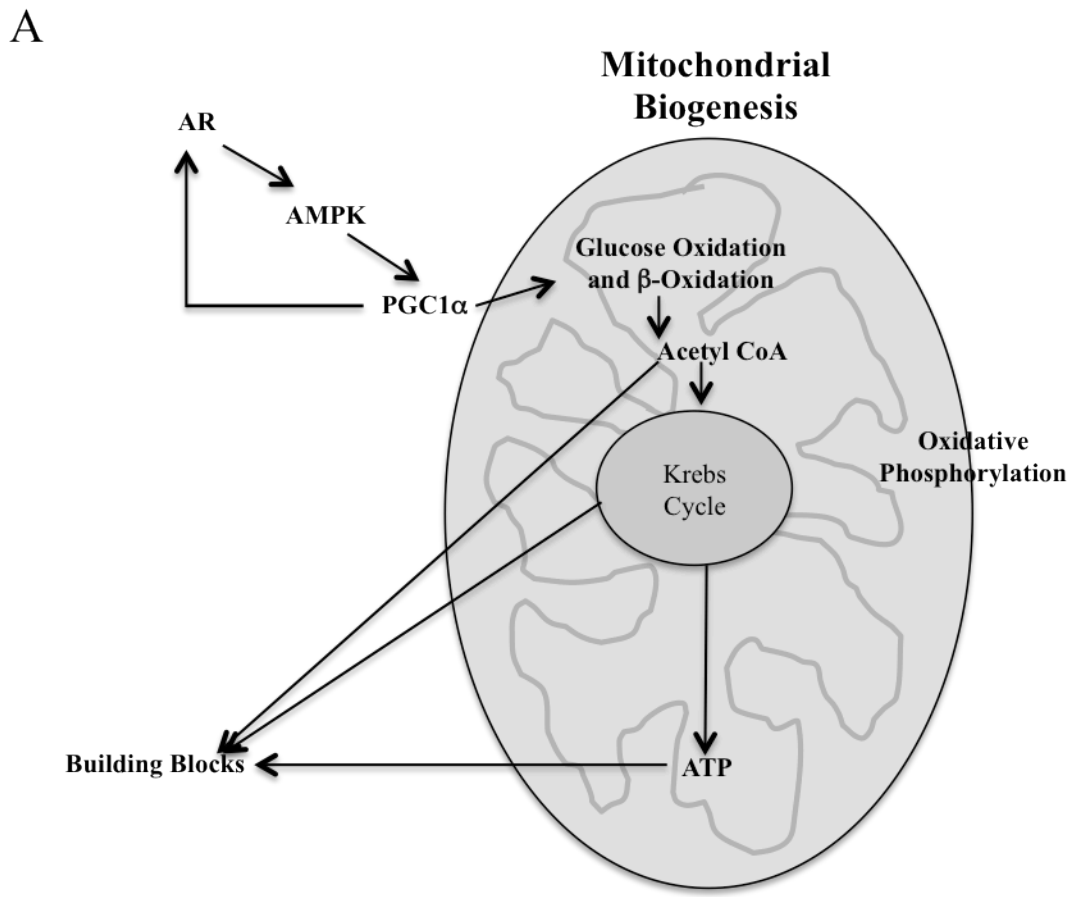

Figure 2.14 Proposed model of the AR-AMPK-PGC-1α signaling axis.

Androgens, through AR, increase AMPK activity. AMPK then potentiates PGC-1α. Increased PGC-1α can then potentiate AR activity via a positive feedback loop and also promote mitochondria biogenesis and function.

DISCUSSION

While much of the research on cancer metabolism has historically focused on glycolysis, it is now becoming apparent that not all cancers depend solely on glycolytic metabolism. Prostate cancer, in particular, appears to utilize other processes to fulfill its metabolic demands. Accordingly, the glycolysis marker ^{18}F-fluorodeoxyglucose is a poor PET imaging marker for prostate cancer (85, 86). Conversely, labeled fatty acid and acetate analogs, which can be shuttled to fatty acid metabolism and/or enter the TCA cycle, have shown more promising results (85, 87, 88). Interestingly, zinc and citrate levels are higher in normal prostate epithelial cells than any other cell in the body. When prostate epithelial cells become cancerous, they are uniquely characterized by decreased zinc and citrate levels, which parallels with increased citrate oxidation and OXPHOS (72, 73). Further, mitochondrial biogenesis, TCA cycle and OXPHOS signatures correlate with unfavorable outcomes in other cancer types as well as prostate cancer (70, 78, 80, 82, 83, 105-108). Inhibition of mitochondrial function/OXPHOS results in cell death or cell cycle arrest in multiple cancer types (75-77, 84). Thus, while glycolysis is a major metabolic pathway in cancer, mitochondrion-mediated functions still appear essential for many cancer cell types including prostate.

The findings above suggest that mitochondria could be an important target for various oncogenic and tumor suppressor signaling cascades. Correspondingly, the telomerase oncogene promotes mitochondrial biogenesis and prostate cancer bone metastasis while the tumor suppressor p53 suppresses PGC-1-mediated mitochondrial biogenesis (80, 106, 107). Our data presented here indicate that AR signaling, upregulated in 100% of metastatic prostate cancers (89), also increases AMPK-PGC-1-mediated mitochondrial biogenesis and prostate cancer cell growth (Fig.2.11 and 2.12 and 2.13). This raises the question of how mitochondrial biogenesis contributes to cell growth. One obvious possibility is that rapidly dividing cells have high

bioenergetic demands. By increasing the mitochondrial content of the cell, androgens also increased the intracellular levels of ATP (Fig. 2.5). Recently, however, it has been determined that the level of building blocks (ex. amino acids for protein production, phospholipids for new plasma membranes, etc), rather than the level of ATP, may be the major rate-limiting factor for rapidly dividing cells (71). As such, making sure a high level of TCA cycle intermediates are maintained, a process termed anaplerosis, would be essential as the TCA cycle serves as a central metabolic hub from which many of the cellular building blocks are derived (Fig.2.14). Our findings that androgens increase TCA cycle intermediate levels and promote the metabolism of glucose and fatty acids through the TCA cycle (Fig. 2.2 and 2.3), suggest that AR signaling is also anaplerotic. Current studies are ongoing to determine where substrates are ultimately shuttled following androgen treatment.

The data presented here indicate that AMPK signaling is required for androgen-mediated prostate cancer cell growth (Fig. 2.1). To date, the role of AMPK in cancer has been enigmatic. We (data not shown), and others (109), have demonstrated that 5-aminoimidazole-4-carboxamide 1-b-D-ribo-furanoside (AICAR) and the antidiabetic drugs metformin and rosiglitazone, which all activate AMPK, also inhibit prostate cancer cell growth. Conversely, while Massie *et al.,* also found that metformin inhibited LNCaP cell growth, they showed AICAR increased LNCaP cell growth in the presence or absence of androgens. Additionally, AICAR was able to rescue the growth inhibitory effects of either CaMKKβ RNAi knockdown or STO-609 (CaMKK antagonist) treatment (91). Further, AMPK has been shown to be activated in clinical prostate cancer samples and inhibition of its activity by compound C or siRNAs targeting AMPK blocks cancer cell growth (Fig. 2.1)(92). These discrepancies may be due to the pleiotropic effects of the various small molecules being used to modulate AMPK activity. For example, AICAR functions by inducing cellular stress. One of the results of this increased cellular stress is the activation of

AMPK. However, the widespread increase in cellular stress may undoubtedly function to inhibit cellular growth through other stress signaling pathways. Alternatively, the pro-growth effects of AMPK may, similar to many signaling cascades, occur within a defined window of activity where some controlled AMPK activity promotes a metabolic shift that enhances cell growth but too much AMPK activity signals stress and subsequent cell cycle arrest.

In prostate cancer cells, androgens increase PGC-1α protein and mRNA levels (Figs. 2.6 A-D). While we know AMPK is required for this PGC-1α regulation (Figs. 2.8 and 2.9), we still do not understand the exact mechanism. Previously, Bruce Spiegelman's laboratory demonstrated that AMPK increases both PGC-1α protein and mRNA levels in skeletal muscle (99). In that study, they found that AMPK directly phosphorylates PGC-1α on threonine-177 and serine-538. These phosphorylation events then increase the activity of PGC-1α protein on its own promoter, increasing its expression through a mechanism that may involve the transcription factors GATA-4 and Upstream Stimulatory Factor-1 (110). Hence, the AR-AMPK mediated increase in PGC-1α protein and mRNA levels may occur through the direct post-translational phosphorylation of PGC-1α protein by AMPK and subsequent positive feedback expression of the *PPARGC1A* gene.

Our data correlate with recent findings that indicate PGC-1α signaling is upregulated in endometrial cancer (79), drives breast cancer tumor growth *in vivo* (111), and *Pgc1α*-/- mice are resistant to chemically-induced models of colon and liver cancer (74). Correspondingly, Shiota *et al.,* also demonstrated that PGC-1α was essential for prostate cancer cell growth (104). Interestingly, in that study, PGC-1α was shown to function as a coactivator of AR. These data, combined with our own, indicate a positive feedback loop whereby AR, via AMPK, increases PGC-1α levels. Increased PGC-1α can then transactivate AR to further promote the feed forward

cycle (Fig. 2.14). Hence, while PGC-1α signaling promotes prostate cancer cell growth in part through increasing mitochondrial function (known because inhibition of mitochondrial function decreases cell growth/survival (Fig. 2.2I) (77)), PGC-1α signaling likely also enhances prostate cancer cell growth through AR-dependent, mitochondrion-independent mechanisms (ex. increasing cyclin D levels, etc). This could also help explain why knockdown of PGC-1α had a more dramatic effect on cell growth (Fig. 2.13 B) than it did on mitochondrial biogenesis (Fig.2.11). The more modest effects on mitochondrial biogenesis were likely due to the suboptimal efficacy of our PGC-1α-targeting siRNAs (Fig 2.11 A and C). Conversely, the dramatic effect of molecular PGC-1α inhibition on growth suggests that PGC-1α may potentiate androgen-mediated prostate cancer cell growth through additional mechanisms. As a result, the modest inhibition of a single protein, PGC-1α, would result in pronounced overall growth effects. Hence, our findings here that demonstrate AR-AMPK-PGC-1α signaling promotes mitochondrial biogenesis, combined with Shiota *et al's* data, indicate PGC-1α can increase androgen-mediated cell growth through both a direct mitochondrially-dependent mechanism and an independent mechanism involving an AR positive feedback loop (Fig. 2.14).

Collectively, the data presented here suggest that AR signaling promotes AMPK-PGC-1α-mediated mitochondrial biogenesis and cell growth. This is important because while AR's role in prostate cancer has been well established, the mechanisms by which AR manifests its biological actions and how these are dysregulated during disease progression are poorly understood. As a result, it is essential to identify the AR signaling networks that truly drive disease progression. Our understanding of these signaling pathways will ultimately yield new therapeutic targets. Hence, as our data indicate, modulators of mitochondrial function may offer new therapeutic avenues for AR-driven prostate cancer.

CHAPTER 3:

Dicer mediated epigenetic and post-transcriptional regulation of imprinted genes in mouse embryonic stem cells

ABSTRACT

Although the conventional role of Dicer in regulating gene expression through post-transcriptional regulation of transcripts is well established, its effect on epigenetic modifications leading to gene expression changes remains poorly understood. In order to investigate a potential role for Dicer in regulating developmentally critical imprinted genes in mammals we carried out a series of qRT-PCR and ChIP-qPCR experiments on a panel consisting of wild type mouse embryonic stem (mES) cells, Dicer deficient mES cells ($Dicer^{-/-}$) and mouse trophoblast stem cells (TS). Our initial observations revealed that loss of Dicer in ES cells leads to increased mRNA levels of imprinted genes Pwcr1, Atp10a, Sfmbt2 and Snord 116 resembling the expression pattern observed in TS cells. Closer examination of the promoter region of the maternally imprinted, paternally expressed and extra embryonically enriched, polycomb repressor gene Sfmbt2 revealed that Dicer impacts Sfmbt2 expression by affecting the overall balance between transcriptionally favorable (H3K4me3 and H3K36me3) vs. transcriptionally unfavorable (H3K9me2 and H3K27me3) marks. Interestingly, further investigation employing Luciferase assays proved that Dicer also post-transcriptionally regulates the expression of Sfmbt2 mRNA levels in mES cells through a miRNA mediated feed back loop. Our combined findings, argue in favor of a case where Dicer regulates the expression of key imprinted genes in wild type mES cells through epigenetic as well as post-transcriptional repression.

MATERIALS AND METHODS

Cell Culture:

Mouse ES cells were seeded at a density of 250,000 cells per well on 0.2% gelatin coated six well plates in DMEM (Gibco, Invitrogen, Carlsbad California catalog number-31053). The growth medium was supplemented with 15% FBS (Invitrogen, Carlsbad California catalog number-10439-024), Glutamine (Gibco, Grand Island New York catalog number-25030-024), non-essential amino acids (Gibco, Grand Island New York catalog number-11140-035), Penstrep (Gibco, Grand Island New York catalog number-15140-122), pyruvate and and 0.1 mM beta mercapto ethanol (Sigma, St. Louis Missouri catalog number-M7522). LIF (LIF 2010, Millipore, Billerica, Massachusetts) was added to the media at a concentration of 1,000 U/ml. LIF containing media was replaced with RA containing media after day zero and the cells were sustained in this medium until day 6. TS cells were cultured in feeder-conditioned medium as described Tanaka *et al*., (33).

Cell transfections and Luciferase assays:

NIH 3T3 cells were co-transfected with Dharmacon miRNA mimics and inhibitors along with Promega dual luciferase vector plasmids using Lipofectamine 2000 (Catalog number11668-019, Invitrogen, Carlsbad, California) reagent according to manufacturer's protocols. Two micrograms of plasmid were coated with the lipofectamine reagent and introduced 3T3 cells seeded at a density of 60,000 cells per well in six well plates 24 hours prior to transfection on DMEM (Gibco, Invitrogen, Carlsbad California catalog number-31053) medium supplemented with 10% FBS (Invitrogen, Carlsbad California catalog number-10439-024). Four hours after the initial transfection the medium was drawn off and 2 ml of fresh media were introduced.

Thereafter respective miRNA mimics or inhibitors were coated with Lipofectamine on optimum (Invitrogen) medium and introduced to each well to attain a final concentration of 10 nM miRNA. Luciferase assays were carried out 72 hours post-transfection on a BMG Labtech Flourstar Optima plate reader using a Promega dual glo luciferase reagent system according to manufacturer's protocols.

RNA Extraction:

A Qiagen miRNAeasy mini extraction kit (Catalog number 217004, Qiagen, Maryland, USA)) was used to extract RNA from the cell lines using according to manufacture's instructions. An on column DNAse treatment was carried out according to manufactures' protocols using a Qiagen DNAse reagent kit In order to make sure that the RNA samples were free of DNA contamination.

Quantitative real time PCR:

All Quantitative real-time PCR reactions were performed using Applied Biosystems 7500 real time PCR machine on Chromatin immunoprecipitated DNA and reverse transcribed RNA samples in a 96 well format using SYBR green dye according to manufacturer's protocols (catalog number 4385112, Applied Biosystems, New Jersey, USA). miRNA qRT-PCR reactions were carried out using taqman probes from applied biosystems according to manufacturer's protocols. A mouse 18S ribosomal subunit mRNA was used as an endogenous control for Sybr green based qRT-PCR assays while a mouse U6 snoRNA was used as an endogenous control for the Taqman based assays.

Chromatin Immunoprecipitation:

H3K4me3, HK9me2, H3K27me3 and H3K36me3 Chromatin immunoprecipitation was performed on genomic DNA samples using specific antibodies according to the method described by Shohet *et al.,* (35). The antibodies used for the chromatin immunoprecipitation assays were: Rabbit anti-Trimethyl-H3K9 (Cat# 39765, Active Motif 914 Palomar Oaks Way # 150, Carlsbad,CA) 92008-6509Rabbit anti-Trimethyl-H3K4 (Cat# 07-473, Upstate Biotechnology ,inc., Lake Placid, NY), Rabbit anti-Trimethyl-H3K27 (Cat# 07-449, Upstate Biotechnology ,inc., Lake Placid, NY) Rabbit anti-Trimethyl-H3K36 Cat# ab9050, Abcam Inc., 1 Kendall Sq # B2304 Cambridge, MA 02139 (617) 577-4200)

Primers:

The primer 3 tool (http://frodo.wi.mit.edu/primer3/) was used to design primers used in RT-PCR, qRT-PCRs and ChIP-qPCR assays. All primers for qRT-PCRs ne RT-PCRs were are listed in Table 3.1 and 3.2. Whenever possible primers used for RT-PCR and qRT-PCR assays were designed to span intronic regions of the concerned genes to avoid background resulting from genomic contamination of RNA samples. The Cold Spring Harbor mammalian promoter database (http://rulai.cshl.edu/CSHLmpd2/) was employed in deciding on promoter regions to which primers needed to be designed for the ChIP-qPCR assays.

Statistical analysis:

Graph pad Prism and Excel software were used for statistical analyses. Students' t-tests were carried out to assess significance in differences in quantitative real time PCR results and the

Luciferase assays. All statistical analyses were carried out and tested at confidence levels of 0.05 or less, unless otherwise stated.

Table 3.1 List of primers used for RT-PCR and qRT-PCR assays

Gene	Forward primer	Reverse primer
Pwcr1	GCCTATGCAGTCGAAGAAGG	GAGAGGGGGTTTCCTTTCAG
Atp10a	AGACCAACCACGACAAAAGG	GCTGTTTGACCCAGCTTCTC
Gtl2	GTTTAAGGCTTGGCTTGCTG	ATCCTGGGGTCCTCAGTCTT
Snord115	CCTCAGCGTAATCCTATTGAGC	TGACAACCCAATGTCATGAAG
Snord116	TCTATGATGATTCCCAGTCAAA	ACCTCAGTTCCGATGAGAGTG
Sfmbt2 Exon3	AACTTCCAGCCAGGAATGAA	CCGCTATGATCACGTCACAC
Sfmbt2 Exon10	GAGTCTGCTTTCTTATCCACTGGG	TTCAGGTCTTAGGTCATCAATGGC
Sfmbt2 Intron10	TCACTATTGCTCCCCACCTTGG	TGGACCCTAAGAGTATCTGACCCG
β-actin	GTACATGGCTGGGGTGTTG	CTGAACCCTAAGGCCAACC

Table 3.2 List of primers used for ChIP-PCR and ChIP-qPCR assays

Gene	Forward primer	Reverse primer
Sfmbt2 promoter	GTGAGTTTTGTCTACCTGGGCATC	CGTCCAAGAGTTTTTGAAGTGAGG
Sfmbt2 Exon10	GAGTCTGCTTTCTTATCCACTGGG	TTCAGGTCTTAGGTCATCAATGGC
Sfmbt2 Intron10	TCACTATTGCTCCCCACCTTGG	TGGACCCTAAGAGTATCTGACCCG
Sfmbt2 Exon11	TGGATTACCACAAGCAGCGTC	ATCAGGAGCAGACTCTCTCTTACCC

INTRODUCTION

Dicer is an RNAseIII enzyme known to mediate microRNA (miRNA) biogenesis by promoting cleavage of precursor miRNAs into their mature form (23, 37). Besides its role in catalyzing miRNA biogenesis Dicer is also known to facilitate regulation of gene expression through formation of the RNA induced silencing complex (RISC) where translational repression or Argonaut mediated mRNA degradation takes place (14). In spite of the presence of Dicer independent miRNA biogenesis mechanisms such as the mirtron pathway (112) loss of Dicer significantly reduces the overall number of miRNAs produced in mES cells and thereby strongly impacts cellular development (41). The fact that Dicer deficient embryos begin to show defects at day 6.5 of embryonic development signifies the importance of Dicer in mammalian embryogenesis (23, 24). It is well established that the numerous roles which Dicer mediated miRNAs play in mammals such as differentiation control in ES cells, development and progression of cancers, heterochromatic silencing and regulating alternative splicing factors in muscle development are executed through 3'UTR element based mechanisms (14, 113). Although numerous studies have implicated a role for Dicer in regulating epigenetic silencing in plants, flies and fission yeast it remains unclear to what extent Dicer regulates epigenetic modifications and thus gene expression in higher order mammals (42-44). In higher order mammals, genetic imprinting is a critical epigenetic process where 1-2% of the total number of genes are expressed from a parent-specific allele (114). Most of the mammalian imprinted regions are clustered and show tissue specific expression (115, 116). Defects in imprinting can lead to severe developmental abnormalities such as Prader-Willi and Angelman syndromes (117, 118). Mechanisms facilitating imprinting include methylation of the imprinted allele, which needs to remain silent while the allele, which needs to be expressed is kept unmethylated (119, 120). Non-coding RNA specific *cis* acting element mediated silencing which is under the control

of imprinting centers is one of the regulatory molecules involved in the maintenance of the imprinted state (121). Although extraembryonic lineage specific genes are for the most part repressed by DNA methylation in the embryo, there is also evidence showing that they remain silenced through polycomb repressor complex 2 (PRC2) and G9a mediated repressive histone methylation mechanisms (119, 120, 122-124). Numerous mechanisms have been studied and implicated in maintaining genetic imprinting, nonetheless there remains no simple answer to all cases involved (114). Given the proposed models for small non-coding RNAs in maintaining imprinting we were intrigued as to the potential role for Dicer- in this phenomenon in mES cells. We hypothesized that Dicer either directly or indirectly through miRNA-based mechanisms play a role in genetic imprinting in mammals. In order to test this hypothesis we initially carried out a series of RT-PCR and qRT-PCR experiments on a panel of key imprinted genes comprising, Pwcr1, Atp10a, Snrpn and Gtl2 in mES cells, Dicer$^{-/-}$ES cells and TS cells. Our initial observations showed that imprinted genes were consistently upregulated in Dicer$^{-/-}$ ES cells as compared to wild type ES cells and resembled the expression pattern of TS cells. Upon further investigation combining ChIP-qPCR, qRT-PCR and Luciferase assays we found that Dicer regulates key imprinted gene expression in mammals through epigenetic histone modifications as well as through a feed back loop involving 3'UTR based post-transcriptional mechanisms.

RESULTS

Loss of Dicer leads to increased mRNA levels of key imprinted genes in mES cells

To assess effects due to loss of Dicer on gene expression in mES cells we carried out a series of RT-PCR experiments on a panel of developmentally critical imprinted genetic regions of the

mouse genome. The first set of genes we chose for our experiments consisted of Pwcr1, Atp10a, Snord115, Snord116, Snrpn, Gtl2 and Sfmbt2 genes. This panel of genes was chosen taking into account their significance in mouse embryonic development and as models for human disease. For example, imprinting defects in the Pwcr1 region leads to the Prader-Willi syndrome phenotype (117). Recent reports have shown that single nucleotide polymorphisms in the Snord 115 and Snord116 snoRNA clusters to be associated with Prader-Willi Angelmans phenotypes (125). Atp10a and Snrpn, mediated regulation also plays critical roles in the development of Prader-Willi, Angleman's phenotypes (126). Imprinting defects in Gtl2 are associated with abnormalities in skeletal muscle, bone development, prenatal lethality and placental size and organization variations (127, 128). The polycomb repressor gene Sfmbt2, which functions as a subunit of the polycomb repressor complex2 in mouse, has been shown to be maternally imprinted extraembryonically enriched and paternally expressed during mouse embryogenesis (129). Our initial experiments revealed that in Dicer$^{-/-}$ ES cells markedly increased expression of imprinted genes occurs, compared to mES cells. Furthermore expression patterns of Dicer$^{-/-}$ ES cells were similar to expression patterns of the same genes in TS cells. When we assayed for Sfmbt2, Exon 3 (E3) and Exon 10 regions (E10) we found that the expression levels were consistently high in the Dicer$^{-/-}$ ES cells compared to the mES cells while the TS cells as well showed expression (Figure 3.1A). Since previous studies have implicated Dicer-dependent miRNAs in alternative splicing mechanisms we probed for different intronic regions of the Sfmbt2 gene and found that Intron 10 region is expressed in both Dicer$^{-/-}$ ES cells and TS cells while it is not expressed in mES cells. This implies possible intron retaining mechanisms being suppressed by Dicer in mES cells (Figure 3.2A). As far as Pwcr1, Atp10a and Snord 116 genes are concerned we found expression patterns similar to Sfmbt2 where, out of the three cell lines, expression was present in TS cells, while Dicer$^{-/-}$ ES cell expression levels were always greater than those observed in mES cells (Figure 3.2 B, C and D). Snord 115 and Gtl2 mRNA were

detectable in Dicer$^{-/-}$ ES cells, however for these two genes we found no mRNA present in either mES cells or TS cells (Figure 3.2E). Snrpn mRNA was found to be higher in Dicer$^{-/-}$ ES cells compared to mES cells (Figure 3.2F). Given the higher expression levels of these developmentally critical imprinted genes we hypothesized that Dicer-mediated mechanisms potentially regulate expression of genetically imprinted genes either through direct intervention or miRNA mediated indirect mechanisms in mES cells.

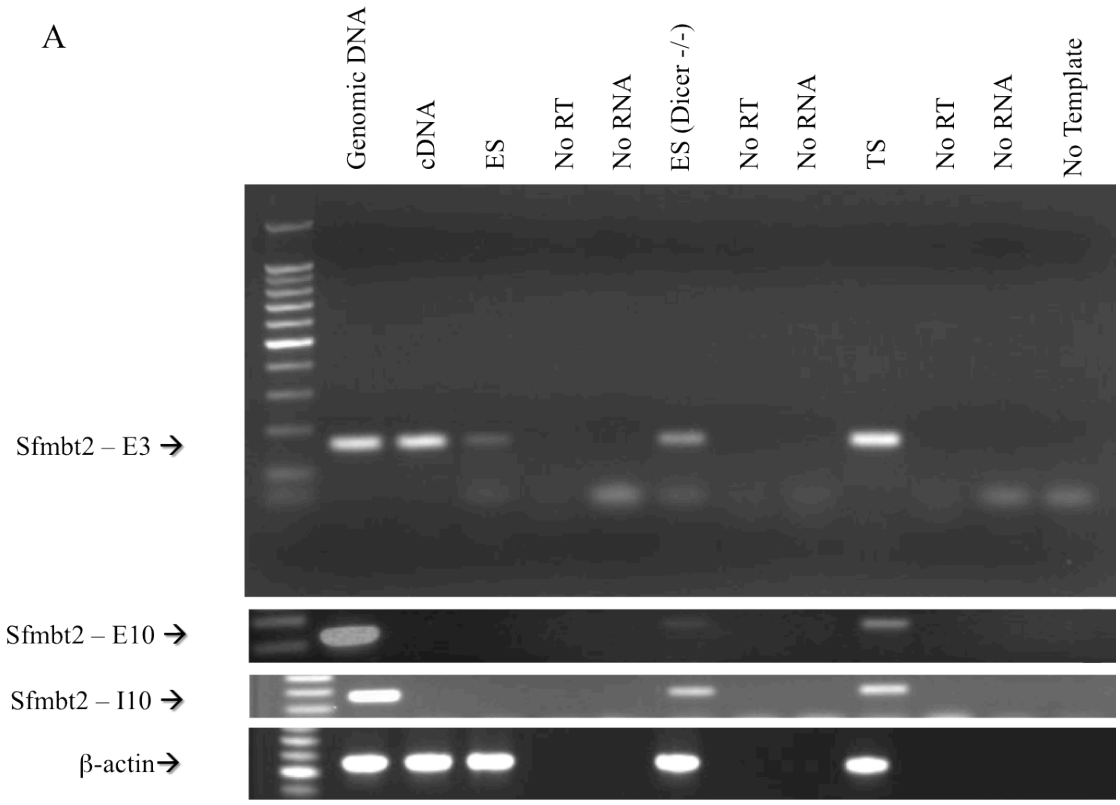

Figure 3.1 Loss of Dicer impacts expression of maternally imprinted paternally expressed polycomb repressor gene Sfmbt2.

A)RT-PCR results showing, loss of Dicer leads to increased mRNA levels of Sfmbt2. Note higher intensities of bands in the Dicer$^{-/-}$ ES cells and TS cell lanes. E3 and E10 represent Exon 3 and Exon 10 while I10 represents Intron 10. β-Actin was used as an integrity and loading control.

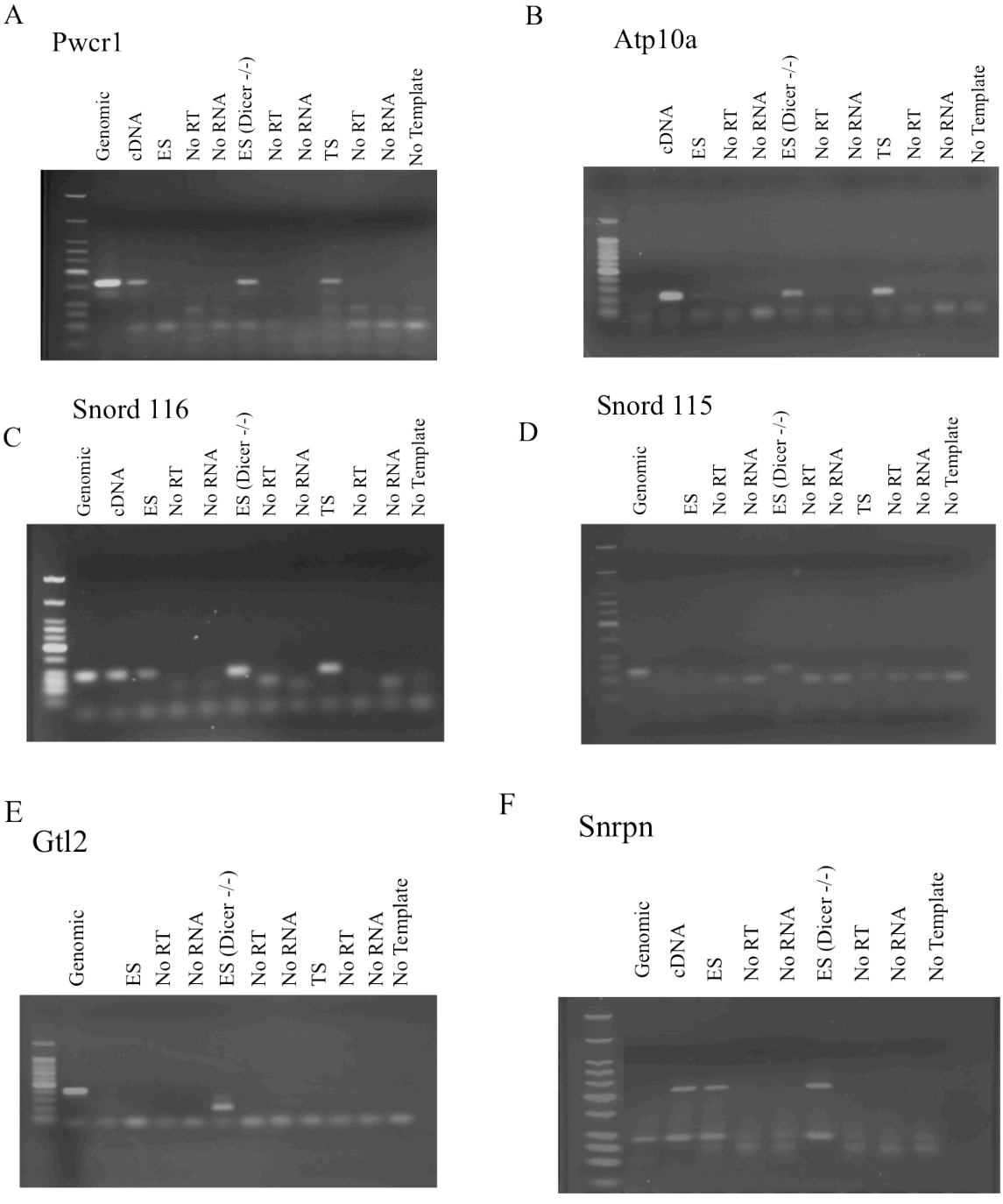
A
Pwcr1
Genomic
cDNA
ES
No RT
No RNA
ES (Dicer -/-)
No RT
No RNA
TS
No RT
No RNA
No Template
B
Atp10a
cDNA
ES
No RT
No RNA
ES (Dicer -/-)
No RT
No RNA
TS
No RT
No RNA
No Template
C
Snord 116
Genomic
cDNA
ES
No RT
No RNA
ES (Dicer -/-)
No RT
No RNA
TS
No RT
No RNA
No Template
D
Snord 115
Genomic
ES
No RT
No RNA
ES (Dicer -/-)
No RT
No RNA
TS
No RT
No RNA
No Template
E
Gtl2
Genomic
ES
No RT
No RNA
ES (Dicer -/-)
No RT
No RNA
TS
No RT
No RNA
No Template
F
Snrpn
Genomic
cDNA
ES
No RT
No RNA
ES (Dicer -/-)
No RT
No RNA
No Template

Figure 3.2 Loss of Dicer impacts expression of key mammalian imprinted genes in mouse ES cells.

A, B, C, D, E and F, RT-PCR results showing increased expression of key mammalian imprinted genes in Dicer$^{-/-}$ ES cells and TS cells. Either genomic or pooled cDNA was used as positive controls, no RT and no template represent the negative controls. β-Actin was used as an integrity and loading control.

Imprinted genes Pwcr1, Atp10a and Sfmbt2 remain significantly over expressed in Dicer$^{-/-}$ES cells upon RA induced differentiation

To assess how the Dicer-dependent changes that we uncovered through our initial RT-PCR experiments behave during differentiation we used retinoic acid (RA) containing medium and qRT-PCR to analyze the expression of the Pwcr1, Atp10 and Sfmbt2 genes. We cultured mES and Dicer$^{-/-}$ ES cells in LIF containing media on day 0 (D0) and thereafter in RA containing medium through day 6 (D6). RNA was isolated from each culture at respective time points of day 0, 3 and 6. We found that expression levels of these genes were consistently higher in Dicer$^{-/-}$ ES cells compared to mES cells throughout the course of RA-induced differentiation (Figure 3.3A, B and C). These striking observations suggest that Dicer-mediated regulation is critical for maintaining appropriate expression levels of imprinted genes during differentiation of mES cells.

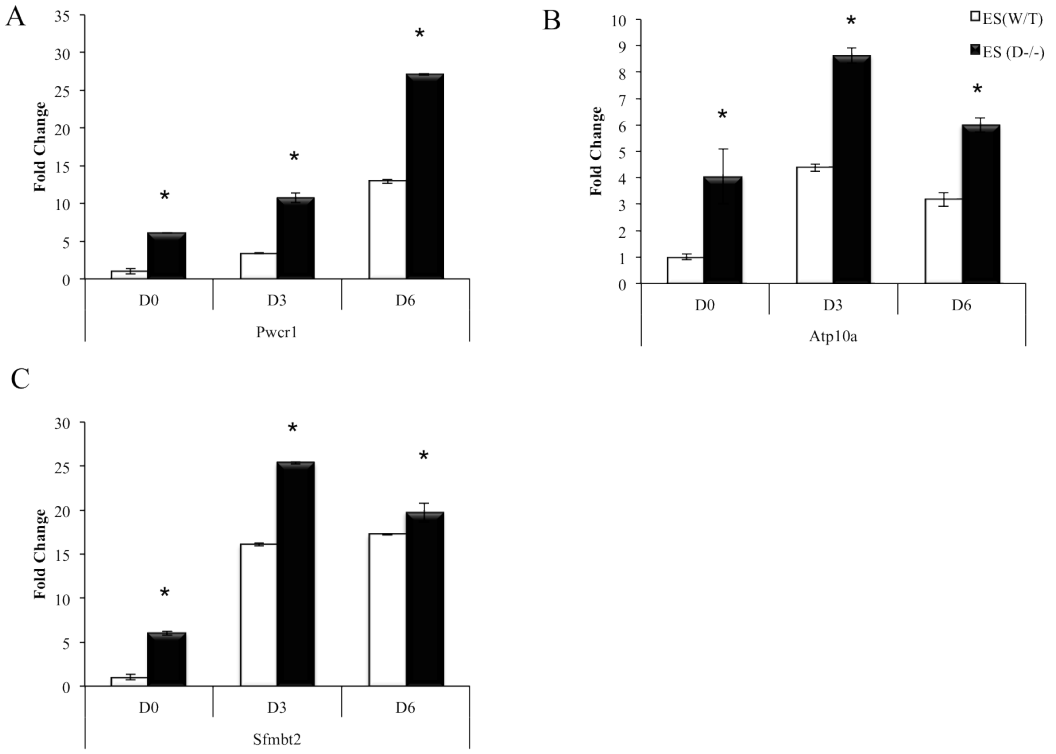

Figure 3.3 qRT-PCR results showing increased expression of the imprinted genes Pwcr1, Atp10a and Sfmbt2 upon RA induced differentiation.

Note significant increases of mRNA in the Dicer$^{-/-}$ ES cells compared to mES cells through day zero (D0) through day six (D6) of RA induced differentiation. The * symbol denotes that the differences between mES and Dicer$^{-/-}$ ES cells were significant in a students t-test at confidence levels of 0.05

Loss of Dicer impacts the overall balance between transcriptionally favorable (H3K4me3 and H3K36me3) vs. transcriptionally unfavorable (H3K9me2 and H3K27me3) histone modifications in the Sfmbt2 gene.

It is known that DNA methylation affects the expression patterns of extraembryonically enriched imprinted genes. However, there is also evidence suggesting that in some of the extraembryonically enriched genes histone modifications also affect imprinting and therefore expression (114). In order to investigate whether Dicer regulates epigenetic modifications in mouse ES cells, which affect imprinted gene expression we decided to carry out ChIP-PCR and ChIP-qPCR assays in different genetic elements of the Sfmbt2 gene. As H3K9me2 enrichment in the promoter regions is widely thought to delineate genomic regions for DNA methylation we initially chromatin immunoprecipitated genomic DNA from mouse mES cells as well as mouse Dicer$^{-/-}$ ES cells using H3K9me2 specific antibodies and carried out a conventional ChIP-PCR assay in the promoter, Exon 10, intron 10 and exon 11 regions of the Sfmbt2 gene. We were struck by the observation that Promoter, Intron 10 and Exon 11 regions showed noticeably higher levels of H3K9me2 in Dicer$^{-/-}$ ES cells (Figure 3.4A). Since the effect of H3K9me2 enrichment on genetic silencing or remaining active for transcription is context dependent and as enrichment of H3K9me2 marks in the promoter regions are widely considered repressive (130) we questioned as to how expression levels of Sfmbt2 were higher in Dicer$^{-/-}$ES cells compared to mES cells. As H3K9me2 enrichment in the promoter region of Sfmbt2 gene in Dicer$^{-/-}$ES cells is likely to repress gene expression on its own we reasoned that there could be additional histone modifications being affected in the promoter region of Sfmbt2 in Dicer$^{-/-}$ES cells. It was shown by two groups that key differentiation genes in ES cells are kept silenced but poised for activation when differentiating through concomitant modification of promoter chromatin regions by

H3K4me3 and H3K27me3 histone modifications and that actively transcribed genes are occupied by transcriptionally favorable H3K4me3 and H3K36me3 marks (51, 131). To probe the enrichment levels of these histone modifications in the promoter region of the Sfmbt2 gene we carried out chromatin immunopreciptations in genomic DNA from mES cells and Dicer$^{-/-}$ ES cells using antibodies specific for H3K4me3, H3K36me3, H3K27me3 and H3K9me2. Thereafter, we assayed for enrichment of these marks in the promoter region of Sfmbt2 through quantitative real time PCR. Upon completing the experiment we found that Dicer$^{-/-}$ ES cells showed consistently enriched amounts of transcriptionally favorable H3K4me3 and H3K36me3 marks and transcriptionally unfavorable H3K9me2 marks. The repressive H3K27me3 marks were found at comparable level in both cell lines (Figure 3.4B). These combined observations argue in favor of a case where Dicer is essential to maintain the desired balance between transcriptionally favorable versus unfavorable histone mark enrichment in mouse ES cells to maintain precise gene expression critical for differentiation.

A

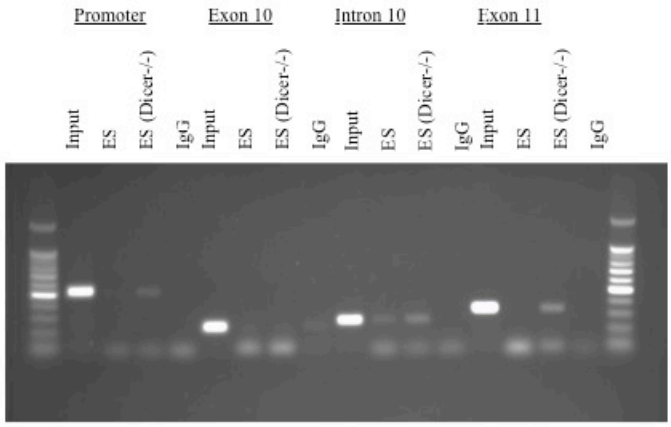
Promoter
Exon 10
Intron 10
Exon 11
Input
ES
ES (Dicer-/-)
IgG

B

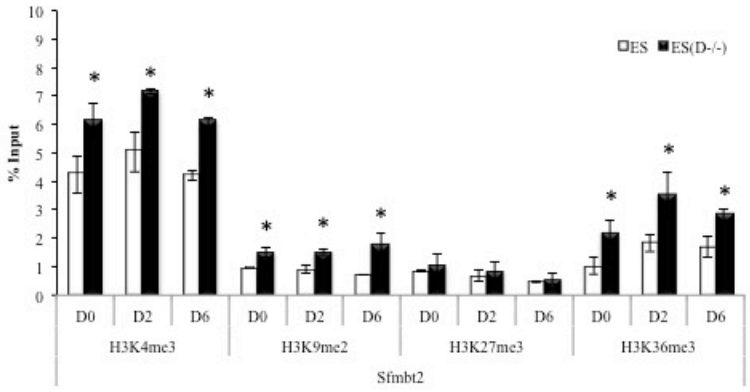
% Input
ES
ES(D-/-)
D0
D2
D6
H3K4me3
H3K9me2
H3K27me3
H3K36me3
Sfmbt2

Figure 3.4 ChIP-PCR and ChIP-qPCR results of different regions of the Sfmbt2 gene showing changes in enrichment of transcriptionally favorable (H3K4me3 and H3K36me3) vs transcriptionally unfavorable (H3K9me2 and H3K27me3) histone modification marks in ES mES and Dicer$^{-/-}$ ES cells.

A) ChIP-PCR result showing increased H3K9me2 occupation in the promoter, intron 10 and exon 11. The input sample was used as a positive control while the immunoprecipitated IgG fraction was used as a negative control. B) ChIP-qPCR results showing enrichment of different histone marks in the promoter region of the Sfmbt2 gene upon RA induced differentiation. Note significantly increased levels of transcriptionally favorable H3K4me3 and H3K36me3 marks in Dicer$^{-/-}$ cells compared to mES cells H3K9me2 marks are higher in Dicer$^{-/-}$ cells while repressive H3K27me3 marks are comparable in mES and Dicer$^{-/-}$ cells through day 0 (D0) to Day (6) of RA induced differentiation. The * symbol denotes that the differences between mES and Dicer$^{-/-}$ ES cells were significant in a students t-test at confidence levels of 0.05.

Dicer-dependent miR-467a post-transcriptionally regulates the extra embryonically enriched polycomb repressor gene Sfmbt2

Having found that Dicer impacts gene expression in mouse ES cells through epigenetic modifications in the extraembryonically enriched Sfmbt2 gene promoter we asked the question whether there could be additional Dicer-mediated miRNA related post-transcriptional regulatory mechanism involved in affecting its expression. Through our previous work we have shown that mmu-miR-467a is found in high abundance in mouse ES cells (132). Interestingly miR-467a is located in intron 10 of the Sfmbt2 gene. To assess the amounts of miR-467a and Sfmbt2 expression levels in mES and TS cells we carried out Taqman and SYBR green based qRT-PCR assays on a series of ES cells in different stages of differentiation and TS cells. We observed that as the ES cells began to differentiate in RA containing media and in TS cells Sfmbt2 mRNA levels increase while the miR-467a levels decrease (Figures 3.5 A an B). Given the inverse relationship between expression levels of miR-467a and Sfmbt2 mRNA in mES cells and TS cells we hypothesized that miR-467a and Sfmbt2 are co-transcribed, however Sfmbt2 mRNA levels are kept at low levels via a feed back loop where miR-467a post-transcriptionally down regulates Sfmbt2 mRNA by targeting its own 3'UTR element. To determine whether there are any predicted binding sites in the 3'UTR of the Sfmbt2 gene for miR-467a we carried out an *in silico* folding analysis using the publicly accessible algorithm RNA hybrid (http://bibiserv.techfak.uni-bielefeld.de/rnahybrid/) (133). Our analysis showed that there are numerous binding sites corresponding to miR-467a in the full length 3'UTR of the Sfmbt2 gene (Appendix). To functionally validate whether miR-467a binds and reduces Sfmbt2 mRNA levels of the Sfmbt2 gene we cloned the full length 3'UTR of the Sfmbt2 gene into a Promega Psi-check dual glo luciferase vector and carried out luciferase reporter assays by transfecting NIH3T3 cells with the cloned plasmid in the presence of appropriate controls and test samples (Fig. 3.6A). As we predicted the results indicated that there was significant decrease in signal in the test sample when

the Sfmbt2 3'UTR reporter was co-transfected with a miR-467a mimic, whereas no significant changes were observed in the control samples when compared to the signals from the sample transfected with the cloned 3'UTR containing plasmid alone (Fig. 3.6A).

A

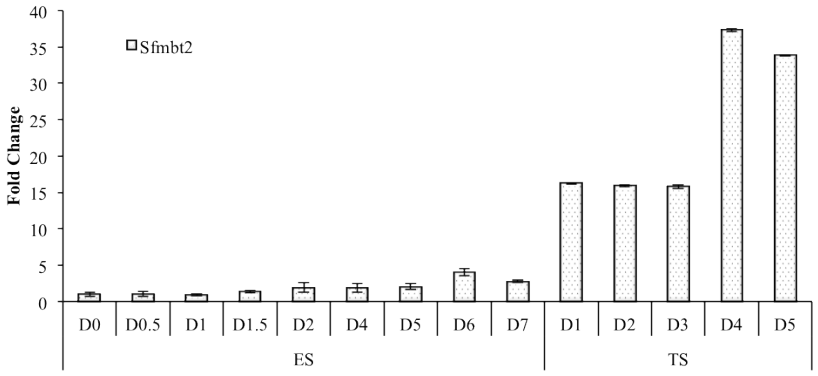

B

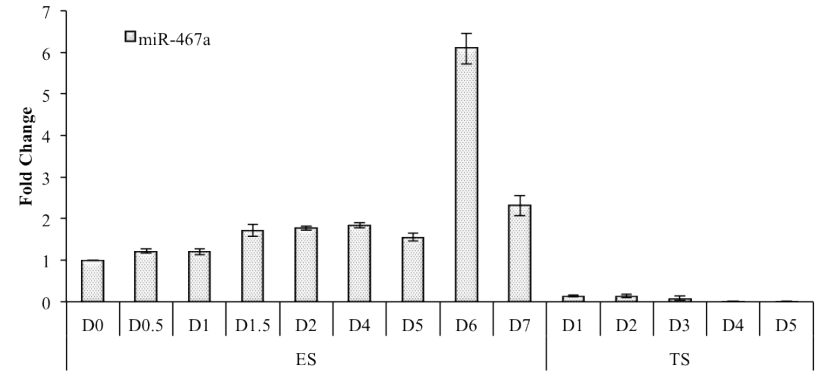

Figure 3.5 Sfmbt2 mRNA and mir467 expression levels show an opposite corelation.

A and B) qPCR data showing opposite correlation in expression patterns of Sfmbt2 mRNA and mir-467a miRNA in mES cells subject to RA induced differentiation and TS cells. Note the gradual increase of Sfmbt2 mRNA levels and the gradual decrease of mir467a during the course of transition from mES cells to TS cell state.

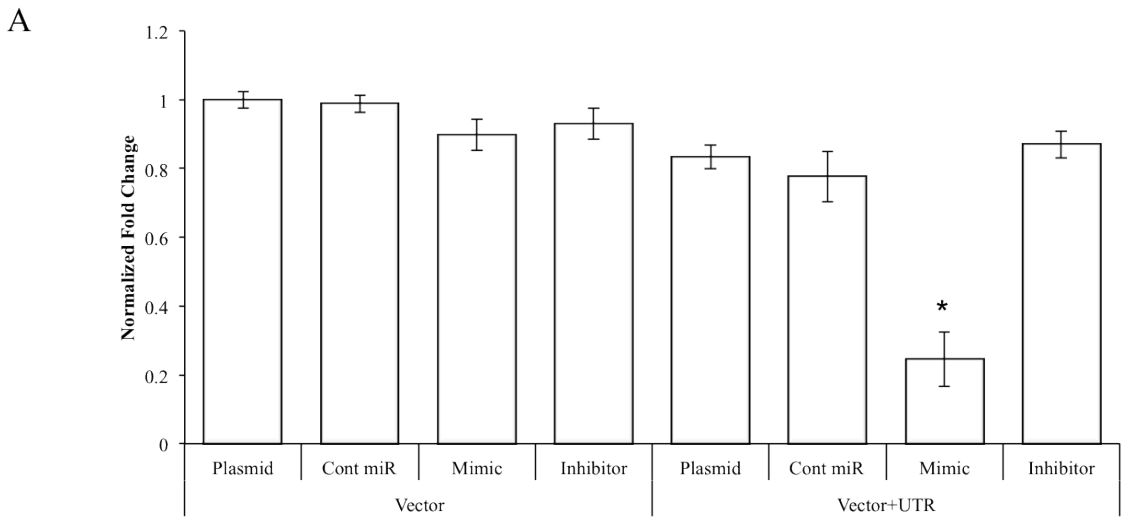

Figure 3.6 miR-467a post-transcriptionally regulates Sfmbt2 mRNA in mES cells.

A) Luciferase assay data showing that mir467a binds to the 3'UTR of the Sfmbt2 gene. The first four bars on the left panel show the strength of the luciferase signals in the four respective conditions where a Promega dual glo^{TM} luciferase vector, the luciferase vector was co-transfected into NIH3T3 cells with a negative control miRNA (Scrambled), miR-467a mimic and mir467a inhibitor miRNAs. Bar 5 through 8 represent similar conditions with the exception of using a dual glo vector to which the full length 3'UTR was cloned. The * symbol denotes that the change in signal in the mimic cotranscribed with the sfmbt2, 3'UTR cloned luciferase vector was significant in a students t-test at 0.05 confidence limits compared to the same clone co-transfected with scrambled miRNA.

DISCUSSION

Through a series of qRT-PCR, ChIP-qPCR and Luciferase assay based experiments we have shown that loss of Dicer can profoundly impact gene expression in mouse ES cells through epigenetic as well as post-transcriptional mechanisms. The significance of Dicer in aiding precise embryonic development is highlighted by the fact that Dicer deficient embryos begin to show morphological differences at day 6.5 (23, 24). The Prader-Willi critical (Pwcr1) region is one the largest imprinted regions in the human genome. This region is known for its genetic complexity, where antisense-based mechanisms (114, 134) play roles in regulating gene expression. From a functional point of view expression levels of genes in this region are extremely critical to direct developmentally robust embryos void of defects (129). Imprinting defects associated with this region are most well known for the Prader-willi and Angelman syndromes (126). Dicer$^{-/-}$ ES cells showing elevated levels of expression of the Pwcr1 critical region genes is an interesting observation which emerged from our study. Sahoo and colleagues have suggested that a single nucleotide polymorphism in the SnoRNA clusters Snord 115 and 116 to have direct relationship to the pathogenicity of the Prader Willi syndrome diseases (125). We found that both Snord 115 and 116 were over expressed in Dicer$^{-/-}$ ES cells. Given the connotations of small RNA mediated regulatory roles and pathogenicity in the imprinted Prader-Willi, Angelman region, and consistently increased expression of the developmentally critical imprinted genes, Pwcr1, Atp10a, Snord115, Snord116, Snrpn, Gtl2 and Sfmbt2 our observations question whether miRNAs too have potential regulatory roles in establishing genetic imprints in developmentally critical regions if not all imprinted regions of the mouse genome.

Moreover employing the same polycomb repressor gene Sfmbt2 which is extraembryonically enriched maternally imprinted and paternally expressed (129) which hosts a large cluster of miRNAs having targets on its own 3'UTR we demonstrate an event where Dicer-dependent

miRNAs post-transcriptionally repress its host gene in mouse ES cells. In mES cells miR-467a regulates its host gene Sfmbt2 by targeting the 3'UTR element, however in TS cells miR-467a is expressed to a lesser degree compared to mES cells, hence mRNA levels of Sfmbt2 remain higher compared to mES cells in TS cells. It is possible that this regulatory loop may be critical in establishing ES cell to TS cell transition. A plausible mechanism in maintaining the opposite and inverse expression relationship of Sfmbt2 mRNA and miR-467a between mES and TS cells is that miR-467a, which is hosted in intron 10 of the Sfmbt2 gene is co-transcribed with Sfmbt2 mRNA under the control of a single promoter in mES cells. However miR-467a may be produced at lesser levels through a miRNA specific promoter in TS cells. The abundance of matching target sites in the 3'UTR of Sfmbt2 exposes itself to repression through a feedback loop facilitating low levels of Sfmbt2 expression in mES cells compared to Dicer$^{-/-}$ ES cells and TS cells.

The interesting observation in our RT-PCR experiments is the retention of intron 10 of the Sfmbt2 gene in the Dicer$^{-/-}$ ES cells while it is absent in the wild type mES cells suggesting that aberrations to normal splicing events may occur in the absence of Dicer (Figure 3.1A). Therefore it is reasonable to assume that presence of Dicer may be necessary for precise splicing to operate in mES cells although this remain speculative until confirmed through additional experiments.

It is established that Dicer mediated miRNAs affect DNA methylation by down regulating repressors of DNA methyl transferases such as Rbl via 3'UTR element based mechanisms employing miR-290-295 cluster members(49). This mechanism ensures that DNA methylation takes place precisely in mES cells. However as Dicer$^{-/-}$ ES cells are unable to process miR-290-295 candidates it is possible that reduced methylation in Dicer$^{--/-}$ ES cells leads to loss of imprinting. However it is also known that expression of extraembryonically enriched imprinted

genes are potentially affected by histone modifications as well (114). To this end our ChIP-qPCR experiments of the Sfmbt2 gene show that Dicer is necessary to maintain the critical balance between transcriptionally favorable versus transcriptionally unfavorable histone modifications, which could potentially affect gene expression. Changes in the histone landscape in Dicer$^{-/-}$ ES cells compared to mES cells may also contribute to loss of imprinting. The aberrant expression of histone and DNA methyl transferases in Dicer$^{-/-}$ ES cells explain the differences in epigenetic modifications to a certain extent, which exist between wild type mES and Dicer$^{-/-}$ ES cells. These observations emphasize the significance of Dicer in maintaining an epigenetic landscape necessary for ideal expression of developmentally critical imprinted genes in mES cells.

Taken together our findings argue in favor of a case where Dicer mediated pathways particularly in conjunction with miR-290-295 cluster, miR-467a and other miRNAs play critical roles in regulating epigenetic modifications and post-transcriptional repression to affect precise gene expression critical for healthy mammalian embryogenesis. These combined findings point to the multifaceted roles, which Dicer plays in regulating mammalian development and emphasize its overall importance as a key regulator of epigenetic as well as post-transcriptional events, which ultimately affect gene expression in mouse embryonic stem cells critical for cellular fate.

SUMMARY AND FUTURE DIRECTIONS

Utilizing two different models of embryonic stem cell systems, I have provided insight into regulatory mechanisms that are driven by Dicer-dependent pathways, which apply to differentiation and proliferation of embryonic stem cells. The initial chapter provides a novel observation that over 900 CpG islands in mouse embryonic stem cells require the function of Dicer to repress H3K9me2 enrichment. A second novel observation that was unexpected is that enriched H3K9me2 at promoter regions of relevant genes are associated with an upregulation of transcript levels, which is contrary to the expectation that H3K9me2 is typically a repressive epigenetic mark. However this latter effect was not universally observed within the assayed panel of developmentally critical genes. This in turn directed attention towards probing the combined effect of transcriptionally favorable H3K4me3 and repressive H3K27me3 marks together with H3K9me2 marks in regards to selected genes. A comparative study of the enrichment levels of the said marks and the expression levels lead to the interesting finding that Dicer-dependent pathways play a critical role in the maintenance of the overall balance of transcriptionally favorable versus unfavorable marks at gene promoters. Part of the consequence of loss of Dicer in ES cells may depend on the level of gene transcripts being driven by this dysregulation of the balance between transcriptionally favorable versus unfavorable histone modifications. In future studies it will be interesting and important to extend these observations to the rest of the genome by conducting ChIP-seq using antibodies to H3K4me3, H3K27me3 and H3K36me3 in ES and Dicer knock out cells. Finally extending this to evaluate the impact of Dicer loss on genome-wide DNA methylation will require bi-sulphite sequencing. At the time of writing this dissertation such efforts involving different model systems were in progress. Unraveling the effects of a combination of histone modification on gene transcription beyond what we have noticed may yield insightful information that would facilitate the development of new strategies to manipulate developmental aspects of embryonic stem cells to our advantage. For example reprogramming

somatic cells to become tissue specific progenitor cells, which can be, utilized in replacement therapies have already been performed by other groups (135). The strategies used in these cases have been based on overexpression of transcription factors or miRNAs (135). A limitation of the results derived from methods described so far has been, the reprogrammed cells not having the typical epigenetic signatures of naturally occurring cells (135). Our findings that let-7g and siEzh2 facilitate cellular transition through epigenetic modifications suggest the possibility of utilizing such methods for reprogramming cells to have a closer resemblance of the epigenetic profiles of naturally occurring cells.

A second important finding of the first chapter is the effect of Dicer in regulating stem cell differentiation. We have noticed that Ezh2, which is an H3K27me3 promoting enzyme is expressed to a higher degree in Dicer null ES cells, compared to wild type mouse embryonic stem cells. The elevated expression levels of Ezh2 in the Dicer knock out ES cells coincided with increased H3K27me3 in the promoter regions of Cdx2 and Hoxa1 differentiation genes. The expression levels of these two genes were impaired in comparison to the wild type cells suggesting that this may be one of the causative factors, which render mouse embryonic stem cells lacking Dicer to inefficiently differentiate (24, 25). Knock down studies using let-7g, a microRNA that targets Ezh2 and is known to be elevated during the process of differentiation, revealed that Ezh2 expression levels and in accordance, H3K27me3 enrichment levels at the promoter regions of Cdx2 and Hoxa1 decrease. Expression studies of Cdx2 and Hoxa1 under knock down conditions showed comparable results to those of embryonic stem cells proving the principle possibility of utilizing let-7g for directed differentiation of embryonic stem cells. It remains unclear as to why elevated levels of Ezh2-directed enrichment of H3K27me3 marks at the promoter regions of Cdx2 and Hoxa1 and not the other genes studied. A plausible explanation to this question is that there could be potential accessory factors that facilitate recruitment of

Ezh2 at genes of choice depending on the biological demands of the cells. It has been noticed in drosophila that accessory proteins are necessary for recruitment of heterochromatin protein and thus chromatin condensation at selected loci (50). Whether such a phenomenon applies to mammalian embryonic stem cells and if so, identifying specific factors, remain open for future experimentation. In the event specific recruitment factors are found, utilizing these factors to reprogram cells via epigenetic modifications at specific loci would be an interesting idea to pursue. This method spans beyond the reprogramming strategies that are employed today.

In the second chapter I studied the effects of androgen signaling on prostate cancer cellular proliferation. The principle findings of this chapter are that Androgens mediate AMPK and PGC-1α signaling to yield increased cellular ATP levels, which afford a distinct proliferative advantage to two established cellular models of prostate cancer. Perhaps the most notable finding of this section is that this axis coopts the OXPHOS pathway along with the glycolytic pathway, which is well established as the choice of ATP production of most cancers. The cancer cells utilizing the glycolytic pathway have been well described particularly in tumors subject to hypoxic conditions (68). Radiolabelled fatty acid and glucose oxidation assays prove that acetyl CoA, the molecule of entry into the TCA cycle, is increased upon androgen signaling via AMPK mediated glucose and fatty acid oxidation. Modern metabolomics approaches using GC/MS and Seahorse technologies further prove that androgens signal via AMPK PGC-1α, increase OXPHOS while androgen treatment alone increases the TCA cycle intermediates. These findings complemented the observation that increased mitochondrial numbers dependent on the same signaling axis. Given the observations that CaMKKβ, AMPK and PGC-1α, are all increased in clinical samples of prostate cancers it is possible that this particular pathway has immense potential for the development of drug targets. Targeting the Androgen mediated AMPK-PGC-1α pathway concurrently with existing drugs is an option, which deserves further investigation. In

order to pursue this possibility at the time of writing this dissertation we were in preparation of inducible AMPK and PGC-1α luciferase-tagged cell lines, which will eventually be introduced into mice to study the effects of this pathway *in vivo*. Identifying the particular molecules which provide a growth and proliferative advantage to prostate cancer cells via the androgen regulated CaMKKβ, AMPK and PGC-1α signaling axis would require higher order experiments of flux measurements using mass spectrometric based techniques. At the time of writing this dissertation we were in the process of proposing specific experimental schemes employing MS to investigate differentially expressed candidates in prostate cancers downstream of the AR driven CaMKKβ, AMPK and PGC-1α signaling axis. These experiments could potentially uncover druggable molecules of choice present in higher quantities in rampantly proliferating cancer cells as opposed to healthy normal prostate cellular types. It has been suggested by several groups that ^{18}F-fluoropropionic acid and ^{11}C-acetate are better biomarkers compared to the glycolytic marker ^{18}F-fluorodeoxyglucose used in PET (positron emission tomography) imaging of prostate cancer (85-88). We have shown that AR-AMPK- PGC-1α signaling plays an important role in fatty acid oxidation. This in turn leads to the idea of exploring the possibility of utilizing AMPK and PGC-1α as biomarkers of prostate cancer. To ascertain whether AMPK and PGC-1α serve as representative biomarkers of prostate cancer would require further investigation of expression levels of these molecules in different grades of clinical prostate cancer samples. Another question, which deserves further probing, is whether AR-AMPK- PGC-1α signaling plays a role in the transformation process of prostate cancers from lower grades to higher grades of Gleason scores. As the isoformic variant of CaMKKβ expressed in the prostate has a restricted profile, using small molecular inhibitors against CaMKKβ with lesser off target effects than the already used inhibitor STO-609C is an idea which will be explored in future. As AMPK is one of the major energy homeostatic molecules which functions in several biological reactions globally targeting AMPK in prostate cancer may not be very pragmatic from a therapeutic perspective.

The same case applies to PGC-1α which is an essential cofactor of mitochondrial biogenesis. However using a combination of therapies where the isoformic variant of CaMKKβ is targeted through orally administered drugs together with locally administered inhibitors of AMPK and PGC-1α are options, which warrant further study. Identifying the nodal intersects of signaling pathway which are coopted with AR driven CaMKKβ, AMPK and PGC-1α in prostate cancer and developing inhibitors which target key molecules at nodes is another avenue which may be key to finding next generation of drugs with higher efficacy. Investigating whether dysregulated AMPK and PGC-1α play roles in other types of cancers and degenerative diseases where mitochondria play essential roles are of course questions, which are worth pursuing in future.

Finally in the third chapter I utilized a model system consisting of trophoblastic and embryonic stem cells with and without Dicer to show the effects of the loss of Dicer on genetic imprinting at specific loci. In this chapter I have particularly focused on the Prader Willi (PWCR) and Angelman's critical region associated genes and the paternally expressed Sfmbt2 gene enriched in the extraembryonic lineage. The PWCR region is one the most complicated genetic regions of the human genome playing vital roles in maintaining genetic imprinting (117, 118, 125). Defects in imprinting and therefore aberrant expression of genes in this region can lead to severe diseases such as the Angelmans syndrome and the Prader Willi syndrome. Our group is the first to uncover in close detail that expression differences in these regions are affected by loss of Dicer in embryonic stem cells, which in turn may result from changes in H3K9me2 modifications at the promoters. Mechanistic investigations point to a situation where epigenetic and post-transcriptional level regulation dependent on miRNA candidates can play potential roles in maintaining imprinting in mammals. The observations made in this chapter suggest that there could be new avenues for further investigation of the use of, selected microRNAs for therapeutics of imprinting related genetic defects.

Taken together this dissertation provides novel information on cellular dynamics of several different models *in vitro,* governed by unique molecular genetic backgrounds and mechanistic events. The combined findings presented herein converge to specific cases suggesting potential for further experiments on molecular strategies. Namely, to treat imprinting related illnesses, to reduce proliferative capacity of prostate cancers and ultimately, to develop cell replacement-based therapeutics.

REFERENCES

1. Turner W. The Cell Theory, Past and Present. J Anat Physiol. 1890;24(Pt 2):253-87. Epub 1890/01/01.

2. Tavassoli M. The cell theory: a foundation to the edifice of biology. Am J Pathol. 1980;98(1):44. Epub 1980/01/01.

3. Donaldson IM. Robert Hooke's Micrographia of 1665 and 1667. J R Coll Physicians Edinb. 2010;40(4):374-6. Epub 2010/12/07.

4. Westerlund JF, Fairbanks DJ. Gregor Mendel's classic paper and the nature of science in genetics courses. Hereditas. 2010;147(6):293-303. Epub 2010/12/21.

5. Paweletz N. Walther Flemming: pioneer of mitosis research. Nat Rev Mol Cell Biol. 2001;2(1):72-5. Epub 2001/06/20.

6. Watson JD, Crick FH. Molecular structure of nucleic acids; a structure for deoxyribose nucleic acid. Nature. 1953;171(4356):737-8. Epub 1953/04/25.

7. Meselson M, Stahl FW. The Replication of DNA in Escherichia Coli. Proc Natl Acad Sci U S A. 1958;44(7):671-82. Epub 1958/07/15.

8. Sharp PA. The discovery of split genes and RNA splicing. Trends Biochem Sci. 2005;30(6):279-81. Epub 2005/06/14.

9. Leder P, Nirenberg MW. Rna Codewords and Protein Synthesis, 3. On the Nucleotide Sequence of a Cysteine and a Leucine Rna Codeword. Proc Natl Acad Sci U S A. 1964;52:1521-9. Epub 1964/12/01.

10. Bernfield MR, Nirenberg MW. Rna Codewords and Protein Synthesis. The Nucleotide Sequences of Multiple Codewords for Phenylalanine, Serine, Leucine, and Proline. Science. 1965;147(3657):479-84. Epub 1965/01/29.

11. Khoury GA, Baliban RC, Floudas CA. Proteome-wide post-translational modification statistics: frequency analysis and curation of the swiss-prot database. Sci Rep. 2011;1. Epub 2011/10/29.

12. Bartel DP, Chen CZ. Micromanagers of gene expression: the potentially widespread influence of metazoan microRNAs. Nat Rev Genet. 2004;5(5):396-400. Epub 2004/05/15.

13. Petersen CP, Bordeleau ME, Pelletier J, Sharp PA. Short RNAs repress translation after initiation in mammalian cells. Mol Cell. 2006;21(4):533-42. Epub 2006/02/18.

14. Bartel DP. MicroRNAs: genomics, biogenesis, mechanism, and function. Cell. 2004;116(2):281-97. Epub 2004/01/28.

15. Reid JG, Nagaraja AK, Lynn FC, Drabek RB, Muzny DM, Shaw CA, et al. Mouse let-7 miRNA populations exhibit RNA editing that is constrained in the 5'-seed/ cleavage/anchor regions and stabilize predicted mmu-let-7a:mRNA duplexes. Genome Res. 2008;18(10):1571-81. Epub 2008/07/11.

16. Gunaratne PH, Lin YC, Benham AL, Drnevich J, Coarfa C, Tennakoon JB, et al. Song exposure regulates known and novel microRNAs in the zebra finch auditory forebrain. BMC Genomics. 2011;12(1):277. Epub 2011/06/02.

17. Gunaratne PH, Creighton CJ, Watson M, Tennakoon JB. Large-scale integration of MicroRNA and gene expression data for identification of enriched microRNA-mRNA associations in biological systems. Methods Mol Biol. 2010;667:297-315. Epub 2010/09/10.

18. Barabasi AL, Oltvai ZN. Network biology: understanding the cell's functional organization. Nat Rev Genet. 2004;5(2):101-13. Epub 2004/01/22.

19. Rain JC, Selig L, De Reuse H, Battaglia V, Reverdy C, Simon S, et al. The protein-protein interaction map of Helicobacter pylori. Nature. 2001;409(6817):211-5. Epub 2001/02/24.

20. Tyagi M, Hashimoto K, Shoemaker BA, Wuchty S, Panchenko AR. Large-scale mapping of human protein interactome using structural complexes. EMBO Rep. 2012;13(3):266-71. Epub 2012/01/21.

21. McDermott J, Guerquin M, Frazier Z, Chang AN, Samudrala R. BIOVERSE: enhancements to the framework for structural, functional and contextual modeling of proteins and proteomes. Nucleic Acids Res. 2005;33(Web Server issue):W324-5. Epub 2005/06/28.

22. McDermott JE, Wang J, Mitchell H, Webb-Robertson BJ, Hafen R, Ramey J, et al. Challenges in Biomarker Discovery: Combining Expert Insights with Statistical Analysis of Complex Omics Data. Expert Opin Med Diagn. 2013;7(1):37-51. Epub 2013/01/22.

23. Bernstein E, Kim SY, Carmell MA, Murchison EP, Alcorn H, Li MZ, et al. Dicer is essential for mouse development. Nat Genet. 2003;35(3):215-7. Epub 2003/10/07.

24. Kanellopoulou C, Muljo SA, Kung AL, Ganesan S, Drapkin R, Jenuwein T, et al. Dicer-deficient mouse embryonic stem cells are defective in differentiation and centromeric silencing. Genes Dev. 2005;19(4):489-501. Epub 2005/02/17.

25. Kanellopoulou C, Muljo SA, Dimitrov SD, Chen X, Colin C, Plath K, et al. X chromosome inactivation in the absence of Dicer. Proc Natl Acad Sci U S A. 2009;106(4):1122-7. Epub 2009/01/24.

26. Sobel RE, Sadar MD. Cell lines used in prostate cancer research: a compendium of old and new lines--part 1. J Urol. 2005;173(2):342-59. Epub 2005/01/12.

27. Sobel RE, Sadar MD. Cell lines used in prostate cancer research: a compendium of old and new lines--part 2. J Urol. 2005;173(2):360-72. Epub 2005/01/12.

28. Shen MM, Abate-Shen C. Molecular genetics of prostate cancer: new prospects for old challenges. Genes Dev. 2010;24(18):1967-2000. Epub 2010/09/17.

29. Knudsen KE, Scher HI. Starving the addiction: new opportunities for durable suppression of AR signaling in prostate cancer. Clin Cancer Res. 2009;15(15):4792-8. Epub 2009/07/30.

30. Knudsen KE, Penning TM. Partners in crime: deregulation of AR activity and androgen synthesis in prostate cancer. Trends Endocrinol Metab. 2010;21(5):315-24. Epub 2010/02/09.

31. Shi Y, Han JJ, Tennakoon JB, Mehta FF, Merchant FA, Burns AR, et al. Androgens promote prostate cancer cell growth through induction of autophagy. Mol Endocrinol. 2013;27(2):280-95. Epub 2012/12/20.

32. Frigo DE, Howe MK, Wittmann BM, Brunner AM, Cushman I, Wang Q, et al. CaM kinase kinase beta-mediated activation of the growth regulatory kinase AMPK is required for androgen-dependent migration of prostate cancer cells. Cancer Res. 2011;71(2):528-37. Epub 2010/11/26.

33. Tanaka S, Kunath T, Hadjantonakis AK, Nagy A, Rossant J. Promotion of trophoblast stem cell proliferation by FGF4. Science. 1998;282(5396):2072-5. Epub 1998/12/16.

34. Murchison EP, Stein P, Xuan Z, Pan H, Zhang MQ, Schultz RM, et al. Critical roles for Dicer in the female germline. Genes Dev. 2007;21(6):682-93. Epub 2007/03/21.

35. Shohet JM, Ghosh R, Coarfa C, Ludwig A, Benham AL, Chen Z, et al. A genome-wide search for promoters that respond to increased MYCN reveals both new oncogenic and tumor suppressor microRNAs associated with aggressive neuroblastoma. Cancer Res. 2011;71(11):3841-51. Epub 2011/04/19.

36. Coarfa C, Yu F, Miller CA, Chen Z, Harris RA, Milosavljevic A. Pash 3.0: A versatile software package for read mapping and integrative analysis of genomic and epigenomic variation using massively parallel DNA sequencing. BMC Bioinformatics. 2010;11:572. Epub 2010/11/26.

37. Bernstein E, Caudy AA, Hammond SM, Hannon GJ. Role for a bidentate ribonuclease in the initiation step of RNA interference. Nature. 2001;409(6818):363-6. Epub 2001/02/24.

38. Gan J, Tropea JE, Austin BP, Court DL, Waugh DS, Ji X. Structural insight into the mechanism of double-stranded RNA processing by ribonuclease III. Cell. 2006;124(2):355-66. Epub 2006/01/28.

39. Macrae IJ, Zhou K, Li F, Repic A, Brooks AN, Cande WZ, et al. Structural basis for double-stranded RNA processing by Dicer. Science. 2006;311(5758):195-8. Epub 2006/01/18.

40. Babiarz JE, Ruby JG, Wang Y, Bartel DP, Blelloch R. Mouse ES cells express endogenous shRNAs, siRNAs, and other Microprocessor-independent, Dicer-dependent small RNAs. Genes Dev. 2008;22(20):2773-85. Epub 2008/10/17.

41. Calabrese JM, Seila AC, Yeo GW, Sharp PA. RNA sequence analysis defines Dicer's role in mouse embryonic stem cells. Proc Natl Acad Sci U S A. 2007;104(46):18097-102. Epub 2007/11/09.

42. Bao N, Lye KW, Barton MK. MicroRNA binding sites in Arabidopsis class III HD-ZIP mRNAs are required for methylation of the template chromosome. Dev Cell. 2004;7(5):653-62. Epub 2004/11/05.

43. Lippman Z, Martienssen R. The role of RNA interference in heterochromatic silencing. Nature. 2004;431(7006):364-70. Epub 2004/09/17.

44. Reinhart BJ, Bartel DP. Small RNAs correspond to centromere heterochromatic repeats. Science. 2002;297(5588):1831. Epub 2002/08/24.

45. Das PP, Bagijn MP, Goldstein LD, Woolford JR, Lehrbach NJ, Sapetschnig A, et al. Piwi and piRNAs act upstream of an endogenous siRNA pathway to suppress Tc3 transposon mobility in the Caenorhabditis elegans germline. Mol Cell. 2008;31(1):79-90. Epub 2008/06/24.

46. Mochizuki K, Fine NA, Fujisawa T, Gorovsky MA. Analysis of a piwi-related gene implicates small RNAs in genome rearrangement in tetrahymena. Cell. 2002;110(6):689-99. Epub 2002/09/26.

47. Viswanathan SR, Daley GQ, Gregory RI. Selective blockade of microRNA processing by Lin28. Science. 2008;320(5872):97-100. Epub 2008/02/23.

48. Marson A, Levine SS, Cole MF, Frampton GM, Brambrink T, Johnstone S, et al. Connecting microRNA genes to the core transcriptional regulatory circuitry of embryonic stem cells. Cell. 2008;134(3):521-33. Epub 2008/08/12.

49. Sinkkonen L, Hugenschmidt T, Berninger P, Gaidatzis D, Mohn F, Artus-Revel CG, et al. MicroRNAs control de novo DNA methylation through regulation of transcriptional repressors in mouse embryonic stem cells. Nat Struct Mol Biol. 2008;15(3):259-67. Epub 2008/03/04.

50. Boyer LA, Plath K, Zeitlinger J, Brambrink T, Medeiros LA, Lee TI, et al. Polycomb complexes repress developmental regulators in murine embryonic stem cells. Nature. 2006;441(7091):349-53. Epub 2006/04/21.

51. Bernstein BE, Mikkelsen TS, Xie X, Kamal M, Huebert DJ, Cuff J, et al. A bivalent chromatin structure marks key developmental genes in embryonic stem cells. Cell. 2006;125(2):315-26. Epub 2006/04/25.

52. Huff JT, Plocik AM, Guthrie C, Yamamoto KR. Reciprocal intronic and exonic histone modification regions in humans. Nat Struct Mol Biol. 2010;17(12):1495-9. Epub 2010/11/09.

53. Andersson R, Enroth S, Rada-Iglesias A, Wadelius C, Komorowski J. Nucleosomes are well positioned in exons and carry characteristic histone modifications. Genome Res. 2009;19(10):1732-41. Epub 2009/08/19.

54. Tilgner H, Nikolaou C, Althammer S, Sammeth M, Beato M, Valcarcel J, et al. Nucleosome positioning as a determinant of exon recognition. Nat Struct Mol Biol. 2009;16(9):996-1001. Epub 2009/08/18.

55. Jenuwein T. Molecular biology. An RNA-guided pathway for the epigenome. Science. 2002;297(5590):2215-8. Epub 2002/09/28.

56. Jenuwein T. The epigenetic magic of histone lysine methylation. Febs J. 2006;273(14):3121-35. Epub 2006/07/22.

57. Bannister AJ, Kouzarides T. Regulation of chromatin by histone modifications. Cell Res. 2011;21(3):381-95. Epub 2011/02/16.

58. Gu P, Xu X, Le Menuet D, Chung AC, Cooney AJ. Differential recruitment of methyl CpG-binding domain factors and DNA methyltransferases by the orphan receptor germ cell nuclear factor initiates the repression and silencing of Oct4. Stem Cells. 2011;29(7):1041-51. Epub 2011/05/25.

59. Newman MA, Thomson JM, Hammond SM. Lin-28 interaction with the Let-7 precursor loop mediates regulated microRNA processing. Rna. 2008;14(8):1539-49. Epub 2008/06/21.

60. Fuhrmann G, Chung AC, Jackson KJ, Hummelke G, Baniahmad A, Sutter J, et al. Mouse germline restriction of Oct4 expression by germ cell nuclear factor. Dev Cell. 2001;1(3):377-87. Epub 2001/11/13.

61. Hummelke GC, Cooney AJ. Germ cell nuclear factor is a transcriptional repressor essential for embryonic development. Front Biosci. 2001;6:D1186-91. Epub 2001/10/02.

62. Ringrose L, Paro R. Epigenetic regulation of cellular memory by the Polycomb and Trithorax group proteins. Annu Rev Genet. 2004;38:413-43. Epub 2004/12/01.

63. Koves TR, Ussher JR, Noland RC, Slentz D, Mosedale M, Ilkayeva O, et al. Mitochondrial overload and incomplete fatty acid oxidation contribute to skeletal muscle insulin resistance. Cell Metab. 2008;7(1):45-56. Epub 2008/01/08.

64. Shi Y, Han JJ, Tennakoon JB, Mehta FF, Merchant FA, Burns AR, et al. Androgens Promote Prostate Cancer Cell Growth through Induction of Autophagy. Mol Endocrinol. 2012. Epub 2012/12/20.

65. Frigo DE, McDonnell DP. Differential effects of prostate cancer therapeutics on neuroendocrine transdifferentiation. Mol Cancer Ther. 2008;7(3):659-69. Epub 2008/03/19.

66. Koves TR, Ussher JR, Noland RC, Slentz D, Mosedale M, Ilkayeva O, et al. Mitochondrial overload and incomplete fatty acid oxidation contribute to skeletal muscle insulin resistance. Cell Metab. 2008;7(1):45-56. Epub 2008/01/08.

67. Collins CL, Bode BP, Souba WW, Abcouwer SF. Multiwell 14CO2-capture assay for evaluation of substrate oxidation rates of cells in culture. Biotechniques. 1998;24(5):803-8. Epub 1998/05/20.

68. Warburg O. On the origin of cancer cells. Science. 1956;123(3191):309-14. Epub 1956/02/24.

69. Hanahan D, Weinberg RA. Hallmarks of cancer: the next generation. Cell. 2011;144(5):646-74. Epub 2011/03/08.

70. Ertel A, Tsirigos A, Whitaker-Menezes D, Birbe RC, Pavlides S, Martinez-Outschoorn UE, et al. Is cancer a metabolic rebellion against host aging? In the quest for immortality, tumor cells try to save themselves by boosting mitochondrial metabolism. Cell Cycle. 2012;11(2):253-63. Epub 2012/01/12.

71. DeBerardinis RJ, Lum JJ, Hatzivassiliou G, Thompson CB. The biology of cancer: metabolic reprogramming fuels cell growth and proliferation. Cell Metab. 2008;7(1):11-20. Epub 2008/01/08.

72. Dakubo GD, Parr RL, Costello LC, Franklin RB, Thayer RE. Altered metabolism and mitochondrial genome in prostate cancer. J Clin Pathol. 2006;59(1):10-6. Epub 2006/01/06.

73. Costello LC, Franklin RB, Feng P. Mitochondrial function, zinc, and intermediary metabolism relationships in normal prostate and prostate cancer. Mitochondrion. 2005;5(3):143-53. Epub 2005/07/30.

74. Bhalla K, Hwang BJ, Dewi RE, Ou L, Twaddel W, Fang HB, et al. PGC1alpha promotes tumor growth by inducing gene expression programs supporting lipogenesis. Cancer Res. 2011;71(21):6888-98. Epub 2011/09/15.

75. Skrtic M, Sriskanthadevan S, Jhas B, Gebbia M, Wang X, Wang Z, et al. Inhibition of mitochondrial translation as a therapeutic strategy for human acute myeloid leukemia. Cancer Cell. 2011;20(5):674-88. Epub 2011/11/19.

76. Guo JY, Chen HY, Mathew R, Fan J, Strohecker AM, Karsli-Uzunbas G, et al. Activated Ras requires autophagy to maintain oxidative metabolism and tumorigenesis. Genes Dev. 2011;25(5):460-70. Epub 2011/02/15.

77. Xiao D, Powolny AA, Moura MB, Kelley EE, Bommareddy A, Kim SH, et al. Phenethyl isothiocyanate inhibits oxidative phosphorylation to trigger reactive oxygen species-mediated death of human prostate cancer cells. J Biol Chem. 2010;285(34):26558-69. Epub 2010/06/24.

78. Chang CY, Kazmin D, Jasper JS, Kunder R, Zuercher WJ, McDonnell DP. The metabolic regulator ERRalpha, a downstream target of HER2/IGF-1R, as a therapeutic target in breast cancer. Cancer Cell. 2011;20(4):500-10. Epub 2011/10/22.

79. Cormio A, Guerra F, Cormio G, Pesce V, Fracasso F, Loizzi V, et al. The PGC-1alpha-dependent pathway of mitochondrial biogenesis is upregulated in type I endometrial cancer. Biochem Biophys Res Commun. 2009;390(4):1182-5. Epub 2009/10/29.

80. Hu J, Hwang SS, Liesa M, Gan B, Sahin E, Jaskelioff M, et al. Antitelomerase therapy provokes ALT and mitochondrial adaptive mechanisms in cancer. Cell. 2012;148(4):651-63. Epub 2012/02/22.

81. Ramanathan A, Wang C, Schreiber SL. Perturbational profiling of a cell-line model of tumorigenesis by using metabolic measurements. Proc Natl Acad Sci U S A. 2005;102(17):5992-7. Epub 2005/04/21.

82. Stoss O, Werther M, Zielinski D, Middel P, Jost N, Ruschoff J, et al. Transcriptional profiling of transurethral resection samples provides insight into molecular mechanisms of hormone refractory prostate cancer. Prostate Cancer Prostatic Dis. 2008;11(2):166-72. Epub 2007/07/25.

83. Whitaker-Menezes D, Martinez-Outschoorn UE, Flomenberg N, Birbe RC, Witkiewicz AK, Howell A, et al. Hyperactivation of oxidative mitochondrial metabolism in epithelial cancer cells in situ: visualizing the therapeutic effects of metformin in tumor tissue. Cell Cycle. 2011;10(23):4047-64. Epub 2011/12/03.

84. Chen SD, Yang DI, Lin TK, Shaw FZ, Liou CW, Chuang YC. Roles of Oxidative Stress, Apoptosis, PGC-1alpha and Mitochondrial Biogenesis in Cerebral Ischemia. Int J Mol Sci. 2011;12(10):7199-215. Epub 2011/11/11.

85. Oyama N, Miller TR, Dehdashti F, Siegel BA, Fischer KC, Michalski JM, et al. 11C-acetate PET imaging of prostate cancer: detection of recurrent disease at PSA relapse. J Nucl Med. 2003;44(4):549-55. Epub 2003/04/08.

86. Hofer C, Laubenbacher C, Block T, Breul J, Hartung R, Schwaiger M. Fluorine-18-fluorodeoxyglucose positron emission tomography is useless for the detection of local recurrence after radical prostatectomy. Eur Urol. 1999;36(1):31-5. Epub 1999/06/12.

87. Pillarsetty N, Punzalan B, Larson SM. 2-18F-Fluoropropionic acid as a PET imaging agent for prostate cancer. J Nucl Med. 2009;50(10):1709-14. Epub 2009/09/18.

88. Yu EY, Muzi M, Hackenbracht JA, Rezvani BB, Link JM, Montgomery RB, et al. C11-acetate and F-18 FDG PET for men with prostate cancer bone metastases: relative findings and response to therapy. Clin Nucl Med. 2011;36(3):192-8. Epub 2011/02/03.

89. Taylor BS, Schultz N, Hieronymus H, Gopalan A, Xiao Y, Carver BS, et al. Integrative genomic profiling of human prostate cancer. Cancer Cell. 2010;18(1):11-22. Epub 2010/06/29.

90. Karacosta LG, Foster BA, Azabdaftari G, Feliciano DM, Edelman AM. A regulatory feedback loop between Ca2+/calmodulin-dependent protein kinase kinase 2 (CaMKK2) and the androgen receptor in prostate cancer progression. J Biol Chem. 2012;287(29):24832-43. Epub 2012/06/02.

91. Massie CE, Lynch A, Ramos-Montoya A, Boren J, Stark R, Fazli L, et al. The androgen receptor fuels prostate cancer by regulating central metabolism and biosynthesis. Embo J. 2011;30(13):2719-33. Epub 2011/05/24.

92. Jung SN, Park IJ, Kim MJ, Kang I, Choe W, Kim SS, et al. Down-regulation of AMP-activated protein kinase sensitizes DU145 carcinoma to Fas-induced apoptosis via c-FLIP degradation. Exp Cell Res. 2009;315(14):2433-41. Epub 2009/05/30.

93. Jeon SM, Chandel NS, Hay N. AMPK regulates NADPH homeostasis to promote tumour cell survival during energy stress. Nature. 2012;485(7400):661-5. Epub 2012/06/05.

94. Laderoute KR, Amin K, Calaoagan JM, Knapp M, Le T, Orduna J, et al. 5'-AMP-activated protein kinase (AMPK) is induced by low-oxygen and glucose deprivation conditions found in solid-tumor microenvironments. Mol Cell Biol. 2006;26(14):5336-47. Epub 2006/07/01.

95. Moon JS, Jin WJ, Kwak JH, Kim HJ, Yun MJ, Kim JW, et al. Androgen stimulates glycolysis for de novo lipid synthesis by increasing the activities of hexokinase 2 and 6-phosphofructo-2-kinase/fructose-2,6-bisphosphatase 2 in prostate cancer cells. Biochem J. 2011;433(1):225-33. Epub 2010/10/21.

96. Liu Y, Zuckier LS, Ghesani NV. Dominant uptake of fatty acid over glucose by prostate cells: a potential new diagnostic and therapeutic approach. Anticancer Res. 2010;30(2):369-74. Epub 2010/03/25.

97. Zha S, Ferdinandusse S, Hicks JL, Denis S, Dunn TA, Wanders RJ, et al. Peroxisomal branched chain fatty acid beta-oxidation pathway is upregulated in prostate cancer. Prostate. 2005;63(4):316-23. Epub 2004/12/16.

98. Liu P, Ramachandran S, Ali Seyed M, Scharer CD, Laycock N, Dalton WB, et al. Sex-determining region Y box 4 is a transforming oncogene in human prostate cancer cells. Cancer Res. 2006;66(8):4011-9. Epub 2006/04/19.

99. Jager S, Handschin C, St-Pierre J, Spiegelman BM. AMP-activated protein kinase (AMPK) action in skeletal muscle via direct phosphorylation of PGC-1alpha. Proc Natl Acad Sci U S A. 2007;104(29):12017-22. Epub 2007/07/05.

100. Varambally S, Yu J, Laxman B, Rhodes DR, Mehra R, Tomlins SA, et al. Integrative genomic and proteomic analysis of prostate cancer reveals signatures of metastatic progression. Cancer Cell. 2005;8(5):393-406. Epub 2005/11/16.

101. Arredouani MS, Lu B, Bhasin M, Eljanne M, Yue W, Mosquera JM, et al. Identification of the transcription factor single-minded homologue 2 as a potential biomarker and immunotherapy target in prostate cancer. Clin Cancer Res. 2009;15(18):5794-802. Epub 2009/09/10.

102. Chandran UR, Ma C, Dhir R, Bisceglia M, Lyons-Weiler M, Liang W, et al. Gene expression profiles of prostate cancer reveal involvement of multiple molecular pathways in the metastatic process. BMC Cancer. 2007;7:64. Epub 2007/04/14.

103. Tamura K, Furihata M, Tsunoda T, Ashida S, Takata R, Obara W, et al. Molecular features of hormone-refractory prostate cancer cells by genome-wide gene expression profiles. Cancer Res. 2007;67(11):5117-25. Epub 2007/06/05.

104. Shiota M, Yokomizo A, Tada Y, Inokuchi J, Tatsugami K, Kuroiwa K, et al. Peroxisome proliferator-activated receptor gamma coactivator-1alpha interacts with the androgen receptor (AR) and promotes prostate cancer cell growth by activating the AR. Mol Endocrinol. 2010;24(1):114-27. Epub 2009/11/04.

105. Marin-Valencia I, Yang C, Mashimo T, Cho S, Baek H, Yang XL, et al. Analysis of tumor metabolism reveals mitochondrial glucose oxidation in genetically diverse human glioblastomas in the mouse brain in vivo. Cell Metab. 2012;15(6):827-37. Epub 2012/06/12.

106. Sahin E, Colla S, Liesa M, Moslehi J, Muller FL, Guo M, et al. Telomere dysfunction induces metabolic and mitochondrial compromise. Nature. 2011;470(7334):359-65. Epub 2011/02/11.

107. Ding Z, Wu CJ, Jaskelioff M, Ivanova E, Kost-Alimova M, Protopopov A, et al. Telomerase reactivation following telomere dysfunction yields murine prostate tumors with bone metastases. Cell. 2012;148(5):896-907. Epub 2012/02/22.

108. O'Mahony F, Razandi M, Pedram A, Harvey BJ, Levin ER. Estrogen modulates metabolic pathway adaptation to available glucose in breast cancer cells. Mol Endocrinol. 2012;26(12):2058-70. Epub 2012/10/03.

109. Xiang X, Saha AK, Wen R, Ruderman NB, Luo Z. AMP-activated protein kinase activators can inhibit the growth of prostate cancer cells by multiple mechanisms. Biochem Biophys Res Commun. 2004;321(1):161-7. Epub 2004/09/11.

110. Irrcher I, Ljubicic V, Kirwan AF, Hood DA. AMP-activated protein kinase-regulated activation of the PGC-1alpha promoter in skeletal muscle cells. PLoS One. 2008;3(10):e3614. Epub 2008/11/01.

111. Klimcakova E, Chenard V, McGuirk S, Germain D, Avizonis D, Muller WJ, et al. PGC-1alpha promotes the growth of ErbB2/Neu-induced mammary tumors by regulating nutrient supply. Cancer Res. 2012;72(6):1538-46. Epub 2012/01/24.

112. Ruby JG, Jan CH, Bartel DP. Intronic microRNA precursors that bypass Drosha processing. Nature. 2007;448(7149):83-6. Epub 2007/06/26.

113. Boutz PL, Chawla G, Stoilov P, Black DL. MicroRNAs regulate the expression of the alternative splicing factor nPTB during muscle development. Genes Dev. 2007;21(1):71-84. Epub 2007/01/11.

114. Barlow DP. Genomic imprinting: a mammalian epigenetic discovery model. Annu Rev Genet. 2011;45:379-403. Epub 2011/09/29.

115. Edwards CA, Ferguson-Smith AC. Mechanisms regulating imprinted genes in clusters. Curr Opin Cell Biol. 2007;19(3):281-9. Epub 2007/05/01.

116. Wan LB, Bartolomei MS. Regulation of imprinting in clusters: noncoding RNAs versus insulators. Adv Genet. 2008;61:207-23. Epub 2008/02/20.

117. Kim SJ, Miller JL, Kuipers PJ, German JR, Beaudet AL, Sahoo T, et al. Unique and atypical deletions in Prader-Willi syndrome reveal distinct phenotypes. Eur J Hum Genet. 2012;20(3):283-90. Epub 2011/11/03.

118. Tan WH, Bacino CA, Skinner SA, Anselm I, Barbieri-Welge R, Bauer-Carlin A, et al. Angelman syndrome: Mutations influence features in early childhood. Am J Med Genet A. 2011;155A(1):81-90. Epub 2011/01/05.

119. Hublitz P, Albert M, Peters AH. Mechanisms of transcriptional repression by histone lysine methylation. Int J Dev Biol. 2009;53(2-3):335-54. Epub 2009/05/05.

120. Hudson QJ, Kulinski TM, Huetter SP, Barlow DP. Genomic imprinting mechanisms in embryonic and extraembryonic mouse tissues. Heredity (Edinb). 2010;105(1):45-56. Epub 2010/03/18.

121. Koerner MV, Pauler FM, Huang R, Barlow DP. The function of non-coding RNAs in genomic imprinting. Development. 2009;136(11):1771-83. Epub 2009/05/12.

122. Black JC, Whetstine JR. Chromatin landscape: methylation beyond transcription. Epigenetics. 2011;6(1):9-15. Epub 2010/09/22.

123. Caspary T, Cleary MA, Baker CC, Guan XJ, Tilghman SM. Multiple mechanisms regulate imprinting of the mouse distal chromosome 7 gene cluster. Mol Cell Biol. 1998;18(6):3466-74. Epub 1998/06/20.

124. Li E, Beard C, Jaenisch R. Role for DNA methylation in genomic imprinting. Nature. 1993;366(6453):362-5. Epub 1993/11/25.

125. Sahoo T, del Gaudio D, German JR, Shinawi M, Peters SU, Person RE, et al. Prader-Willi phenotype caused by paternal deficiency for the HBII-85 C/D box small nucleolar RNA cluster. Nat Genet. 2008;40(6):719-21. Epub 2008/05/27.

126. Royo Perez D, Monge Galindo L, Lopez Pison J, Perez Delgado R, Lafuente Hidalgo M, Pena Segura JL, et al. [Prader-willi and angelman syndromes: 21 years of experience.]. An Pediatr (Barc). 2012. Epub 2012/03/13. Sindromes de Prader-Willi y de Angelman. Expriencia de 21 anos.

127. Miyoshi N, Wagatsuma H, Wakana S, Shiroishi T, Nomura M, Aisaka K, et al. Identification of an imprinted gene, Meg3/Gtl2 and its human homologue MEG3, first mapped on mouse distal chromosome 12 and human chromosome 14q. Genes Cells. 2000;5(3):211-20. Epub 2000/04/12.

128. Zhang X, Rice K, Wang Y, Chen W, Zhong Y, Nakayama Y, et al. Maternally expressed gene 3 (MEG3) noncoding ribonucleic acid: isoform structure, expression, and functions. Endocrinology. 2010;151(3):939-47. Epub 2009/12/25.

129. Kuzmin A, Han Z, Golding MC, Mann MR, Latham KE, Varmuza S. The PcG gene Sfmbt2 is paternally expressed in extraembryonic tissues. Gene Expr Patterns. 2008;8(2):107-16. Epub 2007/11/21.

130. Riddle NC, Minoda A, Kharchenko PV, Alekseyenko AA, Schwartz YB, Tolstorukov MY, et al. Plasticity in patterns of histone modifications and chromosomal proteins in Drosophila heterochromatin. Genome Res. 2011;21(2):147-63. Epub 2010/12/24.

131. Lachner M, O'Sullivan RJ, Jenuwein T. An epigenetic road map for histone lysine methylation. J Cell Sci. 2003;116(Pt 11):2117-24. Epub 2003/05/06.

132. Gu P, Reid JG, Gao X, Shaw CA, Creighton C, Tran PL, et al. Novel microRNA candidates and miRNA-mRNA pairs in embryonic stem (ES) cells. PLoS One. 2008;3(7):e2548. Epub 2008/07/24.

133. Rehmsmeier M, Steffen P, Hochsmann M, Giegerich R. Fast and effective prediction of microRNA/target duplexes. Rna. 2004;10(10):1507-17. Epub 2004/09/24.

134. Kaneda M. Genomic imprinting in mammals-epigenetic parental memories. Differentiation. 2011;82(2):51-6. Epub 2011/06/18.

135. Okano H, Nakamura M, Yoshida K, Okada Y, Tsuji O, Nori S, et al. Steps toward safe cell therapy using induced pluripotent stem cells. Circ Res. 2013;112(3):523-33. Epub 2013/02/02.

APPENDIX

miRNA:mRNA duplex structures between the Sfmbt2 fulllength 3'UTR and mmu-mir-467a

1. Start Position 1581

TGGCAGCATTTTAAGGCATGGTGGTCCCTCAGGCTTTGAA

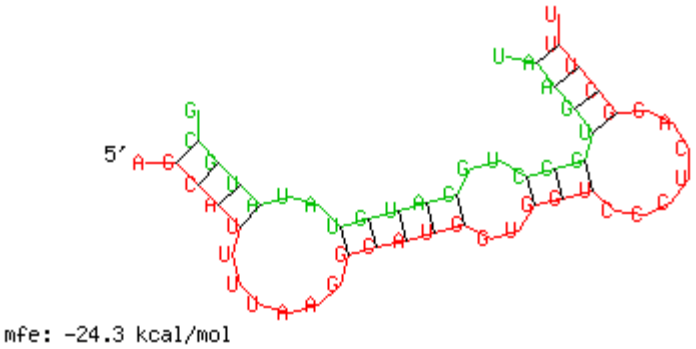

2. Start Position 968

CGTAGCATATGATAGCAGAGCAAATACCGGATCTGGATCT

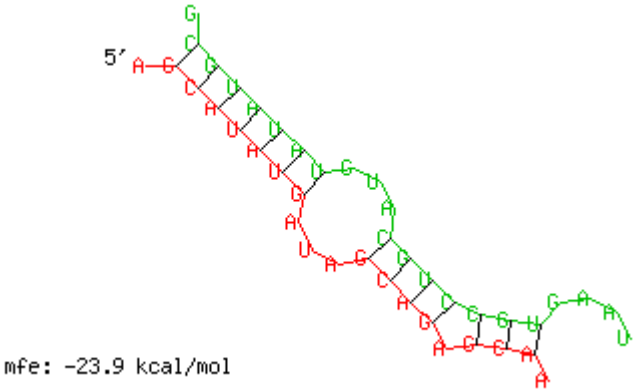

3. Start Position 968

GGATGGCATGCTCACGTGCGGAATGCAATTTTGCCACCGG

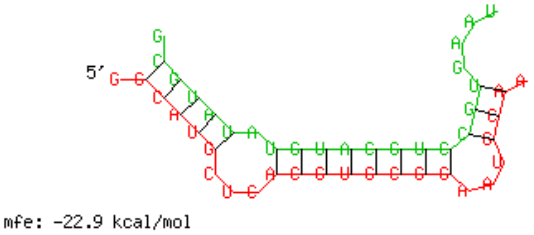

4. Start Position 2141

AATGACGCAGAGGAGGACGTGTTGCCTCAGAACATGGGGA

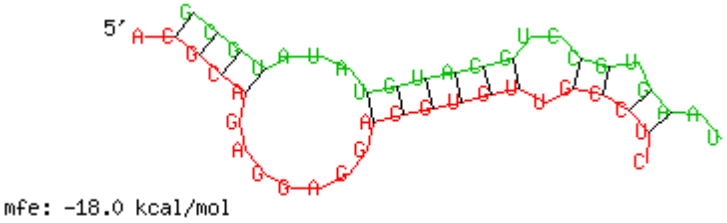

5. Start Position 3914

ACTAGGGTGGTTTGCAGGTATCCAAAAATATGCTATGACA

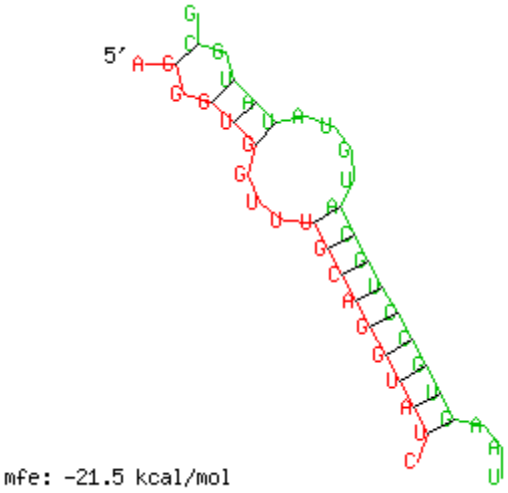

6. Start Position 85

CCTGGGCTTCGTGAAATGGCACAGTCATTGGTAATCTTCA

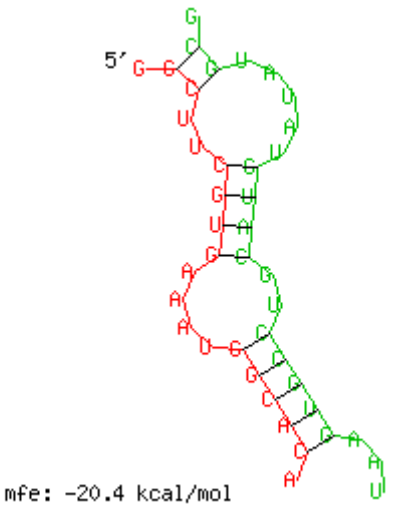

7. Start Position 1320

ATGAGCAGTTCAACCTGTGCCTGCAAAGCCAAAGGGGCTG

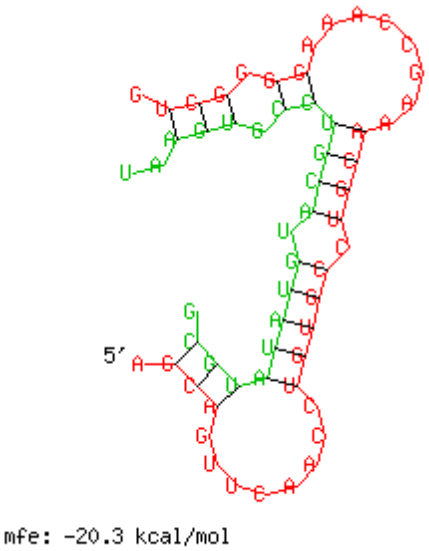

8. Start Position 1098

TTAGGACATTTAGTAGTGAGGCACTGGTACCTTCTCCCTG

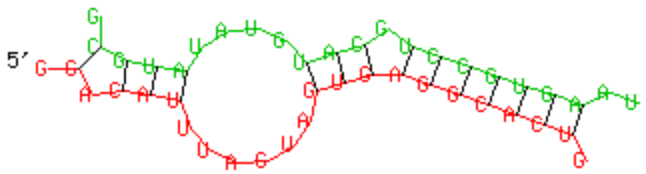

mfe: -20.1 kcal/mol

9. Start Position 1358

CTGAGGTACATTAGAGCATGGAGGACACCTCCACATCTTT

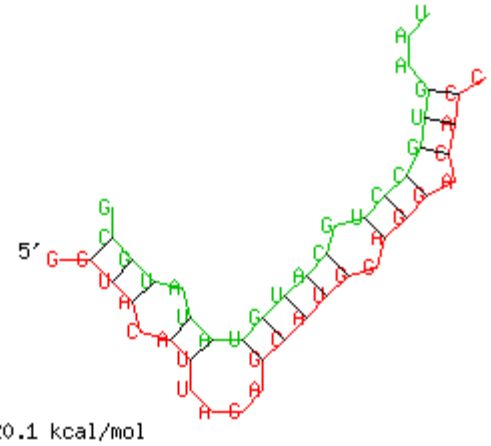

mfe: -20.1 kcal/mol

10. Start position 4451

ATCTTGTGTATTGGTGCATAAAAGAAAAAAAAAACAGTGTT

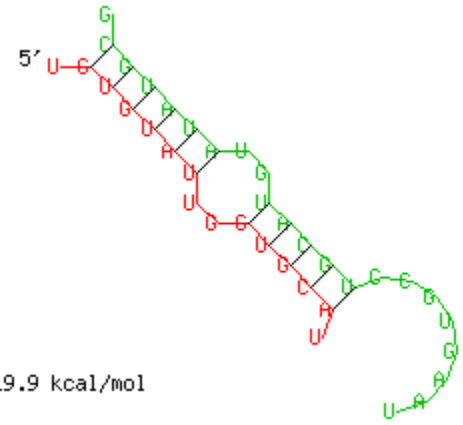

mfe: -19.9 kcal/mol

11. Start position 4141

GTAGGCCATGTCACAGAACCGAGGCAGAGCAGTGCTTTGA

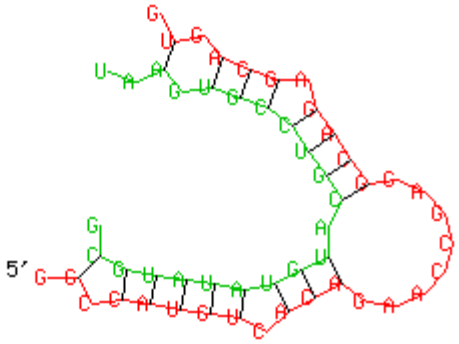

mfe: -19.7 kcal/mol

12. Start position 442

TGTCTGCCACACACGTGCAAGCAATTGTGATTTAGAGTCA

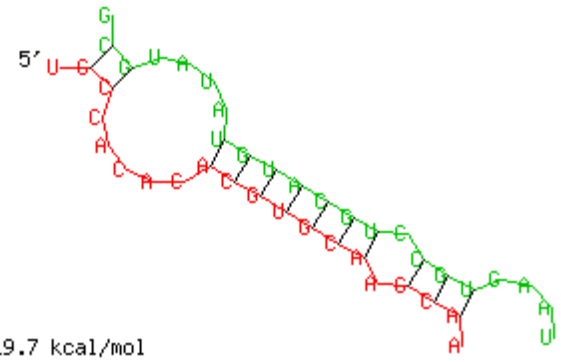

mfe: -19.7 kcal/mol

13. Start position 1915

CTCAGCCACATGCTTTTGGCCATAAATACTCAATCTACCA

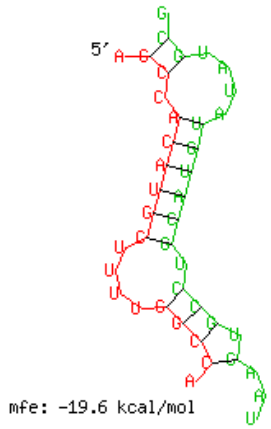

14. Start position 2217

GAAAGCATTAACAGAAAAGCCTGTCAGGACATGTCCACCA

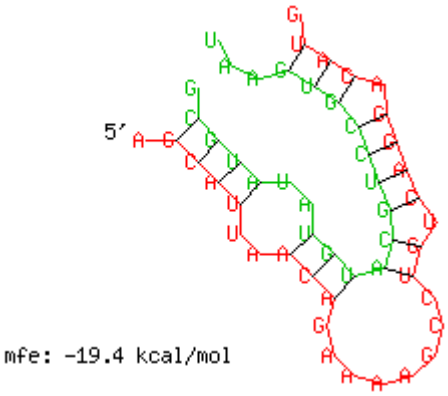

15. Start position 3060

GCCGGCTATACTGGCATTGCATATCTTTGCTATTCAACAA

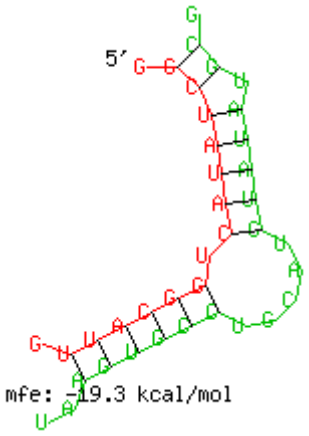

16.Start position 2076

CCATGGCATTGCTAGAATATGGTGTGCTTTTAGAACAAAT

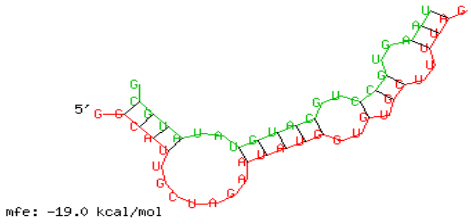

17.Start position 1030

TAATGGCCAACTTCATGTCCTTGGGTAACTTGCCACCACC

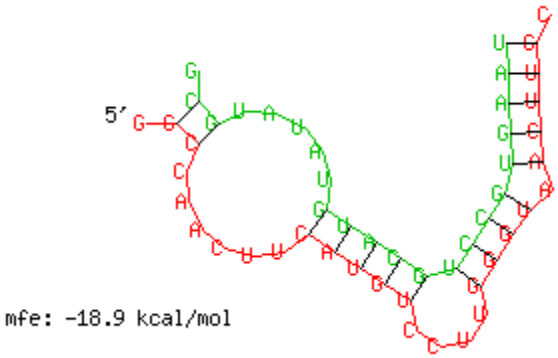

18. Start position 2444

TAGTGGCTCTCAATGTGCATGTCACACCCCCCCTCAGTAG

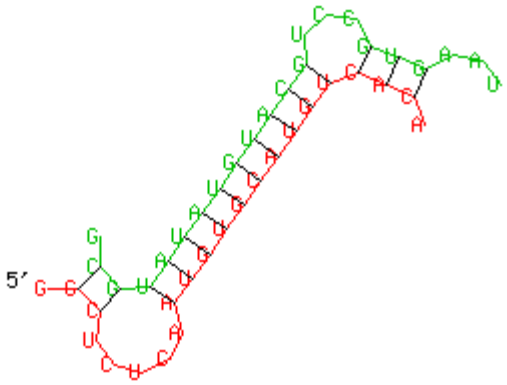

mfe: -18.9 kcal/mol

19. Start position 1843

GATAGGCTCTGTGGAGTTGGCTTGCATTTGGATTTCTCTC

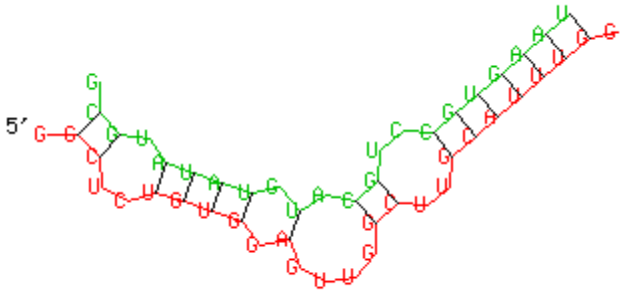

mfe: -18.8 kcal/mol

20. Start position 3404

ATTTTGCATGCTGTATGATTGGCTTTGTCTTCTATCTCCC

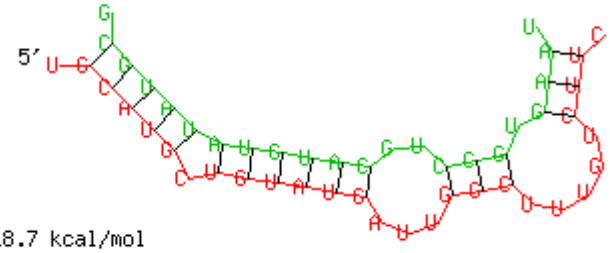

mfe: -18.7 kcal/mol

21. Start position 4562

TTTCCATGTACATAAAGGAAAATATATATCAG*

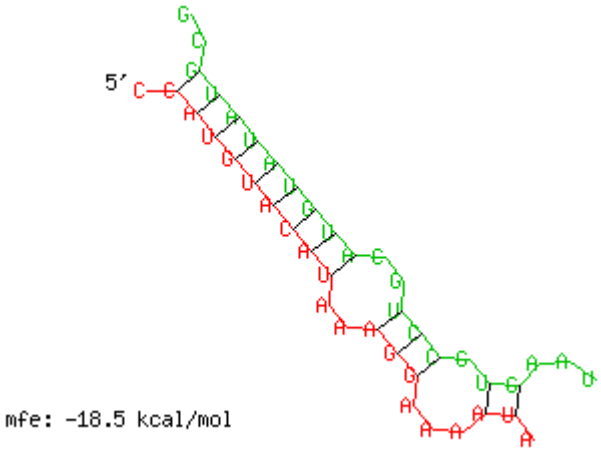

mfe: -18.5 kcal/mol

22. Start position 618

CCTGGGACATTTGCAATAGCAAGCACCCTCTGTAGTCTCC

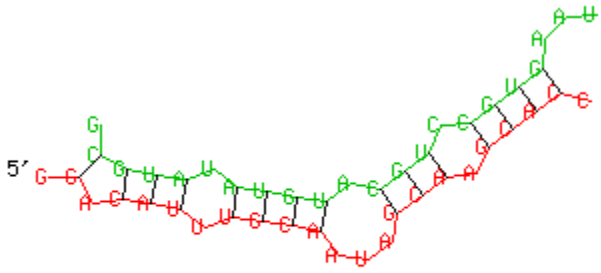

mfe: -18.4 kcal/mol

23. Start position 2

CTCGCCCTTCTTGGCAGGTGTCGCCTGATTCTGATAAT*

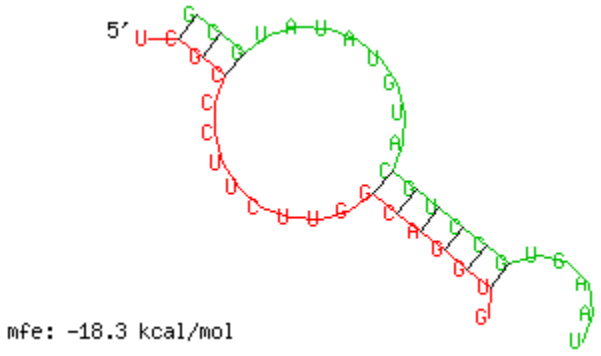

24. Start position 2311

CCTCAGCCTTGCAGTGTAGCATAGGTCTCTCTCTGCACAG

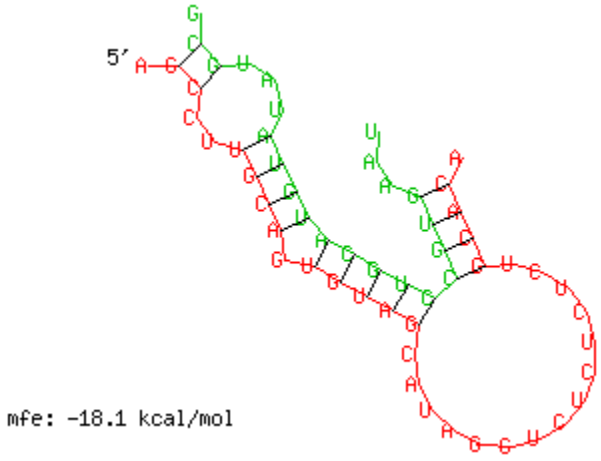

25. Start position 2594

CACCGGTTTGTAATGTGGGTTTTGTTTCTCTCTAGACTTG

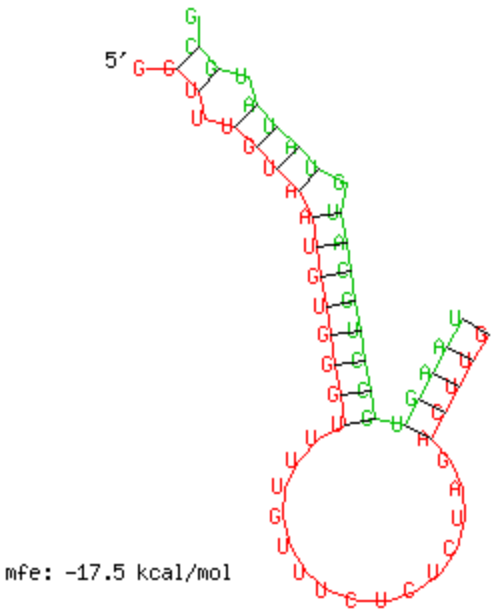

26. Start position 560

GAGGTGCCTTTTCACAAGTATGGCGGCTTACCACGAGATA

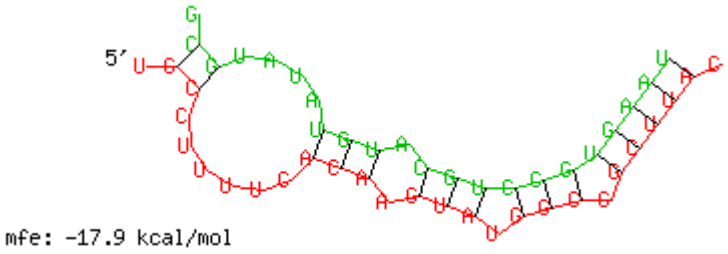

27. Start position 749

GAAAAGCTTTCAGAGGGCATGTATAGGAAGTGATTTTGGG

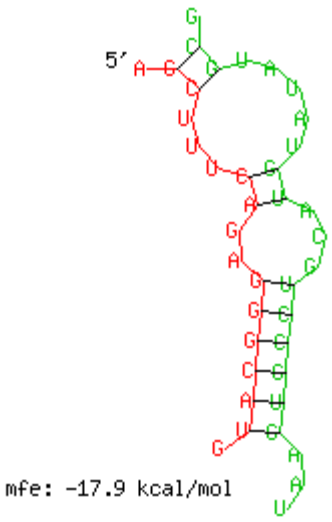

28. Start position 925

GCCTGGCTTGCCACATGGAAAGCAAGCACAAGGGAGCAGT

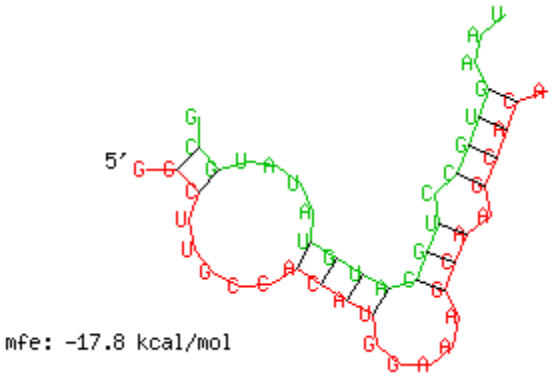

29. Start position 644

CCTCTGTAGTCTCCTGCAGAGCCATAGCTTCAATGTTCTA

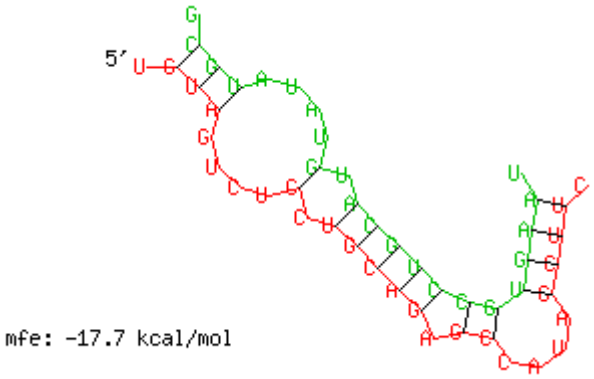

30. Start position 1560

CAGAGCATGTATGACAAGCTTGTGTTTTGGCAGCATTTTA

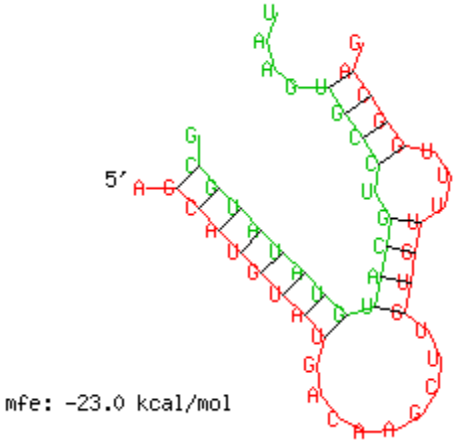

31. Start position 1749

TCAAGCTATAATTCTTTGGTGAATAGGTATGCCTAGGAAC

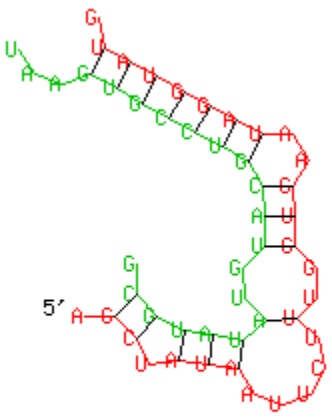

32. Start position 4119

CTAAGGCTCAGTACCAGCGAGCTGTAGGCCATGTCACAGA

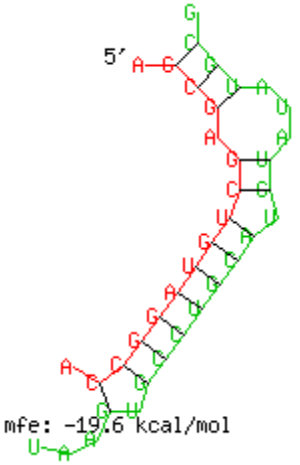

33 . Start position 1775

GGTATGCCTAGGAACAACTGGTGGTTAGTCTGTGTCCTGT

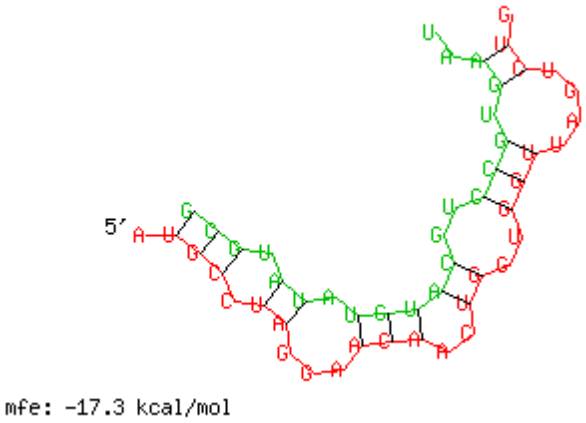

34. Start position 3475

GTTTTGCAAGCGCTCAGGGTTTTCATACTTATTTCATATA

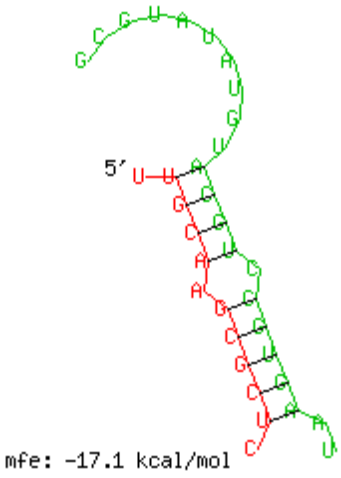

35. Start position 3819

TTGCTCGCTATAGCTTTCTGTTGGCAAATTTTCTCAAAAG

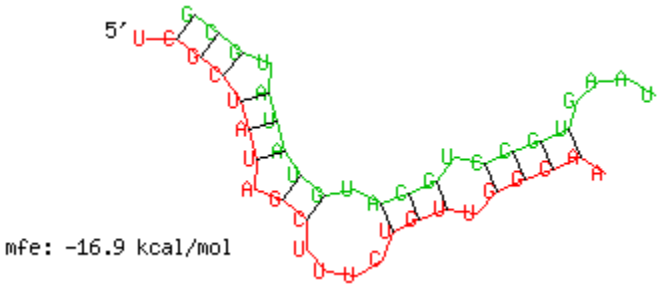

36 . Start position 3695

AGATAGCTGTAGTGTTTATGCCAGAAGTCTCTGGGGACAT

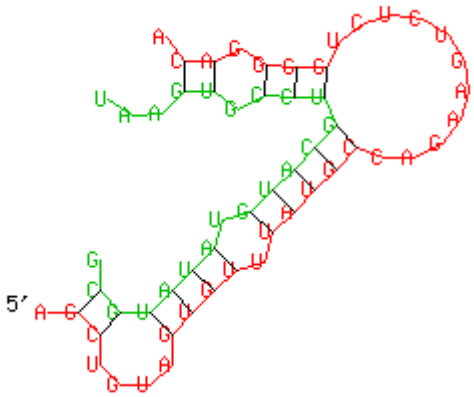

mfe: -16.9 kcal/mol

37. Start position 848

ACTAGCTGTATCCGCTTAGAATGGTAACACAGATGGTCGC

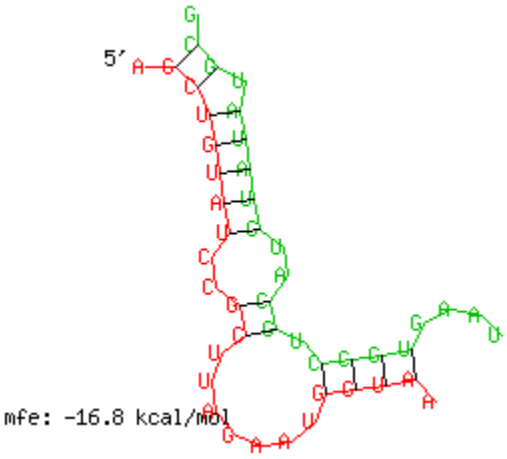

38. Start position 1133

CCCTGCTCCTGTTATAGAGGAGGCTACGTAGACCAAAATG

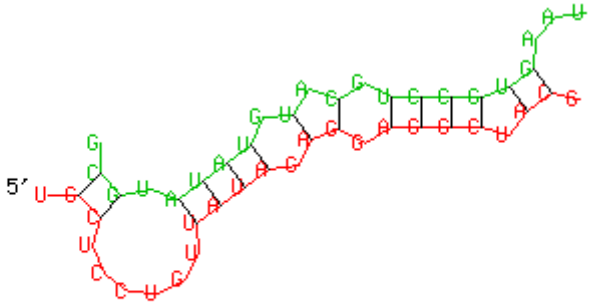

mfe: -16.7 kcal/mol

39. Start position 2738

ACTTGCCAAATTACTTCCTGGGTGGTATCATTTCCTTATC

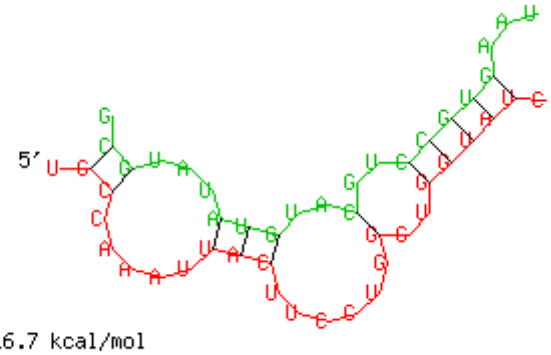

mfe: -16.7 kcal/mol

40. Start position 1959

GGAAAGGGTATCTATTTCAAGATGGGGTGGCGTTTTTCCC

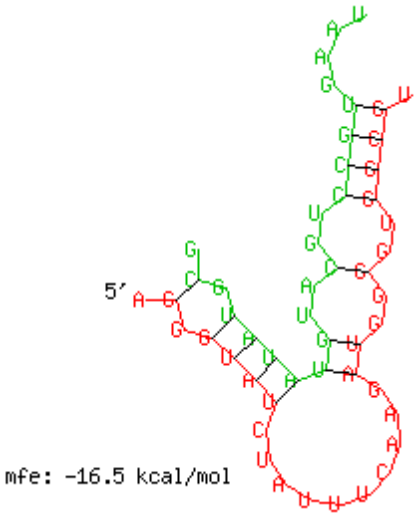

41. Start position 4170

GCAGTGCTTTGAGTAGGACAACAAGGAACATTAAAGAAGG

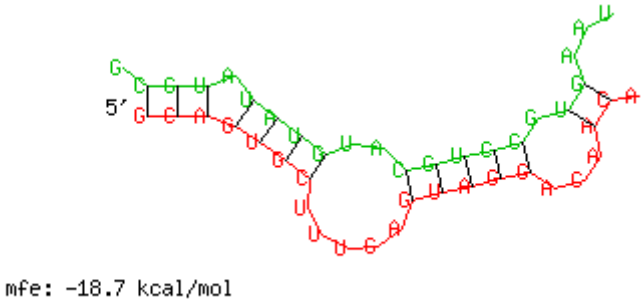

42. Start position 183

TAAAGCACACGGAAGGAGCACCAGCAGCTCTGATAGTATT

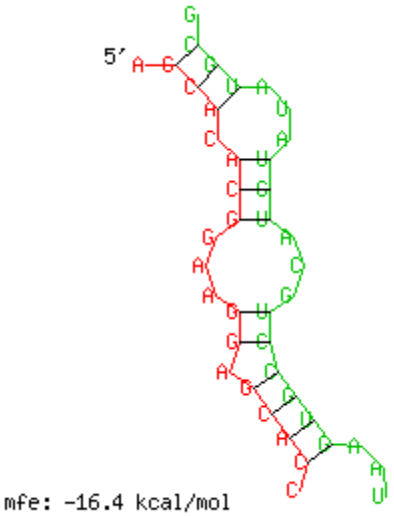

43. Start position 1284

AGTTTGCCTGATACTCAGCACACATCTATGTTTTCCTATG

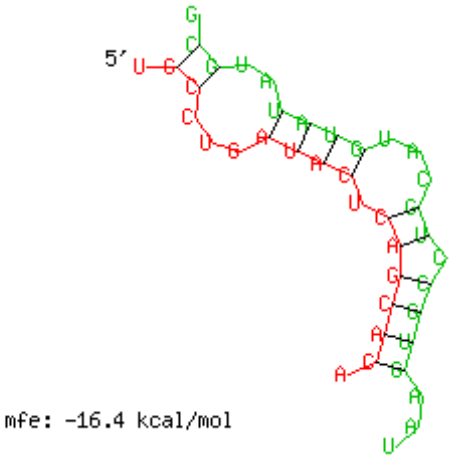

44. Start position 309

GCCAGGTTTCCTTACACTAAGGTAGGTCTAGGTTCTTCGG

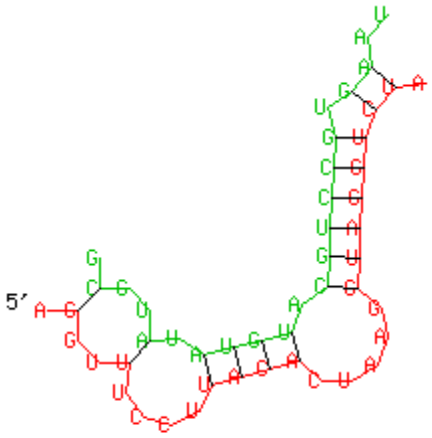

mfe: -16.4 kcal/mol

45 .Start point 2812

TCCACATACCTACACCTTGGGTGCATCACTCCATTCATGG

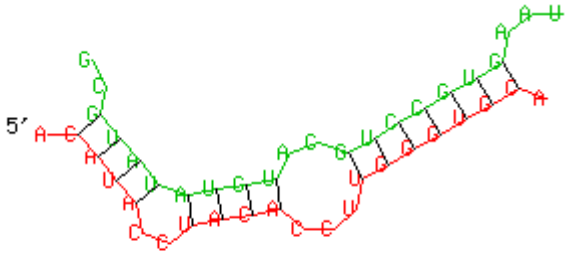

mfe: -16.4 kcal/mol

46. Start point 2403

TCTTGCAACAAGAGTGCCCAACCAGGGACCACTGTCATCA

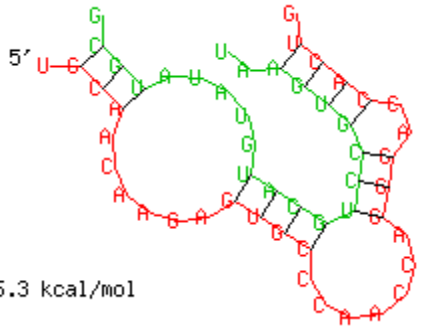

mfe: -16.3 kcal/mol

47. Start point 881

ATGGTCGCTGCAAGCAGATCCCTCTGAGCCTCTCTTCTGC

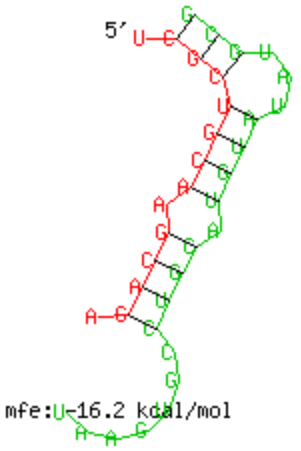

48. Start point 2865

TCATTTCCTTATCTCTCTGATTATCTTCTGGGACCCACGT

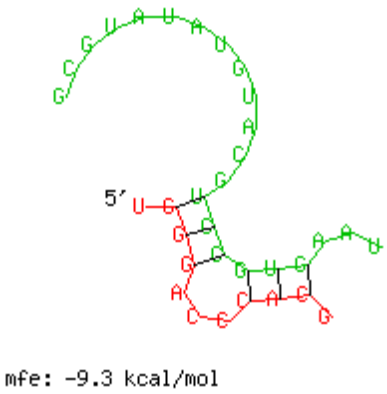

49. Start point 2938

GTTGGTCATTTATGCCCACTTTAAAATGTAGGGAGTCTGT

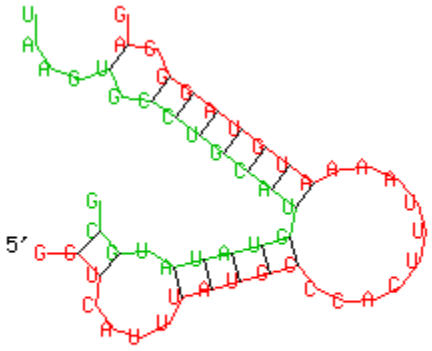

mfe: -15.9 kcal/mol

50 . Start point 3074

CATTGCATATCTTTGCTATTCAACAATGGTGTCCTTCACC

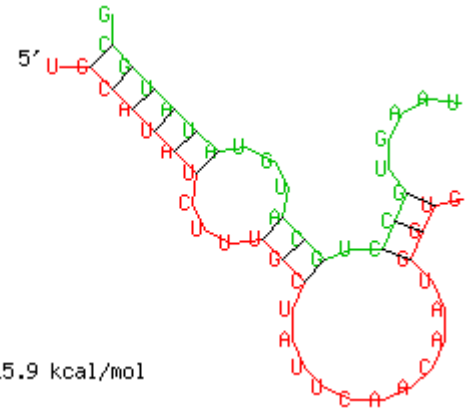

mfe: -15.9 kcal/mol

Supplemental Figure 1: Folded duplex structures from RNA hybrid showing numerous binding sites in the full length 3'UTR of Sfmbt2 for miR467a.